Metal Centers in [NiFe] and [FeFe] Hydrogenase Proteins and Synthetic Model Complexes Studied by X-ray Spectroscopy Techniques

Im Fachbereich Physik der Freien Universität Berlin
eingereichte Dissertation von Oliver Patrick Sanganas

Berlin 2014

Metal Centers in [NiFe] and [FeFe] Hydrogenase Proteins and Synthetic Model Complexes Studied by X-ray Spectroscopy Techniques

Dissertation

zur Erlangung des akademischen Grades eines
Doktors der Naturwissenschaften
(doctor rerum naturalium)

im Fachbereich Physik
der Freien Universität Berlin

eingereicht von

Oliver Patrick Sanganas

Berlin 2014

Erstgutachter: Priv.-Doz. Dr. Michael Haumann
Zweitgutachter: Prof. Dr. Joachim Heberle

Tag der Disputation: 18.09.2014

Contents

Chapter 1

Introduction

1.1 Motivation

The sustainable supply with energy, if possible from renewable resources, is a major global problem. The expected further population growth, the increasing industrial development of the emerging economies, and the constant increase in energy consumption of the industrialized countries turns the search for future energy sources into one of the most important challenges. In addition, this becomes even more prominent considering ecological concerns and limited resources for conventional energy generation from fossil resources or nuclear power.

One possible solution is the development of so-called "green" energies, meaning renewable resources, which are based on unlimited feedstocks such as sunlight, wind, and/or water. Although, for example, photovoltaics and wind power could in principle generate even more than the global energy demand, these have a common problem, which is the storage of the generated energy.

One of the most promising options for storage of renewable energies may be the conversion into hydrogen (H_2), i.e., transformation into chemical energy. The main advantage of hydrogen is that it could serve as a convenient and mobile fuel for transportation and heating or for generation of electricity. The use of hydrogen in efficient fuel cells would reduce the energy conversion losses to a minimum. Today most hydrogen conversion catalysts are based on expensive and rare materials like platinum. However, nature provides efficient and reversible hydrogen catalysts in the form of proteins, which are denoted hydrogenases. These enzymes utilize abundant and cheap first-row transition metals such as nickel and iron to perform hydrogen chemistry.

Hydrogen production in biological organisms has been known for long and natural hydrogen-producing organisms may be directly employed in biotechnological facilities [Melis and Happe, 2001]. Especially interesting are engineered organisms like green algae, which couple photosynthesis, i.e., the generation of high-potential electrons, to the production of hydrogen. The green alga *Chlamydomonas reinhardtii* is a model

organism containing the hydrogenase with the highest known activity for hydrogen formation [Happe and Naber, 1993; Happe and Kaminski, 2002]. This enzyme has been studied in this work. A severe limitation for the use of hydrogenases in applications is their rapid inactivation by oxygen (O_2). Therefore, oxygen-tolerant species are of particular interest. The chemolithoautotrophic Knallgas β-proteobacterium *Ralstonia eutropha* [Lenz and Friedrich, 1998] contains even four oxygen-tolerant hydrogenases, three of which, amongst others, have been investigated in this work.

A long term vision could be the implementation of hydrogenases in photosynthetic hydrogen producing design cells using only sunlight and water as main resources. A further important aspect is the development of novel bio-inspired (semi-)artificial synthetic hydrogen catalysts, which may be based on similar principles as those that facilitate efficient hydrogen catalysis in the hydrogenase enzymes [Armstrong et al., 2012].

1.2 Outline

This thesis is divided into the following chapters:

Chapter Two gives an overview on the different hydrogenases, including their classification, structural features, and redox states of the catalytic cycle. The investigated enzymes and objectives are introduced.

Chapter Three explains the theoretical concepts of X-ray absorption spectroscopy (XAS) and the data analysis procedures. An overview of the experimental setup is provided.

Chapter Four presents the results:
• Section (4.1) summarizes experiments on four oxygen-tolerant membrane-bound [NiFe] hydrogenases (MBH) from *Ralstonia eutropha*, *Aquifex aeolicus*, *Escherichia coli*, and *Hydrogenophaga spec.* AH24, and three oxygen-sensitive periplasmic [NiFe] hydrogenases (PH) from *Desulfovibrio gigas*, *Desulfovibrio fructosovorans*, and *Escherichia coli*. XAS experiments were conducted to reveal structural differences of their metal cofactors.
• Section (4.2) comprises an investigation on the oxygen-tolerant wild-type and four mutant [NiFe] MBHs and the oxygen-sensitive [NiFe] PH from *Escherichia coli*.
• Section (4.3) shows the results of XAS experiments on wild-type and truncated oxygen-tolerant regulatory [NiFe] hydrogenase (RH) constructs from *Ralstonia eutropha*.
• Section (4.4) presents a study on the HoxHY subcomplex of the oxygen-tolerant NAD^+-reducing soluble [NiFe] hydrogenase (SH) from *Ralstonia eutropha*.
• Section (4.5) gives an example for the application of advanced spectroscopic methods (X-ray emission spectroscopy (XES) and resonant inelastic X-ray scattering (RIXS)) on synthetic nickel model compounds and the soluble [NiFe] hydrogenase (SH) from *Ralstonia eutropha*.
• Section (4.6) contains the results of XAS investigations on the H-cluster of the [FeFe] hydrogenase from *Chlamydomonas reinhardtii* revealing structural features of the active site.

Chapter Five concludes this work with a summary of the key results and remarks on future investigations.

Chapter 2

Hydrogenases

All organisms need energy and carbon, besides other nutrients, to sustain life. The carbon either stems from organic compounds (heterotrophs) or from carbon dioxide (autotrophs). Energy sources are light (phototrophs) and organic or inorganic compounds (chemotrophs). Many organisms are able to gain energy from different sources depending on their availability in the environment. One such source is molecular hydrogen. Bacteria can use hydrogen oxidation as an energy supply, which provides electrons for feeding into the respiratory chain. On the other hand, hydrogen can be produced as a byproduct from various reactions, for example during the nitrogen-fixation cycle in nitrogenases or as a valve to release excess reducing equivalents in the cell.

2.1 Overview on Hydrogenase Enzymes

Hydrogenases are metalloenzymes, which contain various transition-metal cofactors. They catalyze the simple and fundamental reaction

$$H_2 \rightleftharpoons 2H^+ + 2e^-. \tag{2.1}$$

Hydrogenase enzymes have been discovered more than 80 years ago [Stephenson and Stickland, 1931] and are meanwhile known to be present in most prokaryotes [Vignais and Colbeau, 2004; Madigan et al., 2010] and archaea. In various eukaryotes, such as entamoeba, fungi, green algae, ciliates, trichomonads, and diplomonads, hydrogenases are also present [Vignais et al., 2001; Vignais and Billoud, 2007]. The vertical distribution of hydrogenase-containing organisms in soil is exemplified in Figure 2.1.

Hydrogenases probably first evolved in phototrophic cyanobacteria around 3.5 billion years ago. Hydrogen metabolizing enzymes perform important functions in the energy balance of the cell [Schwartz and Friedrich, 2003] and are therefore important for homeostasis [Gray and Gest, 1965]. Detailed overviews on the evolution, classification, and function of hydrogenases can be found in respective review articles [Adams, 1990;

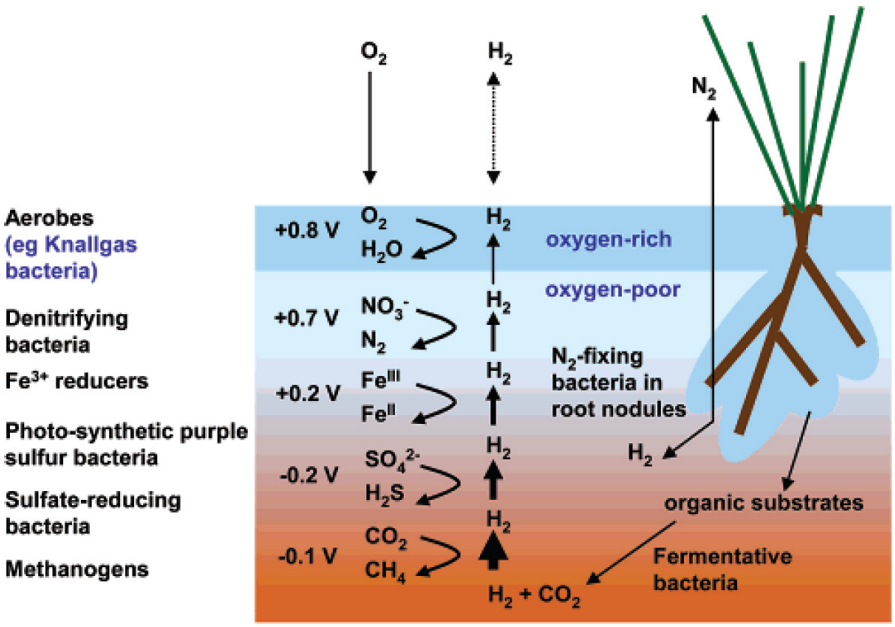

Figure 2.1: Distribution of hydrogenases in soil. The apparent redox potential, relevant catalytic reaction, and the relative concentrations of hydrogen and oxygen are indicated; from [Vincent et al., 2007].

Albracht, 1994; Thauer et al., 1996; Nicolet et al., 2002; Vignais et al., 2001; Vignais and Colbeau, 2004; Vignais and Billoud, 2007; Ghirardi et al., 2007; Madigan et al., 2010; Lubitz et al., 2014].

2.2 Classification of Hydrogenases

Hydrogenases constitute a heterogeneous class of enzymes, which differ with respect to their molecular mass, number and composition of subunits, metal content, cofactors, specific activities, oxygen tolerance, nature of electron donors and acceptors, and reactants. A common feature is that FeS clusters are present in almost all hydrogenases. Only for the methylentetrahydromethanopterin-dehydrogenase (Hmd) found in methanogenic archaea [Pilak et al., 2006], FeS clusters are absent [Zirngibl et al., 1992; Hartmann et al., 1996; Lyon et al., 2004a]). Another general characteristic is a so-called active site where the hydrogen conversion takes place. The classification of hydrogenases is usually based on the metal composition of the active site:

1) In the [NiFe] hydrogenases one nickel and one iron atom form a hetereodinuclear active site complex [Przybyla et al., 1992; Albracht, 1994]. [NiFe] hydrogenases are found in archaea and eubacteria, their main function is the oxidation of hydrogen and hydrogen-formation activities are usually low. The prototypic structure of the [NiFe] cofactor is shown in Figure 2.2. When a sulfur in one cysteine residue bound to the nickel is replaced by a selenium atom (seleno-cysteine) the enzymes are denoted as [NiFeSe] hydrogenases [Garcin et al., 1999]. Such enzymes are also found in eubacteria and archaea [Vignais et al., 2001; Vignais and Billoud, 2007].

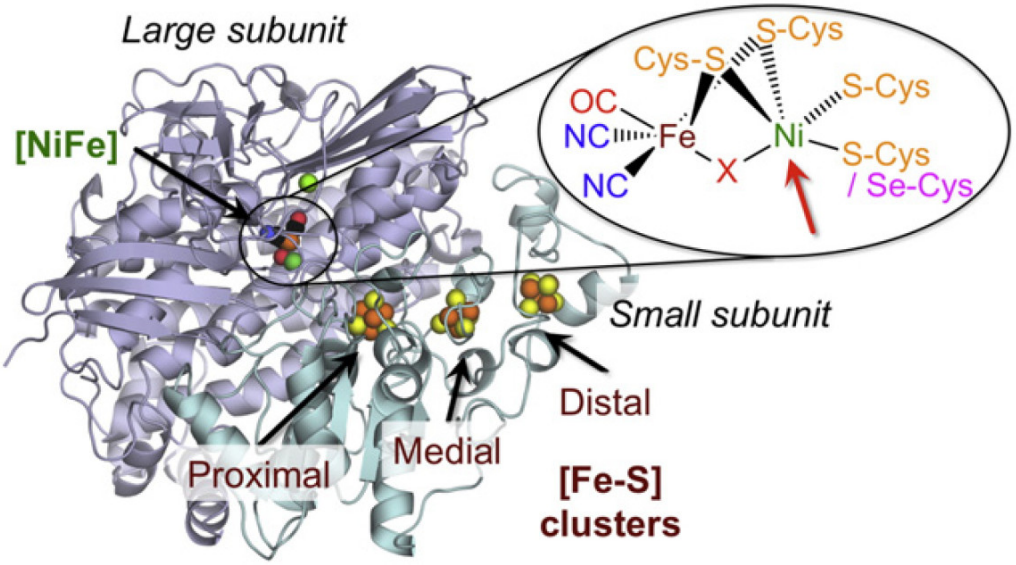

Figure 2.2: X-ray crystal structure of the [NiFe] hydrogenase from *Desulfovibrio vulgaris* Miyazaki F (PDB: 1H2R) showing the large subunit housing the [NiFe] active site and the small subunit binding three FeS clusters. The atomic structure of the [NiFe] active site is shown in magnification: the Ni has four cysteine ligands, two of them in a bridging position, and an additional third bridging ligand X, which is an oxygen species in oxidized states and a hydrogen species at least in the Ni-C state of the enzyme. The active site Fe binds three diatomic ligands (2 CN^-, 1 CO); from [Shafaat et al., 2013].

2) The active site of the [FeFe] hydrogenases is a six-iron unit denoted as H-cluster (Figure 2.7) [Adams, 1990; Akhmanova et al., 1998]. These reversible enzymes are found in anaerobic prokaryotes and eukaryotes such as green algae [Vignais et al., 2001; Vignais and Billoud, 2007]. They are excellent hydrogen producers but also catalyze hydrogen oxidation at high rates [Holtz et al., 1991].

3) The [Fe] hydrogenases contain a mononuclear iron site within a unique iron-guanylyl pyridinol (FeGP) cofactor [Buurman et al., 2000; Lyon et al., 2004b; Shima et al.,

2011]. They have been found only in methanogenic archaea. The Hmd cofactor is light sensitive, i.e., the iron is lost under illumination, which had led to the early assignment of Hmd as metal-free hydrogenase [Zirngibl et al., 1992; Frey, 1998].

A common feature for all [NiFe] and [FeFe] hydrogenases is the presence of iron-bound CO and CN ligands at the active site, which is unusual in nature. Sequence and structural analyses have shown that the three types of hydrogenases have evolved convergently [Vignais and Colbeau, 2004] and are phylogenetically unrelated. [FeFe] hydrogenases are of special interest as hydrogen-forming catalysts because of their much higher hydrogen production rate compared to [NiFe] hydrogenases. The catalytic activity of [FeFe] hydrogenases, however, is irreversible inhibited upon exposure to dioxygen (O_2) [Erbes et al., 1979], while [NiFe] hydrogenases are reversible inhibited by O_2 [Przybyla et al., 1992]. Particularly interesting are those [NiFe] hydrogenases, which exhibit elevated levels or even complete oxygen-tolerance [Burgdorf et al., 2005a; Lubitz et al., 2007; Vincent et al., 2007; Goris et al., 2011; Shafaat et al., 2013].

2.3 Structures of Hydrogenases

Today, crystal structures of all types of hydrogenase proteins are available: structures of [NiFe] hydrogenases from *Desulfovibrio* species, e.g., *D. gigas*, *D. fructosovorans* [Volbeda et al., 1995, 2005], *D. vulgaris* Miyazaki F (Figure 2.2) [Higuchi et al., 1997, 1999; Ogata et al., 2005], and *D. desulfuricans* [Matias et al., 2001] have been reported, which all belong to the oxygen-sensitive so-called "standard" type of enzymes. [NiFeSe] hydrogenase from *Desulfomicrobium baculatum* [Garcin et al., 1999] as well as bacterial [FeFe] hydrogenases from *Clostridium pasteurianum* (Figures 2.3 and 2.6, right) [Peters et al., 1998] and *Desulfovibrio desulfuricans* (Figure 2.6, middle) [Nicolet et al., 1999] have been crystallized. Very recently it was possible to crystallize the membrane-bound [NiFe] hydrogenases from *Ralstonia eutropha* (Figure 2.4) [Fritsch et al., 2011b], *Hydrogenovibrio marinus* [Shomura et al., 2011], and *Escherichia coli* (Figure 2.12) [Volbeda et al., 2012], which all are oxygen-tolerant. The crystal structures show the three dimensional composition of the enzymes at resolutions in the range of about 1 – 3 Å (Figures 2.2, 2.3, 2.4). This includes the domains or subunits, the number, arrangement and type of the FeS clusters as well as the surrounding ligands of the active site. In some structures, hydrophobic cavities and channels can be found and the configurations of all amino acids, in particular around the FeS clusters and the active site, were revealed. These hydrophobic channels, surrounded by conserved histidine and glutamate residues, are involved in hydrogen transportation from the protein surface to the active site and vice versa [Volbeda et al., 1995; Higuchi et al., 1997; Montet et al., 1997; Garcin et al., 1999; Matias et al., 2001; Fontecilla-Camps et al., 2007].

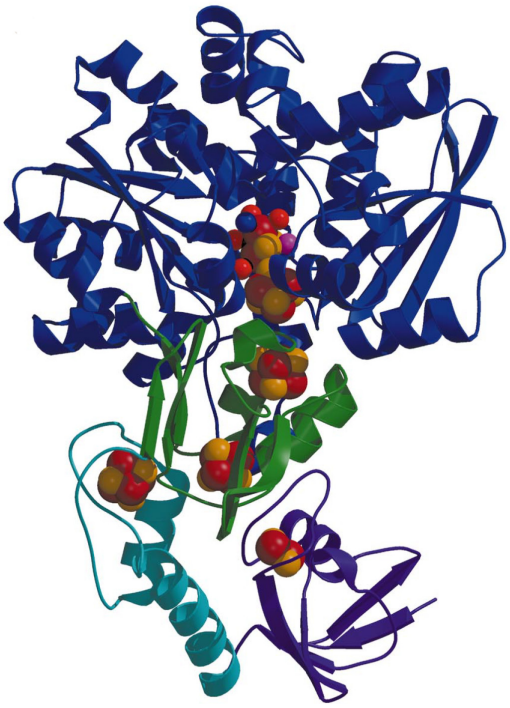

Figure 2.3: Structure of the [FeFe] hydrogenase from *Clostridium pasteurianum* showing the protein domains, the active site, and the FeS clusters: active site domain with the H-cluster (dark blue), 2 [4Fe4S] binding domain (green), domain with a histidine-coordinated [4Fe4S] cluster (cyan), and [2Fe2S] binding domain (purple). Fe (brown), S (yellow), N (blue), C (black), O (red), unknown bridging ligand (purple); from [Peters, 1999].

2.3.1 Structures of [NiFe] Hydrogenases

The core of [NiFe] hydrogenases consists of two highly conserved subunits (Figures 2.2, 2.4). The small subunit (molecular mass 15 – 45 kDa) binds several FeS clusters, while the large subunit (molecular mass 49 – 86 kDa) contains the [NiFe] active site of hydrogen conversion. The FeS clusters are almost equidistantly (∼10 Å) arranged and function in electron transfer towards and out of the [NiFe] active site, which, according to crystal structures, is deeply buried within the large subunit [Fontecilla-Camps et al., 1997; Fontecilla-Camps et al., 2007]. Depending on the distance from the [NiFe] active site, the FeS clusters are denoted as proximal (p), medial (m) or distal (d). In the standard [NiFe] hydrogenases, $[4Fe4S]_p$, $[3Fe4S]_m$, and $[4Fe4S]_d$ species are present [Cammack et al., 1997]. The Fe atoms of the distal cluster are coordinated by three cysteines and one histidine, those of the medial by three cysteines, and those of the proximal clusters usually by four cysteines [Volbeda et al., 1995; Higuchi et al., 1999]. In the crystallized oxygen-tolerant membrane-bound-type [NiFe] hydrogenases (MBH), the

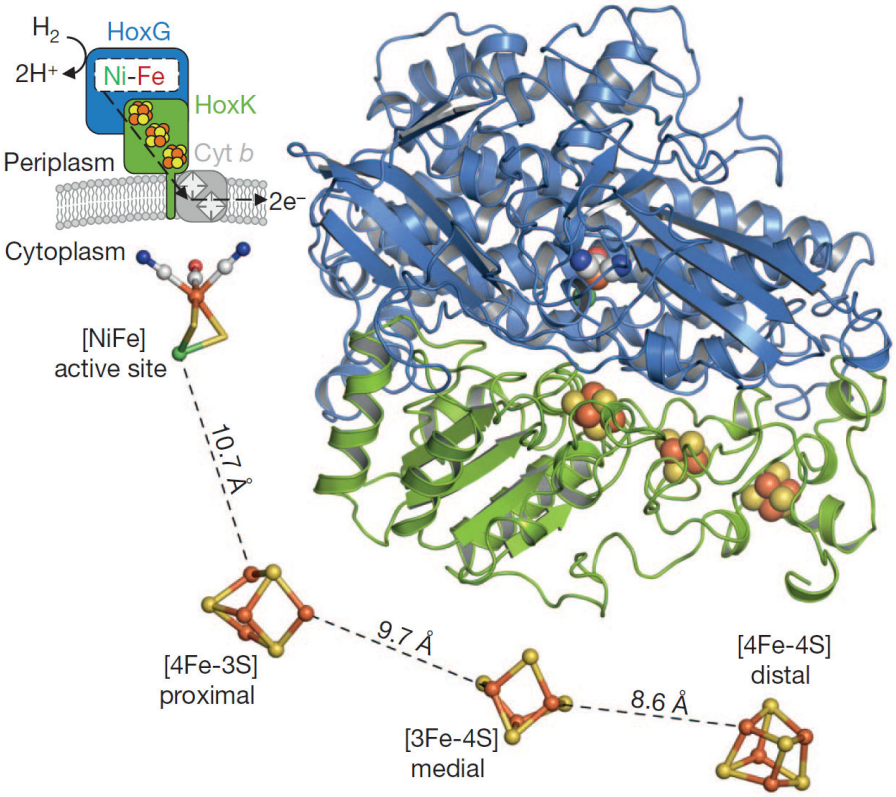

Figure 2.4: X-ray crystal structure of the membrane-bound [NiFe] hydrogenase from *Ralstonia eutropha*. Top right: the large subunit (blue) binds the [NiFe] active site and the small subunit (green) binds three FeS clusters. Top left: scheme of the attachment of the metal centers of the enzyme to the membrane. Bottom: structures and distances of the cofactors; from [Fritsch et al., 2011b].

proximal cluster is coordinated by the sulfurs of two additional cysteine residues in the small subunit and thereby is converted to a [4Fe3S] cluster showing six cysteine ligands. The additional cysteines are positioned on opposite sides of the [4Fe3S] cluster [Fritsch et al., 2011b; Shomura et al., 2011; Volbeda et al., 2012, 2013; Winkler et al., 2013; Fritsch et al., 2014; Lubitz et al., 2014]. Additionally, the [4Fe3S] cluster undergoes structural changes during the catalytic cycle.

At the [NiFe] active site four conserved cysteine ligands surround the Ni ion, with unoccupied binding sites for the potential binding of additional ligands during the catalytic cycle (Figure 2.5). Two cysteine residues connect the Ni and the Fe with their thiolates in a bridging position [Volbeda et al., 1995], establishing a Ni−Fe distance of about ∼2.8 Å [Albracht, 1994; Cammack et al., 1997]. In the [NiFeSe] hydrogenases one cysteine solely bound to the Ni is exchanged with a seleno-cysteine [Garcin et al.,

1999]. A third bridging ligand is often observed in the inactive oxidized state of [NiFe] hydrogenases, which could be a hydroxide (OH^-) or hydroperoxide ($-OOH$) [Stein and Lubitz, 2002; Volbeda et al., 2005], leading to a (distorted) square-pyramidal Ni coordination. In the reduced state (Ni-C, see Section 2.4.1), a bridging hydride (H^-) may be present. The Fe ion coordination is then (distorted) octahedral with three terminal diatomic ligands, i.e., two cyanides (CN^-), one carbon monoxide (CO), and three bridging ligands [Bagley et al., 1994; Volbeda et al., 1995, 1996; Higuchi et al., 1997; Happe et al., 1997; Pierik et al., 1999].

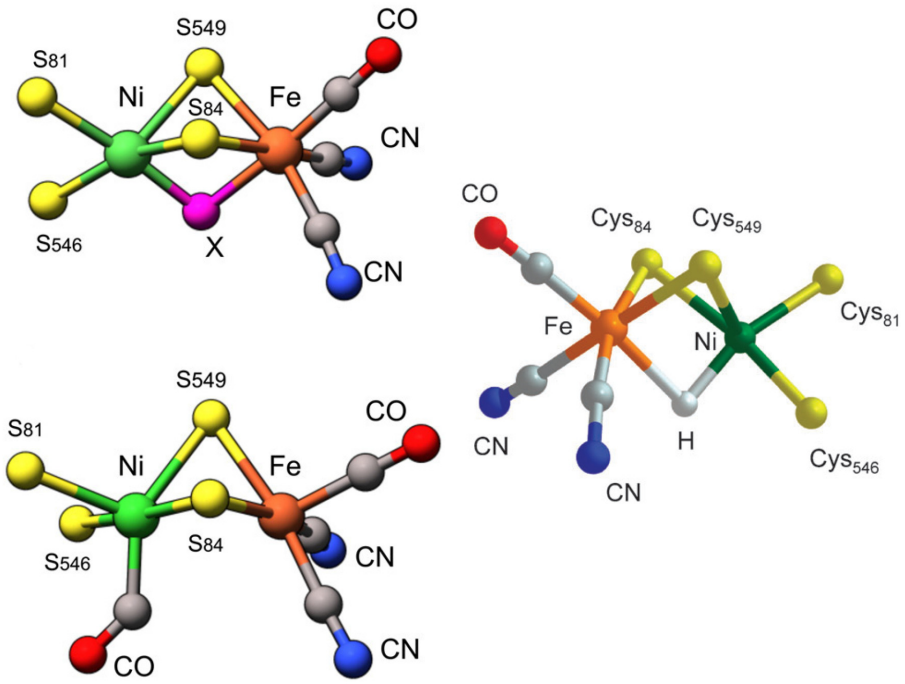

Figure 2.5: Suggested structures for the [NiFe] active site in the hydrogenase from *Desulfovibrio vulgaris* Miyazaki F in three states. Top left: oxidized (X is an oxygen species), bottom left: active form (PDB 1UBJ), right: Ni-C state with a hydride as the bridging ligand. Fe (orange), Ni (green), S (yellow), C (grey), O (red), N (blue); from [Pandelia et al., 2010c; Kellers et al., 2009].

2.3.2 Structures of [FeFe] Hydrogenases

Several types of [FeFe] hydrogenases exist, which show different cofactor complements (Figure 2.6). Bacterial enzymes contain up to four FeS clusters, besides the active site H-cluster [Peters, 1999]. The active site is a unique six-iron cluster, consisting of a [4Fe4S] center (cubane) and a diiron site ($2Fe_H$), which are linked by a cysteine residue

to each other (Figure 2.7) [Lemon and Peters, 1999; Nicolet et al., 2001; Lubitz et al., 2007; Pandey et al., 2008]. The [FeFe] hydrogenase from *Clostridium pasteurianum* has three [4Fe4S] clusters and one [2Fe2S] cluster (Figures 2.3, 2.6 right) [Peters et al., 1998], while the enzyme from *Desulfovibrio desulfuricans* shows only two [4Fe4S] clusters (Figure 2.6 middle) [Nicolet et al., 1999, 2000]. In [FeFe] hydrogenases from green algae, e.g., *Cr*HydA1 from *Chlamydomonas reinhardtii*, only the active site H-cluster is present and relay FeS clusters are absent (Figure 2.6 left).

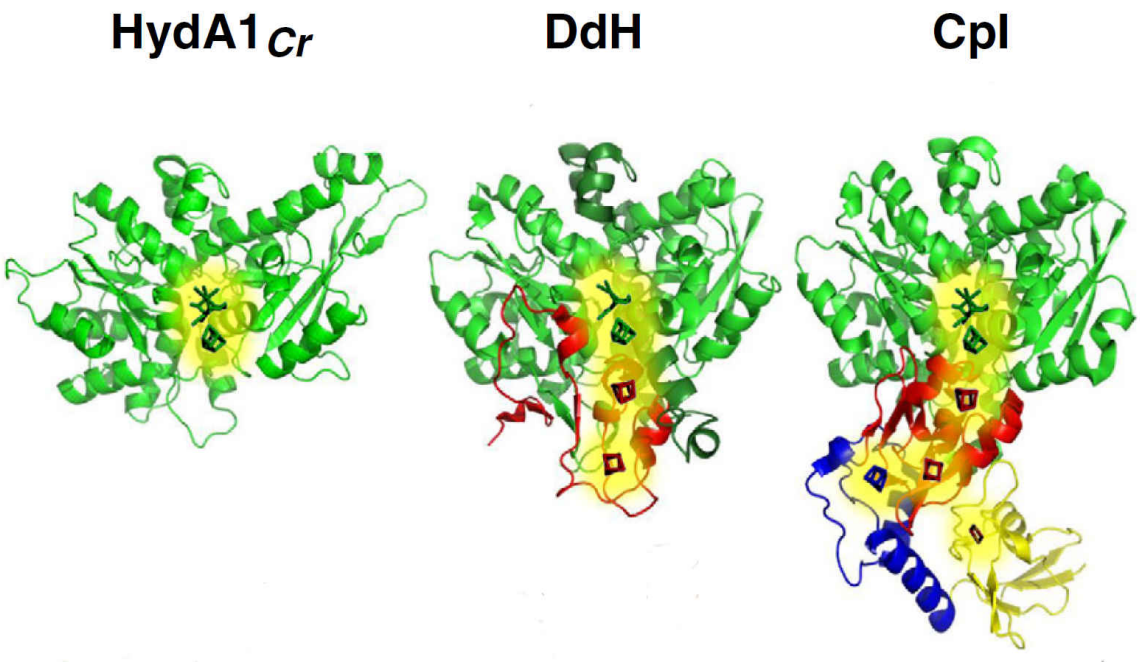

Figure 2.6: Crystal structures of three different [FeFe] hydrogenases: *Cr*HydA1 from *Chlamydomonas reinhardtii* (PDB: 3LX4), *Dd*H from *Desulfovibrio desulfuricans* (PDB: 1HFE), and *Cp*I from *Clostridium pasteurianum* (PDB: 3C8Y). The active site H-cluster and the FeS clusters participating in electron transfer are indicated by stick models (yellow); from [Winkler et al., 2013].

Both Fe atoms of $2Fe_H$ have one carbon monoxide (CO) and one cyanide (CN^-) ligand each [Pierik et al., 1998a,b]. For *Clostridium pasteurianum* only CO ligands have been assigned in one crystal structure, probably due to limited resolution (Figure 2.7) [Nicolet et al., 2000; Fontecilla-Camps et al., 2007]. A further CO molecule is present and located in a bridging position in the oxidized state [Pierik et al., 1998a; Nicolet et al., 2001; Roseboom et al., 2006; Fontecilla-Camps et al., 2007]. A unique bridging ligand is present in $2Fe_H$, which is an azadithiolate group [Berggren et al., 2013]. The Fe of $2Fe_H$ closer to the bridging cysteine residue is denoted as proximal (Fe_p), and the other one as distal (Fe_d). Upon reduction of the H-cluster the bridging CO ligand has

been shown by FTIR to become a terminal ligand to Fe_d [Peters, 1999; Siegbahn et al., 2007]. An open apical binding site at Fe_d is also available for inhibitors such as O_2 or CO.

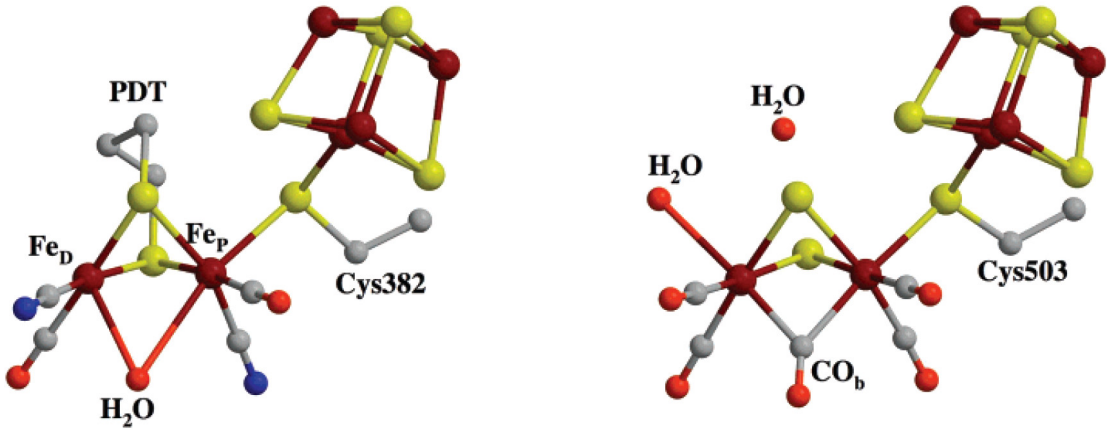

Figure 2.7: Active site structures of the H-cluster in the [FeFe] hydrogenases from *Desulfovibrio desulfuricans* (*Dd*H, left, PDB: 1HFE) and *Clostridium pasteurianum* (*Cp*I, right, PDB: 1FEH). The varying assignment of diatomic ligands is related to the limited crystallographic resolution. The nature of the bridging ligand in $2Fe_H$ has remained unresolved in crystal structures. Recent results assign it to an azadithiolate group. Fe (brown), S (yellow), N (blue), C (grey), O (red, non-labeled), PDT (1,3-propanedithiolate); from [Fontecilla-Camps et al., 2007].

2.4 Redox States and Catalytic Cycle

Based on the crystal structures and, e.g., EPR, FTIR, XAS data, and further spectroscopic investigations on various hydrogenases, considerable information on the catalytic cycles has been gained. A brief overview is given in the following.

2.4.1 Reaction Intermediates of [NiFe] Hydrogenases

Figure 2.8 shows the reaction schemes for the "standard" periplasmic enzymes (PH), the oxygen-tolerant hydrogenases (membrane-bound - MBH, soluble - SH, and regulatory - RH from, e.g., *Ralstonia eutropha*), and the [NiFeSe] hydrogenase, summarizing most of the present knowledge from spectroscopic studies [Fichtner et al., 2006; Kellers et al., 2009; Pandelia et al., 2009, 2010c; Bleijlevens et al., 2001; Pandelia et al., 2010a, 2011, 2012a; Horch et al., 2010; Bernhard et al., 2001; Medina et al., 1996; De Lacey et al.,

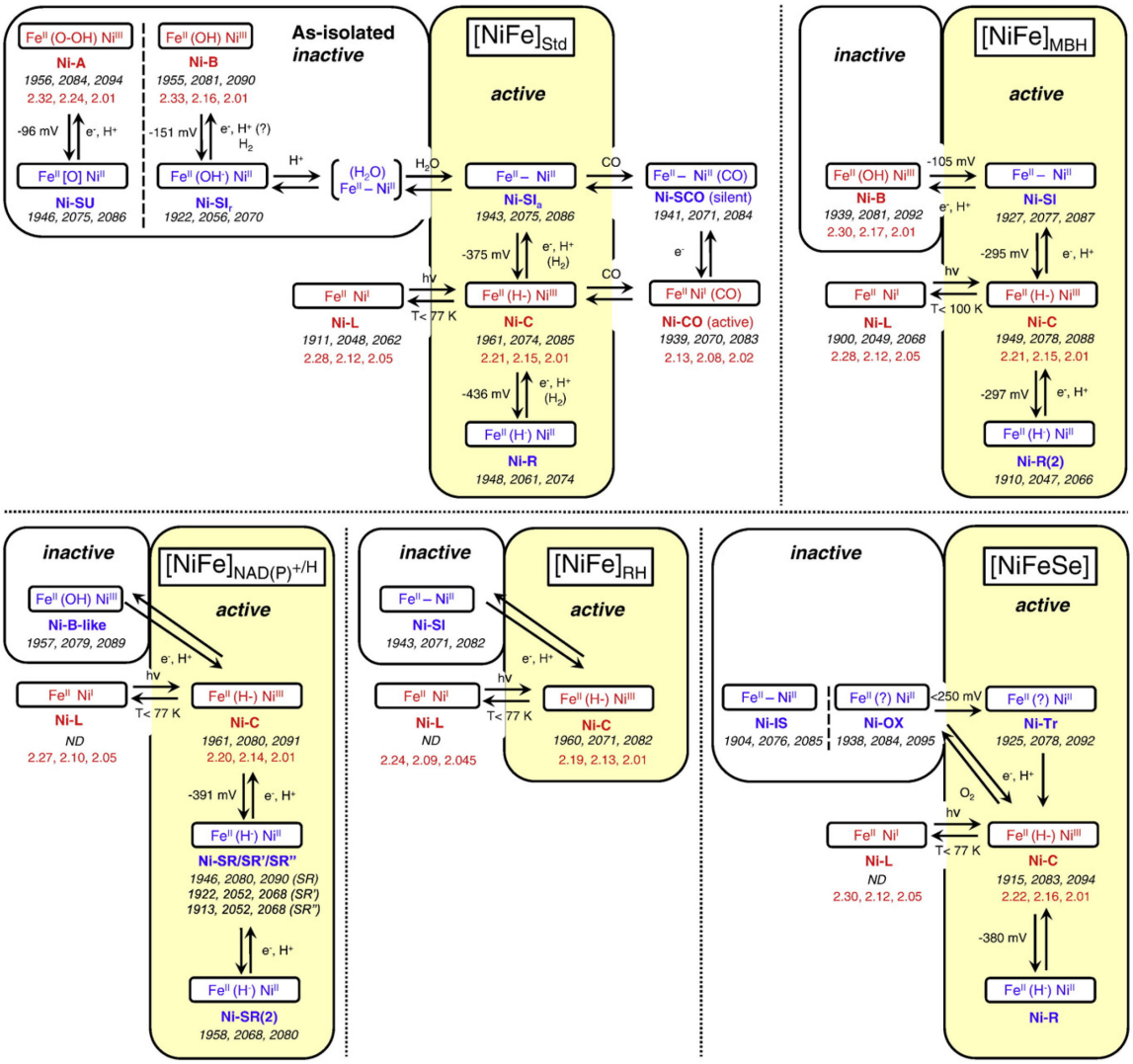

Figure 2.8: Reaction schemes for the different types of [NiFe] hydrogenases: the "standard" periplasmic enzymes, the oxygen-tolerant hydrogenases (MBH, SH, RH) (from, e.g., *Ralstonia eutropha*), and the [NiFeSe] hydrogenase; from [Shafaat et al., 2013].

2008; Saggu et al., 2009, 2010b,a]. Depicted are the respective oxidation states for the Ni and Fe atoms of the [NiFe] active site, the third bridging ligand, the Ni states detected by EPR, the FTIR frequencies of the three diatomic ligands at the [NiFe] active site, the EPR g-values, and the conditions that induce the state transitions (e.g., pH, CO, light). Ni-A and Ni-B are inactive states of the [NiFe] hydrogenases. Ni-A probably has an O−OH bridging ligand instead of an OH likely present in Ni-B. In aerobically oxidized "standard" hydrogenases, Ni-A is the major species, while in

oxygen-tolerant hydrogenases, Ni-A is completely absent and only Ni-B is found. So far, the reasons for this difference are unclear. Under reducing conditions the Ni-A and Ni-B states are converted into a diamagnetic state due to the formation of Ni^{II}. Therefore, no EPR signal can be detected and Ni^{II} states are denoted silent unready (Ni-SU), silent inactive (Ni-SI), or silent ready (Ni-SR). The Fe in the [NiFe] active site remains in the low-spin Fe^{II} state during the whole catalytic cycle due to the strong-field CO and CN^- ligands [Huyett et al., 1997].

Upon activation with H_2 the Ni oxidation state changes to Ni^{III}, H_2 is heterolytically cleaved and oxidizes the Ni to form a Ni−hydride bond. This new highly active state is called Ni-C. The hydride presumably is in a Ni−Fe bridging position (Ni^{III}− H^-− Fe^{II}) [Teixeira et al., 1985; Stein, 2001; Stein and Lubitz, 2001; Brecht et al., 2003; Foerster, 2003; Foerster et al., 2003; Pandelia et al., 2012a]. At temperatures below 100 K the so-called Ni-L state can be created upon illumination with visible light. In this state, the Ni presumably has a formal oxidation state of Ni^{I}. Ni-L is stable only at low temperatures [van der Zwaan et al., 1985], whereas at temperatures above 200 K it relaxes back to the Ni-C state. Crystal structures have shown that the third bridging ligand in the [NiFe] active site is removed during further reduction of the Ni-C state leading to the appearance of the Ni-R or Ni-SR states [Garcin et al., 1999; Higuchi et al., 1999], which are EPR silent and contain Ni^{II}.

Recent studies have shown that the proximal FeS cluster in the oxygen-tolerant MBHs is a unique [4Fe3S] species [Fritsch et al., 2011b; Shomura et al., 2011; Volbeda et al., 2012, 2013]. EPR measurements revealed strong magnetic coupling between the [NiFe] active site and the proximal FeS cluster [Lenz et al., 2010; Saggu et al., 2010b; Pandelia et al., 2011]. The [4Fe3S] cluster can undergo two redox transitions at ambient potentials [Pandelia et al., 2011], as opposed to only one transition of the standard [4Fe4S] cluster. This is possibly related to the coordination by two additional cysteine ligands [Fritsch et al., 2011b; Goris et al., 2011; Pandelia et al., 2011; Parkin and Sargent, 2012], which leads to a structure with one more separated Fe ion. In the MBH of *Ralstonia eutropha* this Fe ion has four sulfur ligands: two bridging sulfurs, one from Cys149 and one from the additional Cys120. The other additional cysteine (Cys19) is located on the opposite side of the [4Fe3S] cluster and connected to two of its Fe ions. Investigations using Mössbauer spectroscopy on the *Aquifex aeolicus* MBH revealed additional large isomer shifts and large quadrupole splittings, due to the geometrical distortions in the [4Fe3S] cluster, as also supported by DFT calculations [Pandelia et al., 2013]. Pronounced structural changes of the [4Fe3S] cluster have been observed in the crystal structures, including coordination of one Fe ion by a nitrogen atom of the protein backbone [Shomura et al., 2011; Volbeda et al., 2012]. In the oxidized state the two additional cysteines elongate the cluster by pulling the more isolated Fe further away from the other three Fe ions. Therefore, the respective Fe−Fe distances are increased to 3.5 Å and 4.0 Å [Fritsch et al., 2011b], while being shorter (∼2.7 Å) in a conventional [4Fe4S] cluster [Volbeda et al., 1995, 2005; Ogata et al., 2010]. The unusual redox

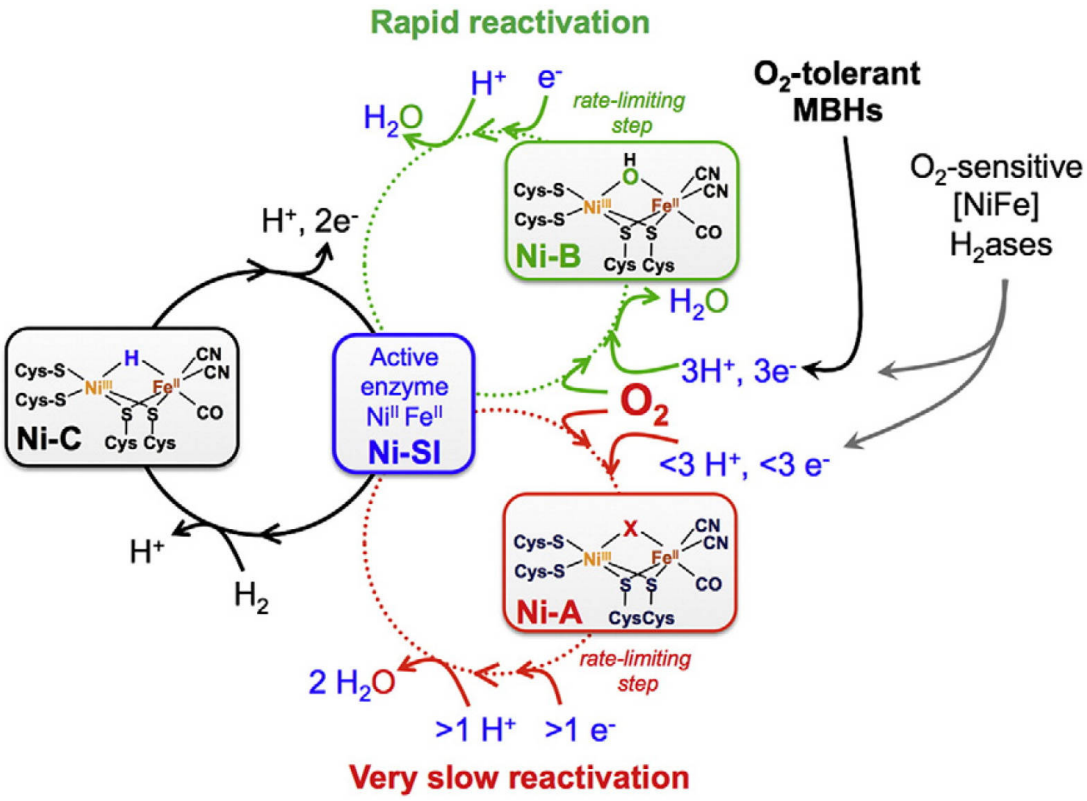

Figure 2.9: General scheme of the catalytic cycle and of oxygen-reduction during reactivation of oxygen-tolerant membrane-bound hydrogenases.; from [Shafaat et al., 2013].

properties of the [4Fe3S] cluster, namely its two-electron donation capacity, have been related to the oxygen-tolerance of the MBHs. It has been proposed that this facilitates full reduction of O_2 to H_2O at the [NiFe] active site, thereby preventing formation of the inactive and slowly reactivated Ni-A state (Figure 2.9).

In this work, characterization of the [NiFe] hydrogenases from *Ralstonia eutropha* by spectroscopic methods is a main topic. XAS is a tool for detection even of subtle structural differences at the [NiFe] active site, which are not resolved in crystals. This holds in particular for diamagnetic states, which are EPR silent, and for intermediates, which have not been crystallized. Also for EPR active and crystallized states of hydrogenases, XAS can provide additional information due to its subangstrom distance resolution. Further, for example the composition of the FeS clusters is not yet determined in the SH and RH enzymes. The reasons for the apparently fewer detectable states in the SH and RH remain unclear as well as the molecular restraints for the different catalytic activities and the oxygen-tolerance. Structural changes detected by XAS can provide possible explanations, in particular if, e.g., wild-type and mutant enzymes are

compared. Oxygen-tolerant [NiFe] hydrogenases are found in many organisms, in particular the enzymes from *Ralstonia eutropha* have been characterized extensively. The oxygen-tolerant hydrogenases of the MBH, SH, and RH types do not show the inactive Ni-A state. However, the Ni-B state has been observed in the MBHs (Figure 2.9).

2.4.2 Redox States and Catalytic Cycle of [FeFe] Hydrogenases

A tentative scheme of the reactions taking place during the catalytic cycle of [FeFe] hydrogenases and the possible reaction sequences upon exposure to CO or O_2 is shown in Figure 2.10 [Winkler et al., 2013]. The H-cluster shows at least two distinct redox states during its catalytic cycle (Figure 2.10). One is the active oxidized state (H_{ox}) in which $2Fe_H$ shows a $Fe^{I}Fe^{II}$ configuration, the other one is the active reduced state (H_{red}) with an $Fe^{I}Fe^{I}$ site [Lubitz et al., 2007]. Hydrogen bonding to the CN ligands is believed to stabilize the orientation of $2Fe_H$ within the enzyme, while the CO ligands are more flexible and may change their orientation during the catalytic cycle. Additionally, a further transition to the so-called super-reduced state (H_{sred}) has been described. The midpoint potential for the red→sred transition differs between the *Dd*H enzyme (-540 mV) and *Cr*HydA1 (-460 mV). FTIR results have suggested that only in the super-reduced state (H_{sred}) the bridging CO ligand moves to a terminal position at Fe_d. The second reduction probably takes place at the [4Fe4S] unit of the H-cluster.

Exogenous CO is a reversible inhibitor of the H-cluster [Adams, 1990; Silakov et al., 2009; Goldet et al., 2009]. Oxygen-exposure leads to fast and irreversible inhibition and subsequent destruction of the H-cluster. The binding of O_2 at the open site at Fe_d presumably is the starting point of oxygen-inhibition and may lead to the formation of reactive oxygen species (ROS) [Stripp et al., 2009; Goldet et al., 2009; Lambertz et al., 2011]. XAS studies on the H-cluster have resolved the Fe−S and Fe−CO/N bond lengths as well as individual Fe−Fe bond lengths in [4Fe4S] and $2Fe_H$. Further, structural changes upon different treatments (H_2, O_2, CO) were detected by XAS, suggesting that the [4Fe4S] unit is degraded first upon exposure to O_2, while the $2Fe_H$ remains intact for longer oxygen-exposure periods [Stripp et al., 2009; Lambertz et al., 2011]. Possibly, O_2 binds first to $2Fe_H$ so that superoxide is formed, which then attacks the [4Fe4S] unit, leading to its degradation [Lambertz et al., 2011]. XAS studies on the H-cluster assembly during the maturation process have been carried out [Czech et al., 2010, 2011; Shepard et al., 2010]. Advanced site-selective XAS methods gave new insight on the individual electronic structures of the [4Fe4S] and $2Fe_H$ units [Lambertz et al., 2014]. Further XAS investigations may lead to deeper insight into O_2-inactivation and the electronic structure of the H-cluster in all intermediate states.

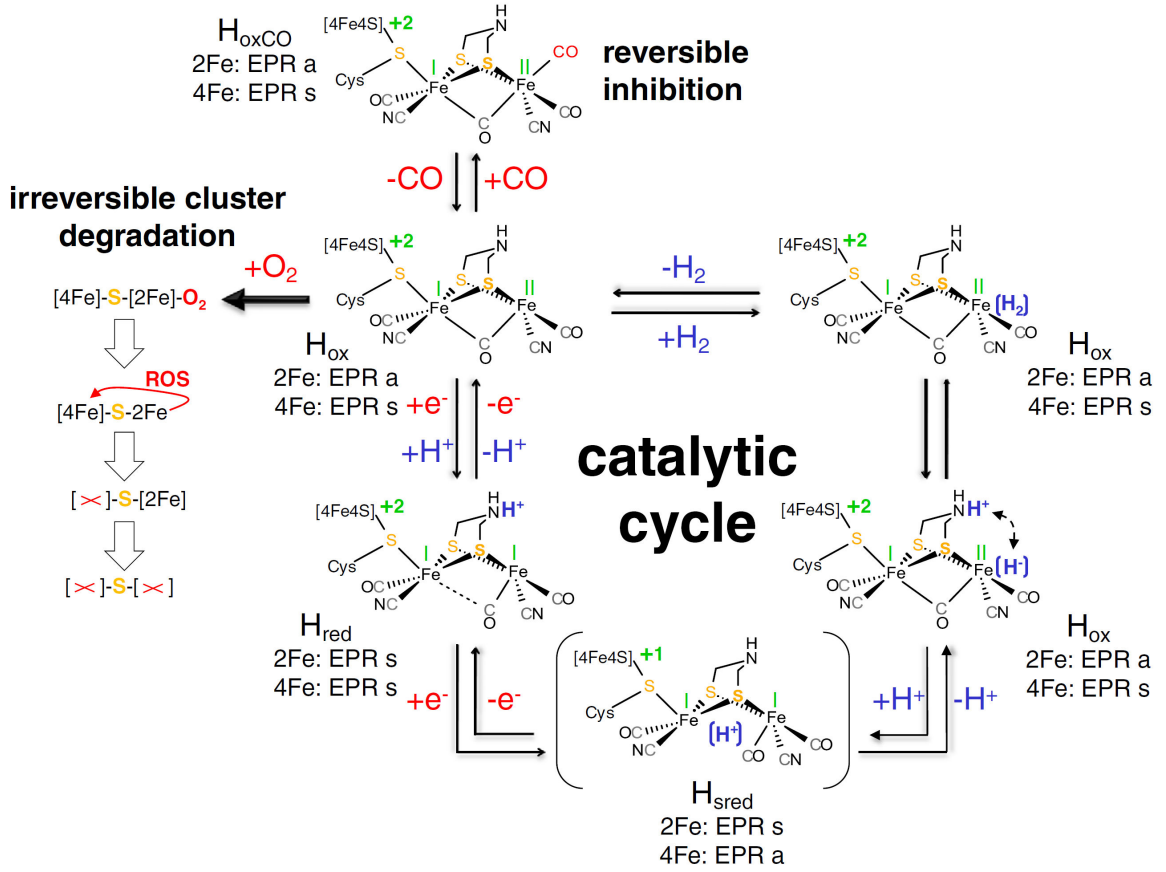

Figure 2.10: Reaction scheme for the H-cluster in [FeFe] hydrogenases. Valence states (green), protons/hydrides/H_2 (blue), oxidation/inhibition (red), S (yellow), EPR s: EPR-silent, EPR a: EPR-active, ROS: reactive oxygen species.; from [Winkler et al., 2013].

2.5 Investigated Enzymes

2.5.1 Standard [NiFe] Hydrogenases

The periplasmic dimeric [NiFe] hydrogenases from the anaerobic bacteria *Desulfovibrio gigas* (Figure 2.11, top right) and *Desulfovibrio fructosovorans* are long known and well studied enzymes. The hydrogenase Hyd-2 from *Escherichia coli* also belongs to the "standard" oxygen-sensitive type. Therefore, these enzymes were studied as reference systems for comparison with the oxygen-tolerant enzymes.

2.5.2 Oxygen-Tolerant Hydrogenases from Ralstonia eutropha

The three hydrogenases (MBH, SH, RH) of *Ralstonia eutropha* H16 [Lenz and Friedrich, 1998] are of particular interest because they show particularly pronounced oxygen-tolerance and have been in the focus of extensive investigation during recent years (Figure 2.11). As a representative of the Knallgas bacteria [Cammack et al., 1997; Lenz et al., 2002] *Ralstonia eutropha* belongs to the group of chemolithoautotrophic β-proteobacteria and is found, for example, close to the surface, in ponds, where O_2 is present at almost atmospheric partial pressure. Therefore, *Ralstonia eutropha* can use H_2 as an energy source in the presence of O_2.

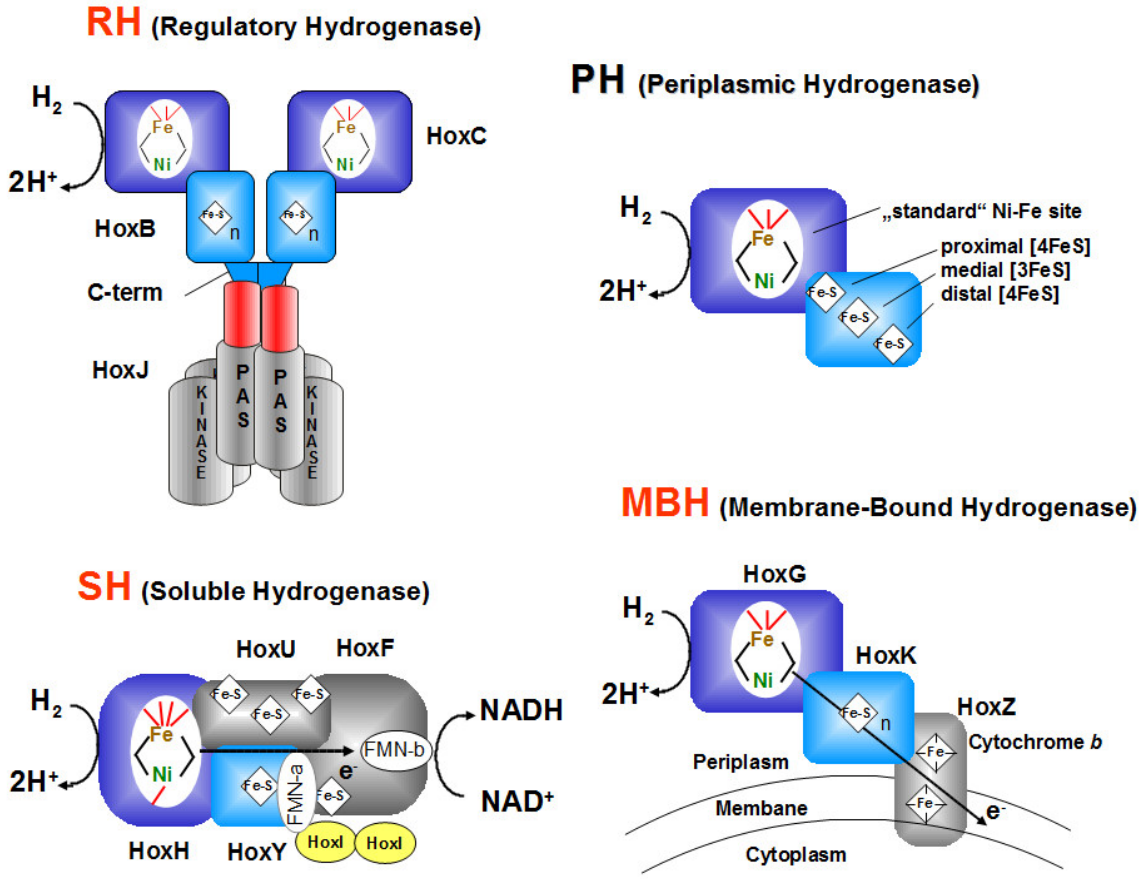

Figure 2.11: Organisation of the oxygen-tolerant [NiFe] hydrogenases MBH, SH, and RH from *Ralstonia eutropha* compared to the "standard" oxygen-sensitive periplasmic [NiFe] hydrogenase PH (from *Desulfovibrio species*); from [Burgdorf et al., 2005a,c].

The **membrane-bound hydrogenase (MBH)** is involved in energy conservation and attached to the cytoplasmic membrane via a b-type cytochrome (Figure 2.11,

bottom right). *In vivo* it mainly catalyzes the splitting of hydrogen into protons and electrons (H_2 uptake reaction) [Vignais and Colbeau, 2004], while hydrogen formation is catalyzed at low rates [Goldet et al., 2008]. The large subunit HoxG binds the [NiFe] active site and the small subunit HoxK binds three FeS clusters in a typical [NiFe] heterodimeric structure. The Cyt-b serves as an electron acceptor and transfers electrons from the FeS clusters to the respiratory chain [Lenz et al., 2010]. Recently it has become possible to express the enzyme as a heterotrimer including the third HoxZ subunit [Frielingsdorf et al., 2011]. In the cell, three trimers seem to form a complex. The structure of the active site appears to be very similar to that of standard hydrogenases, according to crystal structures. The oxygen-tolerance is probably related to the modified proximal FeS cluster as this is the most significant difference found so far between MBHs and PHs. We aimed at quantitative information on structural differences at the cofactors and their structural changes upon exposure to H_2 and O_2 using XAS experiments. Additionally, wild-type and mutant MBHs from *Ralstonia eutropha* and from other organisms were compared to "standard" type PHs.

The **soluble hydrogenase (SH)** is a bidirectional enzyme [Vignais et al., 2001] consisting of at least six subunits and located in the cytoplasm [Burgdorf et al., 2005c] (Figure 2.11, bottom left). A small HoxY and a larger HoxH subunit form the heterodimeric hydrogenase module. HoxY harbors only one FeS cluster and possibly a flavin mononucleotide molecule (FMN-a) [van der Linden et al., 2004]. The second heterodimeric module functions as a diaphorase (NADH dehydrogenase), which is attached to the hydrogenase. It contains a small subunit (HoxU) harboring one [4Fe4S] and one [2Fe2S] cluster, as well as a larger subunit (HoxF) harboring one [4Fe4S] cluster and FMN-b, which is likely involved in electron transfer to NAD^+. Further, two HoxI subunits are attached to HoxY and HoxF, providing a binding site for NADPH, which is involved in the activation of the enzyme [Burgdorf et al., 2005c]. A truncated SH construct was used to study the FeS cluster in HoxY by XAS and should reveal the composition of the FeS clusters and the ligation at the [NiFe] active site in HoxH.

The **regulatory hydrogenase (RH)** is a hydrogen sensor and controls the expression of the energy conserving hydrogenases (Figure 2.11, top left). It consists of several subunits: a dimeric heterodimeric hydrogenase $(HoxBC)_2$, a PAS domain, and a tetrameric (HoxJ) histidine protein kinase [Kleihues et al., 2000; Bernhard et al., 2001; Lenz et al., 2002; Buhrke et al., 2004]. Each large subunit (HoxC) binds a [NiFe] active site with standard-type ligands [Bernhard et al., 2001]. The small subunit (HoxB) contains FeS clusters of unclear nature. The RH does not show the inactive Ni-A and Ni-B states and is therefore always ready to bind hydrogen, in agreement with its sensor function. Previous studies investigated the [NiFe] active site but could not unambiguously determine the structure of the oxidized and reduced states [Haumann et al., 2003; Buhrke et al., 2005a; Löscher et al., 2005]. Further, the number and nature of the FeS clusters in the small subunit remained unclear [Buhrke et al., 2005b].

Therefore, several RH constructs with different subunit composition were investigated by XAS to study differences in the metal center structures.

2.5.3 Further Non-Standard [NiFe] Hydrogenases

The MBH (H_2ase I) from the hyperthermophilic bacterium *Aquifex aeolicus* (*Aa*), the MBH (Hyd-1) from *Escherichia coli* (*Ec*) (Figure 2.12), and the MBH from the bacterium *Hydrogenophaga spec.* AH24, which are oxygen-tolerant, were compared using Ni- and Fe-XAS.

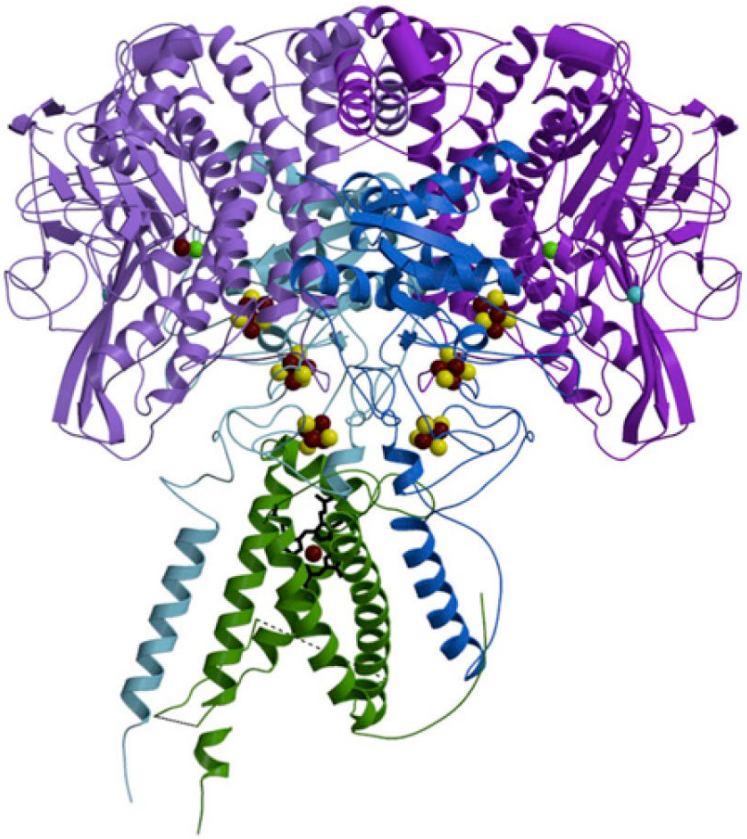

Figure 2.12: Structure of the O_2-tolerant membrane-bound [NiFe] hydrogenase (Hyd-1) from *Escherichia coli*. Fe (brown), Ni (green), S (yellow), and Mg^{2+} (blue); from [Volbeda et al., 2013].

2.5.4 [FeFe] Hydrogenase from Chlamydomonas reinhardtii

The [FeFe] hydrogenase from the green alga *Chlamydomonas reinhardtii* *Cr*HydA1 is the smallest known [FeFe] hydrogenase in nature. It consists of one subunit (47.5 kDa), which binds only the H-cluster, additional FeS clusters as in bacterial enzymes are absent [Happe and Naber, 1993; Happe and Kaminski, 2002; Winkler et al., 2013]. *Cr*HydA1 is located in the chloroplasts of the algae and linked by a ferredoxin to the photosynthetic electron transport chain. XAS experiments were used to study the $2Fe_H$ and [4Fe4S] units of the H-cluster. Due to the unique structure of the H-cluster, extended-range XAS experiments to particularly high energy values facilitated resolution of different Fe−Fe distances in the cubane and the diiron site.

2.5.5 Synthetic Nickel Model Compounds

Seven nickel model compounds with different structural features were investigated by XAS and XES (Section 4.5). The respective compounds had ligands similar in nature (e.g., O, N, S, P), number, and ratio to those found in hydrogenases. With known nickel coordination and oxidation state, these well characterized compounds are suitable as reference systems for comparison with hydrogenases.

2.6 Objectives

Over the last decades, a broad range of experimental methods has been applied to hydrogenase enzymes to gain knowledge on their structure and function. The molecular structure of the proteins and the metal cofactors as well as the catalytic cycle have been studied in detail. However, important questions related to the mechanism of hydrogen catalysis, the reactions of oxygen-inhibition or -tolerance of the enzymes, and structural and redox changes at the active site during hydrogen turnover and electron transfer have remained unclear.

In this work, various hydrogenases were studied using X-ray absorption spectroscopy (XAS) as a method complementary to crystallography, EPR, FTIR, and further spectroscopic techniques within a collaborative research network. Available crystal structures show the overall three-dimensional composition of the enzymes, but at limited resolution ($\geq$ 1 Å). XAS reveals fine-structural information on the metal cofactors at subangstrom resolution. In addition, information on the electronic structure, for example the oxidation states, is provided. A particular strength of the XAS method is that all accessible intermediate states and corresponding structural changes can be characterized.

One main topic was the search for structural features that may be related to the oxygen-tolerance or the extraordinary high activity of certain hydrogenases. In continuation of previous research efforts mainly on the [NiFe] hydrogenases from *Ralstonia eutropha*, a second goal was the application of XAS experiments to a broader set of enzymes of the [NiFe] type, to the [FeFe] hydrogenase *Cr*HydA1, as well as to biomimetic synthetic compounds. To facilitate structural investigations of various types of enzymes by XAS, a broad collaborative approach was pursued. The [NiFe] hydrogenases from *Ralstonia eutropha* were further investigated by XAS in search for structural features concerning their oxygen-tolerance, completing previous work. Another objective was the implementation of advanced spectroscopic methods (e.g., resonant inelastic X-ray scattering (RIXS) and X-ray emission spectroscopy (XES)) to demonstrate their technical feasibility and pave the way for future experiments on enzymes. Therefore, the further improvement of the XAS methodology, of the corresponding experimental setup, the experimental procedures and the data evaluation process were also important topics of this work.

To achieve these goals, various types of [NiFe] hydrogenases, as well as an [FeFe] hydrogenase and synthetic nickel model compounds, as provided by our collaboration partners, were compared by XAS experiments:

1) Membrane-bound [NiFe] hydrogenases (MBH) show surprisingly high oxygen-tolerance. MBHs from *Ralstonia eutropha*, *Escherichia coli*, *Aquifex aeolicus*, and *Hydrogenophaga spec.* AH24 were compared. The oxygen-tolerance distinguishes the MBHs from the so-called standard hydrogenases from, e.g., *Desulfovibrio gigas*.

2) Periplasmic [NiFe] hydrogenases (PHs) from *Desulfovibrio gigas*, *Desulfovibrio fructosovorans*, and *Escherichia coli* are reversibly inhibited by oxygen. Their features were compared to those of the MBHs.

3) The regulatory and the soluble [NiFe] hydrogenase from *Ralstonia eutropha* (RH and SH) act as a hydrogen sensor or as a reversible catalyst for hydrogen cleavage. The RH is located in the cytoplasm. Several constructs of this enzyme were studied, for example dimeric or tetrameric protein complexes. The SH is located in the cytoplasm. A truncated SH construct containing only the hydrogenase unit and the HoxY subunit was studied.

4) The [FeFe] hydrogenase from *Chlamydomonas reinhardtii* (*Cr*HydA1) shows a very high hydrogen turnover rate. It contains only the six-iron active site, denoted as H-cluster, and no accessory FeS clusters as bacterial enzymes. Therefore, *Cr*HydA1 is particularly well suited to study the reactions at the H-cluster by XAS.

5) Synthetic nickel model compounds were measured to evaluate the feasibility and viability of advanced X-ray spectroscopic methods (RIXS, XES) for enzyme studies.

Chapter 3

X-ray Absorption Spectroscopy

3.1 Introduction

X-ray absorption spectroscopy (XAS) relies on the absorption of X-rays by the element (metal) under investigation. This provides absolute element specificity in XAS on biological samples. Incoming photons excite electrons and the process due to absorption intensity loss can be described by the Lambert-Beer-Law

$$I = I_0 \cdot e^{-\mu x}, \tag{3.1}$$

where I is the measured intensity, I_0 is the incident intensity, μ is the absorption coefficient and x is the path length. In the energy range of "hard" X-rays (keV) core-electrons (1s, 2p) are excited into higher unoccupied levels (resonant excitation) or non-resonantly into the continuum (photoelectron generation).

XAS provides complementary information to other methods like crystallography or electron paramagnetic resonance spectroscopy (EPR). Often, proteins cannot be crystallized at all or only in a certain state. Here, XAS allows to study samples in all aggregate states, e.g., liquid, powder, and solution samples as well as crystals. Thus, changes at metal centers during the catalytic cycle and, most importantly, the changes between, for example, different redox states can be studied. In addition, all spin states or isotopes of an element are detectable. However, besides of large quantities of biological samples, highly intense and stable X-ray radiation sources are required to study biological materials. Therefore, Bio-XAS experiments are often carried out at third-generation synchrotrons, which provide a small X-ray spot size, high beam stability, X-ray flux at the sample position of up to 10^{13} s^{-1}, and a linear polarized X-ray beam.

3.2 Theory of X-ray Absorption Spectroscopy

XAS measurements rely on tuning of the energy of the incident X-ray beam by a double-crystal monochromator and recording of the absorption or fluorescence signal of the sample. In general, the absorption intensity continuously decreases with increasing energy as the absorption cross-section is inversely proportional to the X-ray energy ($\mu(E) \propto E^{-3}$, [Haken and Wolf, 1996]). At certain energies, however, a discontinuity occurs due to the onset of the specific absorption of a given element. Whenever the energy of the X-ray photon matches the energy difference between two electronic orbitals, an electron can be excited to the higher energy level while absorbing the incoming photon (Figure 3.1A). This yields an increase of the absorption probability described by the absorption coefficient, leading to an absorption edge in the spectrum. At higher photon energies excitations to higher levels or to the continuum occur. Quantum mechanically the probability for transitions between energy levels can be calculated with Fermi's Golden Rule:

$$\mu(E) \propto| \langle i \mid \widehat{H} \mid f \rangle |^2, \tag{3.2}$$

where $\langle i \mid$ is the initial state with a photon and a core-electron, $\mid f \rangle$ is the final state with a photo-electron and a core-hole and $\widehat{H}$ is the Hamilton interaction operator. Depending on the initial main quantum number of the electron, the absorption edges are denoted K, L, M (for n = 1, 2, 3). After a certain lifetime this core-hole will be filled with an electron of a higher shell accompanied by emission of a photon (X-ray fluorescence, Figure 3.1B).

X-ray absorption spectra can be divided into two main regions providing different information (Figure 3.2). The X-ray absorption near edge structure (XANES) region ranges from about 10 eV before up to about 50 eV after the main edge. This region can also show a so-called pre-edge peak feature, which usually appears shortly prior to the main edge. The edge shape can be complex, depending on the sample characteristics. The edge energy can be determined either by the edge half-height method, the inflection point method (using the first derivative), or the integral method [Dittmer et al., 1998]. At about 50 eV above the edge, the extended X-ray absorption fine structure (EXAFS) region starts. EXAFS data should extend at least up to 500 eV above the edge, with a longer energy range corresponding to improved interatomic distance resolution. The XANES and EXAFS regions provide complementary information and are usually analyzed separately, as outlined below. For a more detailed description of XAS see for example [Teo and Joy, 1981; Teo, 1986; Koningsberger and Prins, 1988; Rehr and Albers, 2000; Newville, 2004].

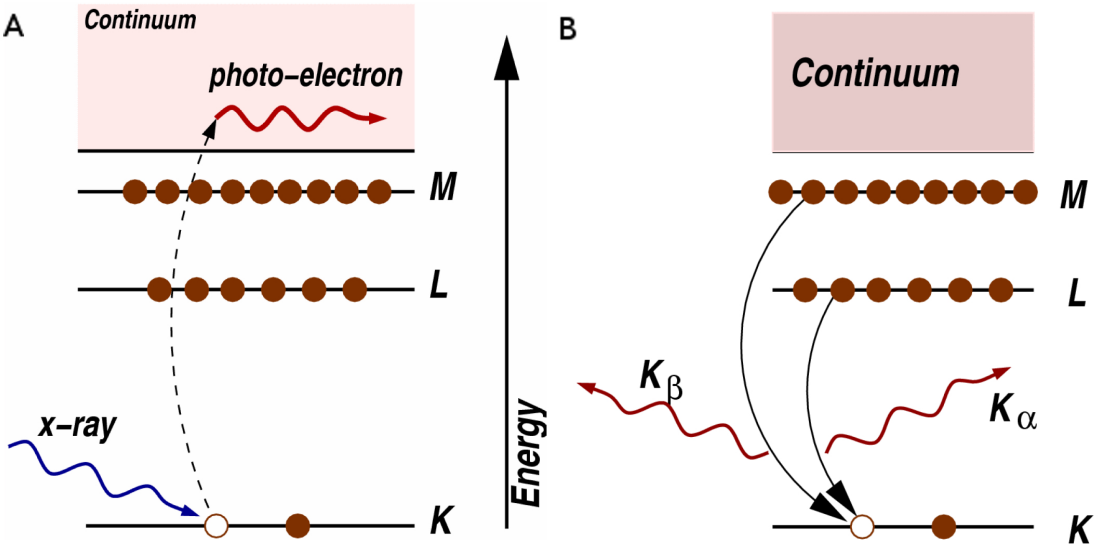

Figure 3.1: Scheme describing (A) the photo-electric effect, i.e., the excitation of core-electrons into the continuum, and (B) the resulting X-ray fluorescence emission. An incoming photon excites a core-electron into higher unoccupied states or the continuum creating a core-hole. This hole is filled after a certain lifetime with an electron of a higher shell, the energy difference corresponds to the energy of the emitted photon (X-ray fluorescence); from [Newville, 2004].

3.3 The XANES and Pre-Edge Region

The XANES including the pre-edge region carries information on the metal site geometry and electronic structure. Excitation of a 1s electron into molecular orbitals with metal 3d character gives rise to pre-edge peak features. 1s→3d transitions are formally dipole-forbidden but gain intensity due to admixture of allowed quadrupole transitions (of usually low intensity) and p/d hybridization. The p/d hybridization results from the crystal field splitting due to the metal ligands, i.e., from deviations from ideal octahedral symmetry at the absorber. The amplitude of the pre-edge features thus is related to the shape, nature, number, and geometric arrangement of the ligands around the absorbing metal ion. Large pre-edge peak features are usually observed for highly distorted geometries. In a tetrahedral environment for example, the pre-edge peak can be as high as the main edge while in octahedral systems almost no pre-edge peak is visible. Furthermore, the pre-edge peak often shows several absorption features due to electronic transitions into 3d orbitals at different energies. The intensities and energies can provide information on d-level energy splitting and the spin state.

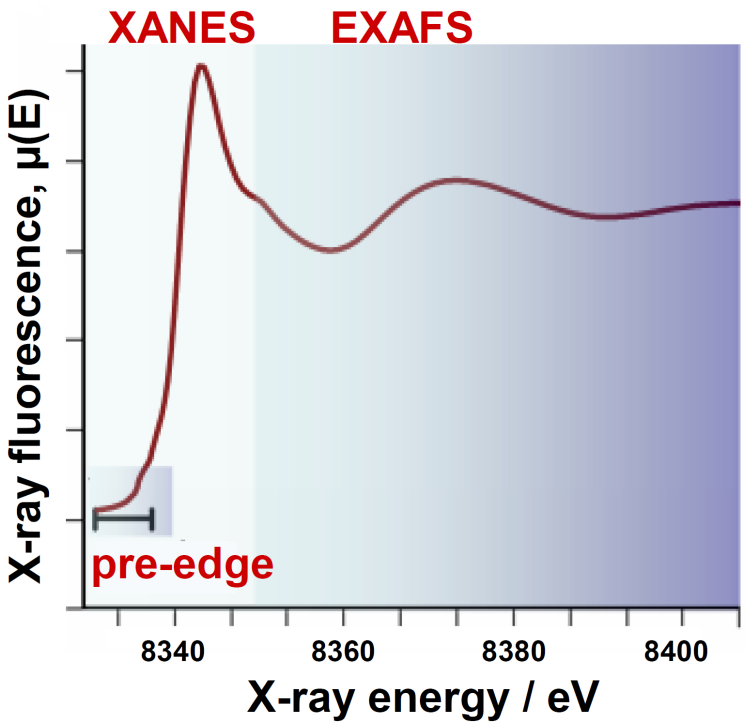

Figure 3.2: Example of an XAS spectrum of a nickel compound with the three main regions indicated (pre-edge, XANES, EXAFS); from [Löscher, 2007].

Excitation to higher-level orbitals, e.g., 4p final states, gives rise to the main edge absorption. The main edge energy provides information on the oxidation state of the absorbing metal ion, i.e., higher edge energies correspond to higher oxidation states. The amplitude of the edge maximum is related to the chemical identity and the number of metal ligands. Empirically, measured XANES spectra of samples, for which the structure of the metal site is not known, are often compared to data from known structures such as metal coordination compounds. Calculations of edge spectra using scattering theory and model structures are feasible for example with the FEFF program [Mustre de Leon et al., 1991; Zabinsky et al., 1995; Rehr and Albers, 2000; Ankudinov and Rehr, 2003; Rehr et al., 2010].

3.4 The EXAFS Region

The EXAFS region provides the inter-atomic distances around the absorber at ∼0.02 Å accuracy. The recorded signal is the absorption coefficient $\mu(E) = log(I_0/I)$. In the theoretical analysis of the data the photo-electron is taken into account as a wave,

therefore absorption spectra are plotted over the electron wavevector k [Teo, 1986; Newville, 2004]. To extract the EXAFS oscillations, a function $\chi(k)$ is then defined as

$$\chi(k) = \frac{\mu(k) - \mu_0(k)}{\Delta\mu_0(k)} \text{ with } k = \sqrt{\frac{2m(E - E_0)}{\hbar^2}} \; [m^{-1}], \tag{3.3}$$

where $\mu_0(k)$ is a smooth background function representing the absorption signal of an absorber atom without surrounding neighbors. $\Delta\mu_0(k)$ is the absorption jump at the edge energy E_0, which is usually defined as an energy close to the bottom of the K-edge, i.e., as an apparent Fermi energy.

In many cases, the metal atom has different types of neighboring atoms at varying distances. Each leads to an oscillation with a certain frequency contributing to the measured EXAFS signal (Figure 3.3). In terms of quantum mechanics the absorption of an X-ray photon leads to a transition between two quantum states usually being calculated with Fermi's Golden Rule (3.2). The initial state remains unaltered independently of the presence or absence of neighbors. In contrast, the photo-electron alters the energy level of the final state. Therefore, the final state $\mid f\rangle$ can be split into two contributions: one from the single isolated atom $\mid f_0\rangle$ and a perturbation resulting from the neighbors $\mid \Delta f\rangle$:

$$\mid f\rangle = \mid f_0\rangle + \mid \Delta f\rangle, \tag{3.4}$$

which leads to the following equation:

$$\mu(E) \propto \mid \langle i \mid \widehat{H} \mid f_0\rangle \mid^2 [1 + \langle i \mid \widehat{H} \mid \Delta f\rangle \frac{\langle f_0 \mid \widehat{H} \mid i\rangle^*}{\mid \langle i \mid \widehat{H} \mid f_0\rangle \mid^2} + c.c.], \tag{3.5}$$

where c.c. is the complex conjugate and $\widehat{H}$ is the Hamiltonian interaction term [Teo, 1986; Newville, 2004]. Comparing this equation to the relation between the absorption coefficient $\mu(E)$ and $\chi(E)$ gives:

$$\mu(E) = \mu_0(E)[1 + \chi(E)]. \tag{3.6}$$

Thus,

$$\mu_0 = \mid \langle i \mid \widehat{H} \mid f_0\rangle \mid^2 \tag{3.7}$$

is the contribution from the isolated atom to the absorption, while

$$\chi(E) \propto \langle i \mid \widehat{H} \mid \Delta f\rangle \tag{3.8}$$

takes the effects of the neighbors into account. The Hamiltonian is proportional to e^{ikr} [Teo, 1986; Stohr, 1992], for the core level initial state $\langle i \mid$ a delta function is an adequate approximation, while the variation $\mid \Delta f\rangle$ of the final state is described by the wave function of the back-scattered photo-electron wave $\psi_{\text{scatt}}(r)$, summing up to

the following relation:

$$\chi(E) \propto \int dr\delta(r)e^{ikr}\psi_{\text{scatt}}(r) = \psi_{\text{scatt}}(0), \tag{3.9}$$

where $\psi_{\text{scatt}}(0)$ is the amplitude of the scattered photo-electron at the position of the absorber atom (r = 0).

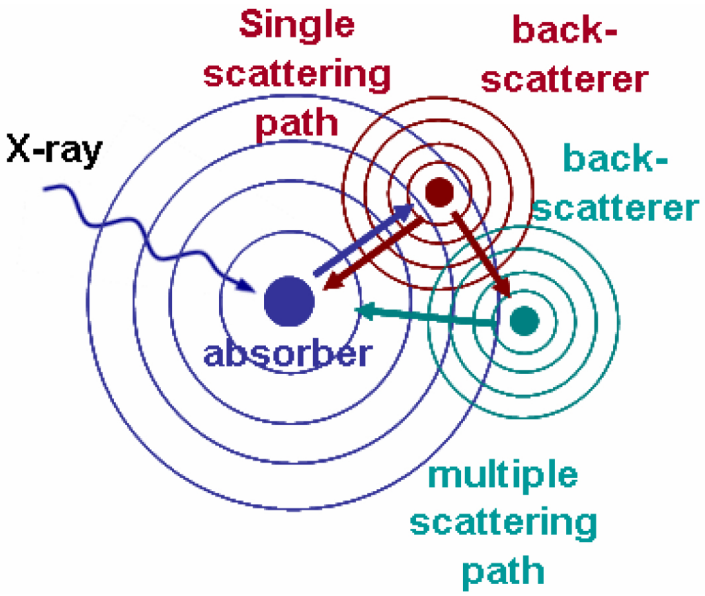

Figure 3.3: Scheme of single and multiple X-ray backscattering paths for two ligand atoms around the absorber; from [Löscher, 2007].

The fine structure in the EXAFS originates in the amplitude modulation of the back-scattered photo-electron wave-function at the metal atom, leading to a modification of the absorption coefficient $\mu(E)$ through the influence of the final state. The wave-function is usually described as a spherical wave $\psi(k,r) = \frac{e^{ikr}}{kr}$, which spreads out towards the neighboring atom and travels back to the central atom after being elastically scattered:

$$\chi(k) \propto \psi_{\text{scatt}}(k, r = 0) = \frac{e^{ikR}}{kR}[2kf(k)e^{i\delta(k)}]\frac{e^{ikR}}{kR} + c.c., \tag{3.10}$$

where $f(k)$ and $\delta(k)$ are related to the scattering atoms and correlated to the atomic number Z.

After expanding all terms and including the complex conjugate, the oscillations can be described as:

$$\chi(k) = \frac{f(k)}{kR^2}sin[2kR + \delta(k)]. \tag{3.11}$$

Taking into account the effects of thermal and static disorder and different types of neighboring atoms, the formula is further extended to give:

$$\chi(k) = \sum_j \frac{N_j e^{-2k^2\sigma_j^2} f_j(k)}{kR_j^2} sin[2kR_j + \delta_j(k)]. \tag{3.12}$$

Each atom type is represented by its own term (also referred to as coordination shell) in the sum, if bond length spread exceeds a certain boundary (about ±0.1 Å). Every coordination shell contributes with its own frequency so that a Fourier transformation is helpful during data analysis to visualize the individual absorber-backscatterer distances. Metal ligands with adjacent atom number Z (C, O, N), which are present at similar distances, are difficult to distinguish by EXAFS analysis, whereas metal-metal distances often are well determined.

Further effects should be taken into account leading to an improved theoretical description. Firstly, after a distinct time the core hole is filled with a higher-orbital electron. After this relaxation process, coherent interference between the outgoing and back-scattered photo-electron wave at the absorber atom is no longer possible, making the EXAFS oscillations time and distance sensitive. Secondly, the photo-electron can undergo extrinsic inelastic interactions, e.g., scattering at other electrons, excitation of phonons, plasmons, or electron-hole pairs, which destroy the coherence due to energy loss. This leads to a reduction of the EXAFS amplitude at higher energies. The fine-structure formula takes this into account by inclusion of an empirical damping factor $e^{-2r/\lambda(k)}$. Here, $\lambda(k)$ is the energy dependent mean free path of the electron. Inelastic losses can also be intrinsic as other electrons in the absorber atom are excited through the generation of a core-hole (e.g., shake-up and shake-off effects) [Rehr and Albers, 2000]. These complicated many-body effects usually are rather accurately accounted for by introducing a phenomenological amplitude-reduction factor (S_0^2), which leads to the well-known EXAFS formula:

$$\chi(k) = \sum_j \frac{N_j S_0^2 e^{-2k^2\sigma_j^2} e^{-2R_j/\lambda(k)} f_j(k)}{kR_j^2} sin[2kR_j + \delta_j(k)]. \tag{3.13}$$

In order to extract the information from experimental EXAFS data using Equation 3.13, values for the scattering amplitude f(k) and the phase shifts $\delta(k)$ have to be calculated. Available ab-initio programs like FEFF [Mustre de Leon et al., 1991; Zabinsky et al., 1995; Rehr and Albers, 2000; Ankudinov and Rehr, 2003; Rehr et al., 2010] facilitate quantitative analysis of EXAFS data. The primary outcomes of EXAFS analysis are the coordination numbers (N), i.e., the numbers of ligands at the metal, inter-atomic distances (R), i.e., the metal-ligand or metal-metal distances, and the apparent radial distance spread (Debye-Waller factor σ).

3.5 Synchrotron Experiments

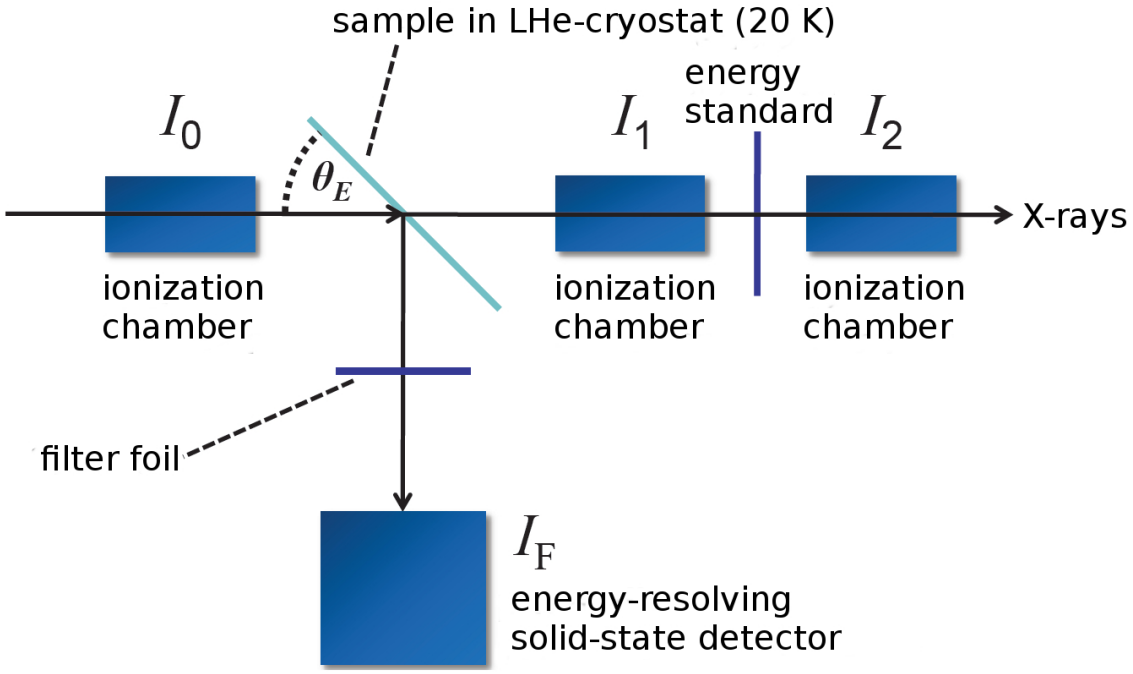

Figure 3.4: Experimental setup for XAS at synchrotron beamlines; from [Grundmeier, 2011] (adapted).

X-ray absorption spectroscopy measurements on biological samples usually are carried out at a synchrotron radiation facility. Very high beam intensities, high stability, a small spot size, a small divergence, as well as linear polarization and pulsed beams allow for different types of experiments on biological samples. We have carried out XAS experiments at BESSY II (Berlin), EMBL Outstation at HASYLAB (DESY/Hamburg), ESRF (Grenoble/France), SOLEIL (Paris/France), ANKA (Karlsruhe), and SRS (Daresbury/UK). Metalloenzymes often contain one or more transition metal species, which can be investigated separately by K-edge spectroscopy utilizing its intrinsic element specificity.

A typical setup for XAS consists of a double-crystal monochromator, a first ionization chamber (I_0) that measures the incident beam intensity in front of the sample, a second (I_1) and third (I_2) chamber measuring the signal after the interaction with the sample and the signal of an energy standard, which often is a metal foil, used for energy calibration (Figure 3.4). A liquid helium cryostat contains the sample in a controlled environment, usually at 10 – 20 K and in a helium atmosphere used for heat exchange.

A multi-element energy-resolving solid-state detector often is used for collecting the X-ray fluorescence.

Dilute protein samples have to be studied using the fluorescence detection mode. For low metal concentrations the absorption signal in transmission mode is too small for obtaining an EXAFS spectrum with suitable signal-to-noise-ratio. The energy-resolving detector is positioned at 90° to the incident beam to monitor the X-ray fluorescence. At this angle the intensity ratio of the X-ray fluorescence and the scattered incident radiation is maximal.

3.6 Data Evaluation

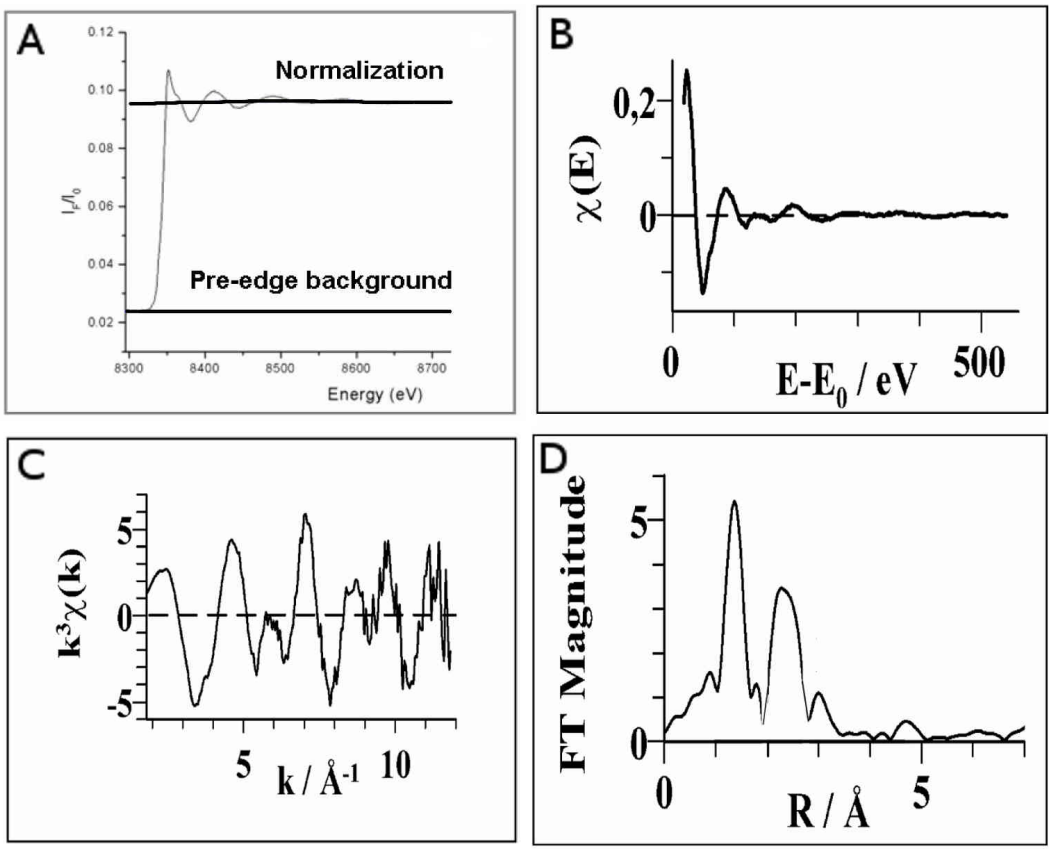

Figure 3.5: EXAFS data evaluation. For further details see text; from [Löscher, 2007]

XAS spectra are processed as outlined below:

The data from each output channel of the detector are individually inspected, selected, and averaged to yield one spectrum per monochromator scan after dead-time correction and energy calibration. All spectra of one sample are averaged to provide one spectrum I_F, which is divided by the incident signal I_0 (Figure 3.5A). The pre-edge background is removed (i.e., by subtracting a straight line) and the signal is normalized to yield the absorbing per metal ion. The EXAFS spectrum ($\chi(E)$) is derived from the correlation $\mu(E) = \mu_o(E)[1 + \chi(E)]$ by dividing the measured absorption ($\mu(E)$) by a post-edge background spline ($\mu_0(E)$):

$$\chi(E) = \frac{\mu(E)}{\mu_0(E)} - 1, \tag{3.14}$$

which yields the raw EXAFS oscillations ($\chi(E)$) (Figure 3.5B). Compensation for the decay of the EXAFS oscillations for increasing energy is achieved by weighting the spectrum by k^3 (Figure 3.5C). After transforming the energy axis into a k axis a Fourier-transformation (FT) converts the data into R-space showing directly the spectral contributions of the different metal-ligand distances (on a reduced distance scale) (Figure 3.5D).

3.7 Materials and Methods

The results in this work were obtained on hydrogenase and model compound samples, which were prepared by our collaboration partners. The [NiFe] hydrogenases (MBH, SH, PH) from *Ralstonia eutropha* were provided by the group of Prof. B. Friedrich and Dr. O. Lenz (Microbiology Department at the Humboldt University Berlin). Samples of other membrane-bound [NiFe] hydrogenases were provided by the group of Dr. M.-T. Giudici-Orticoni (CNRS Marseille) (H_2ase I of *Aquifex aeolicus*), by the group of Prof. F. Armstrong (University of Oxford, Inorganic Chemistry) (H_2ase I and H_2ase II from *Escherichia coli*), and by the group of Prof. H. Nishihara (Ibaraki University, Bioresource Science) (MBH from *Hydrogenophaga spec.* AH24). Periplasmic standard hydrogenases from *Desulfovibrio fructosovorans* and *Desulfovibrio gigas* were provided by the groups of Prof. M. Rousset and S. Dementin (CNRS Marseille) and by the group of Prof. A. De Lacey (University of Madrid). Samples of the [FeFe] hydrogenase from *Chlamydomonas reinhardtii Cr*HydA1 were prepared in the laboratory of Prof. T. Happe (Ruhr University Bochum). Nickel model compounds were obtained from the group of Prof. M. Driess (Technical University Berlin) and from the group of Prof. C. Limberg (Humboldt University Berlin).

XAS experiments were performed at beamline D2 of the European Molecular Biology Laboratory (EMBL) outstation (HAmburger SYnchrotronstrahlungsLABor, HASYLAB, Deutsches Elektronen Synchrotron, DESY, Hamburg, Germany), beamline

KMC-1 of the Berliner Elektronenspeicherring für Synchrotronstrahlung (BESSY II, Helmholtz-Zentrum Berlin, Germany) [Schaefers et al., 2007], beamline 16.5 of the Synchrotron Radiation Source (SRS, Daresbury, UK), beamline ID26 of the European Synchrotron Radiation Facility (ESRF, Grenoble, France), and at the XAS beamline of the Angströmquelle Karlsruhe (ANKA, Karlsruhe Institute of Technology, Karlsruhe, Germany).

EXAFS simulations were carried out with the in-house program SimX [Dau et al., 2003] and with EXCURV [Tomic et al., 2005] using least-square curve fitting algorithms and unfiltered k^3-weighted spectra and the curved-wave multiple-scattering approach. Phase functions were calculated with FEFF7 [Zabinsky et al., 1995] or FEFF8 [Rehr et al., 2010] using model structures derived with Hyperchem [Froimowitz, 1993; Hypercube, 2007]. The full-multiple-scattering (FMS) and the self-consistent-field (SCF) approach was used within the program FEFF8.2 [Zabinsky et al., 1995] for calculations of the XANES region [Burgdorf et al., 2005b; Löscher et al., 2007]. The pre-edge region was extracted from the main edge by applying a polynomial spline using the program XANDA [Klementiev, 2005]. Further details of XAS data analysis are provided in the Materials and Methods sections of the following Chapters.

Chapter 4

Experimental Results

4.1 Structural Differences of Oxidized [FeS] and [NiFe] Cofactors in O_2-Tolerant and O_2-Sensitive Hydrogenases Studied by X-ray Absorption Spectroscopy

Previously published in: K.G.V. Sigfridsson, N. Leidel, O. Sanganas, P. Chernev, O. Lenz, K.-S. Yoon, H. Nishihara, A. Parkin, F.A. Armstrong, S. Dementin, M. Rousset, A.L. De Lacey and M. Haumann (2015). Structural differences of oxidized iron-sulfur and nickel-iron cofactors in O_2-tolerant and O_2-sensitive hydrogenases studied by X-ray absorption spectroscopy, *Biochimica et Biophysica Acta (BBA) - Bioenergetics*, 1847:162-170, Epub ahead of print.

https://dx.doi.org/10.1016/j.bbabio.2014.06.011

Content removed due to copyright restrictions.

Previously published in: K.G.V. Sigfridsson, N. Leidel, O. Sanganas, P. Chernev, O. Lenz, K.-S. Yoon, H. Nishihara, A. Parkin, F.A. Armstrong, S. Dementin, M. Rousset, A.L. De Lacey and M. Haumann (2015). Structural differences of oxidized iron-sulfur and nickel-iron cofactors in O_2-tolerant and O_2-sensitive hydrogenases studied by X-ray absorption spectroscopy, *Biochimica et Biophysica Acta (BBA) - Bioenergetics*, 1847:162-170, Epub ahead of print.

https://dx.doi.org/10.1016/j.bbabio.2014.06.011

Content removed due to copyright restrictions.

Previously published in: K.G.V. Sigfridsson, N. Leidel, O. Sanganas, P. Chernev, O. Lenz, K.-S. Yoon, H. Nishihara, A. Parkin, F.A. Armstrong, S. Dementin, M. Rousset, A.L. De Lacey and M. Haumann (2015). Structural differences of oxidized iron-sulfur and nickel-iron cofactors in O_2-tolerant and O_2-sensitive hydrogenases studied by X-ray absorption spectroscopy, *Biochimica et Biophysica Acta (BBA) - Bioenergetics*, 1847:162-170, Epub ahead of print.

https://dx.doi.org/10.1016/j.bbabio.2014.06.011

Content removed due to copyright restrictions.

Previously published in: K.G.V. Sigfridsson, N. Leidel, O. Sanganas, P. Chernev, O. Lenz, K.-S. Yoon, H. Nishihara, A. Parkin, F.A. Armstrong, S. Dementin, M. Rousset, A.L. De Lacey and M. Haumann (2015). Structural differences of oxidized iron-sulfur and nickel-iron cofactors in O_2-tolerant and O_2-sensitive hydrogenases studied by X-ray absorption spectroscopy, *Biochimica et Biophysica Acta (BBA) - Bioenergetics*, 1847:162-170, Epub ahead of print.

https://dx.doi.org/10.1016/j.bbabio.2014.06.011

Content removed due to copyright restrictions.

Previously published in: K.G.V. Sigfridsson, N. Leidel, O. Sanganas, P. Chernev, O. Lenz, K.-S. Yoon, H. Nishihara, A. Parkin, F.A. Armstrong, S. Dementin, M. Rousset, A.L. De Lacey and M. Haumann (2015). Structural differences of oxidized iron-sulfur and nickel-iron cofactors in O_2-tolerant and O_2-sensitive hydrogenases studied by X-ray absorption spectroscopy, *Biochimica et Biophysica Acta (BBA) - Bioenergetics*, 1847:162-170, Epub ahead of print.

https://dx.doi.org/10.1016/j.bbabio.2014.06.011

Content removed due to copyright restrictions.

Previously published in: K.G.V. Sigfridsson, N. Leidel, O. Sanganas, P. Chernev, O. Lenz, K.-S. Yoon, H. Nishihara, A. Parkin, F.A. Armstrong, S. Dementin, M. Rousset, A.L. De Lacey and M. Haumann (2015). Structural differences of oxidized iron-sulfur and nickel-iron cofactors in O_2-tolerant and O_2-sensitive hydrogenases studied by X-ray absorption spectroscopy, *Biochimica et Biophysica Acta (BBA) - Bioenergetics*, 1847:162-170, Epub ahead of print.

https://dx.doi.org/10.1016/j.bbabio.2014.06.011

Content removed due to copyright restrictions.

Previously published in: K.G.V. Sigfridsson, N. Leidel, O. Sanganas, P. Chernev, O. Lenz, K.-S. Yoon, H. Nishihara, A. Parkin, F.A. Armstrong, S. Dementin, M. Rousset, A.L. De Lacey and M. Haumann (2015). Structural differences of oxidized iron-sulfur and nickel-iron cofactors in O_2-tolerant and O_2-sensitive hydrogenases studied by X-ray absorption spectroscopy, *Biochimica et Biophysica Acta (BBA) - Bioenergetics*, 1847:162-170, Epub ahead of print.

https://dx.doi.org/10.1016/j.bbabio.2014.06.011

Content removed due to copyright restrictions.

Previously published in: K.G.V. Sigfridsson, N. Leidel, O. Sanganas, P. Chernev, O. Lenz, K.-S. Yoon, H. Nishihara, A. Parkin, F.A. Armstrong, S. Dementin, M. Rousset, A.L. De Lacey and M. Haumann (2015). Structural differences of oxidized iron-sulfur and nickel-iron cofactors in O_2-tolerant and O_2-sensitive hydrogenases studied by X-ray absorption spectroscopy, *Biochimica et Biophysica Acta (BBA) - Bioenergetics*, 1847:162-170, Epub ahead of print.

https://dx.doi.org/10.1016/j.bbabio.2014.06.011

Content removed due to copyright restrictions.

Previously published in: K.G.V. Sigfridsson, N. Leidel, O. Sanganas, P. Chernev, O. Lenz, K.-S. Yoon, H. Nishihara, A. Parkin, F.A. Armstrong, S. Dementin, M. Rousset, A.L. De Lacey and M. Haumann (2015). Structural differences of oxidized iron-sulfur and nickel-iron cofactors in O_2-tolerant and O_2-sensitive hydrogenases studied by X-ray absorption spectroscopy, *Biochimica et Biophysica Acta (BBA) - Bioenergetics*, 1847:162-170, Epub ahead of print.

https://dx.doi.org/10.1016/j.bbabio.2014.06.011

Content removed due to copyright restrictions.

Previously published in: K.G.V. Sigfridsson, N. Leidel, O. Sanganas, P. Chernev, O. Lenz, K.-S. Yoon, H. Nishihara, A. Parkin, F.A. Armstrong, S. Dementin, M. Rousset, A.L. De Lacey and M. Haumann (2015). Structural differences of oxidized iron-sulfur and nickel-iron cofactors in O_2-tolerant and O_2-sensitive hydrogenases studied by X-ray absorption spectroscopy, *Biochimica et Biophysica Acta (BBA) - Bioenergetics*, 1847:162-170, Epub ahead of print.

https://dx.doi.org/10.1016/j.bbabio.2014.06.011

Content removed due to copyright restrictions.

Previously published in: K.G.V. Sigfridsson, N. Leidel, O. Sanganas, P. Chernev, O. Lenz, K.-S. Yoon, H. Nishihara, A. Parkin, F.A. Armstrong, S. Dementin, M. Rousset, A.L. De Lacey and M. Haumann (2015). Structural differences of oxidized iron-sulfur and nickel-iron cofactors in O_2-tolerant and O_2-sensitive hydrogenases studied by X-ray absorption spectroscopy, *Biochimica et Biophysica Acta (BBA) - Bioenergetics*, 1847:162-170, Epub ahead of print.

https://dx.doi.org/10.1016/j.bbabio.2014.06.011

Content removed due to copyright restrictions.

Previously published in: K.G.V. Sigfridsson, N. Leidel, O. Sanganas, P. Chernev, O. Lenz, K.-S. Yoon, H. Nishihara, A. Parkin, F.A. Armstrong, S. Dementin, M. Rousset, A.L. De Lacey and M. Haumann (2015). Structural differences of oxidized iron-sulfur and nickel-iron cofactors in O_2-tolerant and O_2-sensitive hydrogenases studied by X-ray absorption spectroscopy, *Biochimica et Biophysica Acta (BBA) - Bioenergetics*, 1847:162-170, Epub ahead of print.

https://dx.doi.org/10.1016/j.bbabio.2014.06.011

Content removed due to copyright restrictions.

Previously published in: K.G.V. Sigfridsson, N. Leidel, O. Sanganas, P. Chernev, O. Lenz, K.-S. Yoon, H. Nishihara, A. Parkin, F.A. Armstrong, S. Dementin, M. Rousset, A.L. De Lacey and M. Haumann (2015). Structural differences of oxidized iron-sulfur and nickel-iron cofactors in O_2-tolerant and O_2-sensitive hydrogenases studied by X-ray absorption spectroscopy, *Biochimica et Biophysica Acta (BBA) - Bioenergetics*, 1847:162-170, Epub ahead of print.

https://dx.doi.org/10.1016/j.bbabio.2014.06.011

Content removed due to copyright restrictions.

Previously published in: K.G.V. Sigfridsson, N. Leidel, O. Sanganas, P. Chernev, O. Lenz, K.-S. Yoon, H. Nishihara, A. Parkin, F.A. Armstrong, S. Dementin, M. Rousset, A.L. De Lacey and M. Haumann (2015). Structural differences of oxidized iron-sulfur and nickel-iron cofactors in O_2-tolerant and O_2-sensitive hydrogenases studied by X-ray absorption spectroscopy, *Biochimica et Biophysica Acta (BBA) - Bioenergetics*, 1847:162-170, Epub ahead of print.

https://dx.doi.org/10.1016/j.bbabio.2014.06.011

Content removed due to copyright restrictions.

Previously published in: K.G.V. Sigfridsson, N. Leidel, O. Sanganas, P. Chernev, O. Lenz, K.-S. Yoon, H. Nishihara, A. Parkin, F.A. Armstrong, S. Dementin, M. Rousset, A.L. De Lacey and M. Haumann (2015). Structural differences of oxidized iron-sulfur and nickel-iron cofactors in O_2-tolerant and O_2-sensitive hydrogenases studied by X-ray absorption spectroscopy, *Biochimica et Biophysica Acta (BBA) - Bioenergetics*, 1847:162-170, Epub ahead of print.

https://dx.doi.org/10.1016/j.bbabio.2014.06.011

Content removed due to copyright restrictions.

Previously published in: K.G.V. Sigfridsson, N. Leidel, O. Sanganas, P. Chernev, O. Lenz, K.-S. Yoon, H. Nishihara, A. Parkin, F.A. Armstrong, S. Dementin, M. Rousset, A.L. De Lacey and M. Haumann (2015). Structural differences of oxidized iron-sulfur and nickel-iron cofactors in O_2-tolerant and O_2-sensitive hydrogenases studied by X-ray absorption spectroscopy, *Biochimica et Biophysica Acta (BBA) - Bioenergetics*, 1847:162-170, Epub ahead of print.

https://dx.doi.org/10.1016/j.bbabio.2014.06.011

Content removed due to copyright restrictions.

Previously published in: K.G.V. Sigfridsson, N. Leidel, O. Sanganas, P. Chernev, O. Lenz, K.-S. Yoon, H. Nishihara, A. Parkin, F.A. Armstrong, S. Dementin, M. Rousset, A.L. De Lacey and M. Haumann (2015). Structural differences of oxidized iron-sulfur and nickel-iron cofactors in O_2-tolerant and O_2-sensitive hydrogenases studied by X-ray absorption spectroscopy, *Biochimica et Biophysica Acta (BBA) - Bioenergetics*, 1847:162-170, Epub ahead of print.

https://dx.doi.org/10.1016/j.bbabio.2014.06.011

Content removed due to copyright restrictions.

Previously published in: K.G.V. Sigfridsson, N. Leidel, O. Sanganas, P. Chernev, O. Lenz, K.-S. Yoon, H. Nishihara, A. Parkin, F.A. Armstrong, S. Dementin, M. Rousset, A.L. De Lacey and M. Haumann (2015). Structural differences of oxidized iron-sulfur and nickel-iron cofactors in O_2-tolerant and O_2-sensitive hydrogenases studied by X-ray absorption spectroscopy, *Biochimica et Biophysica Acta (BBA) - Bioenergetics*, 1847:162-170, Epub ahead of print.

https://dx.doi.org/10.1016/j.bbabio.2014.06.011

4.2 X-ray Absorption Spectroscopy on Escherichia coli [NiFe] Hydrogenases 1 and 2

4.2.1 Abstract

Escherichia coli harbors an oxygen-sensitive periplasmic (PH) and an oxygen-tolerant membrane-bound (MBH) [NiFe] hydrogenase. For the oxidized wild-type PH (WTH2), the oxidized and reduced wild-type MBH (WTH1), and for four oxidized H1 proteins, in which amino acids near the proximal iron-sulfur cluster were exchanged, the metal contents and structural differences of the iron-sulfur cluster were investigated using X-ray absorption spectroscopy (XAS). 12 iron per nickel were found in all samples, except for the H1C20S mutant, in which some Fe was lost. Fe-XAS indicated overall more oxidized iron in a more distorted coordination environment and less ∼2.7 Å Fe−Fe distances with a higher distance spread in WTH1 compared to WTH2. Further, a larger number of longer Fe−Fe distances of ≥3.4 Å, decreased numbers of Fe−S distances of ∼2.3 Å and increased numbers of long Fe−S bonds of ∼2.6 Å were found. These results are in agreement with a 3Fe+1Fe arrangement of the proximal iron-sulfur cluster for the wild-type H1 compared to a standard [4Fe4S] cluster in the PH H2. In the mutated H1, gradual conversion of the 3Fe+1Fe iron-sulfur cluster to a (distorted) [4Fe4S] cluster was supported by the XAS data, the extent of the conversion depending on the actually exchanged amino acid.

4.2.2 Introduction

Hydrogenases (H_2ases) are enzymes responsible for the cleavage or formation of molecular hydrogen (H_2) at high turnover rates [Special Issue on Hydrogenases, 2007; Cammack et al., 1997]. Therefore, these catalysts are interesting candidates for biotechnological applications. Unfortunately, most hydrogenases are oxygen-sensitive and inactivated in the presence of oxygen [Vincent et al., 2005; De Lacey et al., 2007]. A few enzymes, however, show high oxygen-tolerance of hydrogen catalysis [Burgdorf et al., 2005a; Guiral et al., 2005; Yoon et al., 2009; Lukey et al., 2010; Pandelia et al., 2010a; Shafaat et al., 2013; Fritsch et al., 2013; Parkin et al., 2012]. Further insight into the reasons on the atomic level for the oxygen-tolerance may result from comparison of standard and oxygen-tolerant H_2ases, and from determination of the effects of site-divided mutagenesis in the enzymes on the cofactor structures.

Oxygen-tolerant H_2ases so far have only been found among the [NiFe] enzymes and the highest levels of oxygen-tolerance were observed in the membrane-bound [NiFe] H_2ases (MBH). Recently, crystal structures of several MBHs were reported [Fritsch et al., 2011b; Shomura et al., 2011; Volbeda et al., 2012]. The [NiFe] active site in

the MBHs contains two bridging cysteine residues, two further cysteine residues at the Ni, one carbon monoxide (CO) ligand and two cyanides (CN^-) at the Fe [Pierik et al., 1999; Saggu et al., 2009; Pandelia et al., 2010a], similar to the standard [NiFe] H_2ases.

A key finding in the crystal structures was a modified proximal FeS cluster in the oxygen-tolerant MBHs. Two additional cysteine residues bind to the Fe atoms of a unique [4Fe3S] proximal cluster, with the coordination of the Fe ions further depending on the redox state [Goris et al., 2011; Pandelia et al., 2012b; Roessler et al., 2012; Evans et al., 2013]. This suggests that the two additional cysteines in the small subunit are crucial for the structure of the proximal cluster.

The facultative anaerobic bacterium *Escherichia coli* houses an oxygen-tolerant membrane-bound [NiFe] H_2ase (H1) and an oxygen-sensitive periplasmic [NiFe] H_2ase (H2). Therefore, the *Escherichia coli* system is ideal to compare the cofactor structures in H1 and H2. We used X-ray absorption spectroscopy (XAS) at the Fe K-edge to study the structure of the FeS clusters. The wild-type PH (WTH2), the wild-type MBH (WTH1), and four mutants of H1 were compared. The results suggest a modified [4Fe3S] proximal cluster in H1, similar to the MBH from *Ralstonia eutropha*, as opposed to a standard [4Fe4S] cluster in the H2, and a more "standard-like" arrangement of the proximal cluster, depending on which amino acid in its vicinity was exchanged by mutagenesis.

4.2.3 Materials and Methods

H_2ase samples. Samples of *Escherichia coli* [NiFe] H_2ases 1 and 2 were provided by the group of Prof. F. Armstrong (University of Oxford, UK) and characterized by biochemical techniques prior to the XAS experiments.

Metal content quantification. Total-reflection X-ray fluorescence analysis (TXRF) [Klockenkamper, 1996] on a Bruker PicoFox spectrometer was carried out to determine the metal content in H_2ase protein samples.

XAS. XAS at the Fe K-edge was performed at beamline KMC-1 of BESSY (Helmholtz Zentrum Berlin) using a double-crystal Si[111] monochromator, a 13-element energy-resolving Ge detector (Canberra) for fluorescence monitoring, and samples held at 20 K in a liquid helium cryostat (Oxford) as previously described [Dau et al., 2003]. The energy axis of XAS scans was calibrated using the first inflection point at 7112 eV in the absorption edge of an Fe foil as a standard. XAS scans were averaged (7 – 11 scans of 6950 – 8150 eV), normalized, and EXAFS spectra were derived as described in [Dau et al., 2003, 2004]. K-edge energies were determined at 50% of normalized fluorescence (edge half height). Pre-edge features were extracted using the program XANDA [Klementiev, 2005]. Simulations of k^3-weighted EXAFS spectra were carried

out with the program SimX [Dau et al., 2003] using a least-squares global analysis approach (joint fit of spectra) [Dau et al., 2003] and phase functions calculated with FEFF8.4 [Rehr et al., 2010]. E_0 was refined to ∼7116 eV in the simulations; ${S_0}^2$ was 0.85. Fourier transforms (FTs) of EXAFS spectra were calculated for k-values of 2 – 16 Å^{-1} using cos^2 windows extending over 10% of both k-range ends.

4.2.4 Results

Metal contents of H_2ase samples. By TXRF the metal concentrations in the H_2ase samples and the iron to nickel ratios were determined (Figure 4.1). Wild-type H1 and H2 samples contained about 3 – 5 mM Fe, ∼0.35 mM Ni, and <100 µM Cu and Zn. The Fe/Ni ratio was similar, between 11.0 – 11.5 with an error of about ±0.5, for both H_2ases and thus close to 12 Fe per Ni. A value of 12 was expected, which accounts for the active site Fe, two [4Fe4S] clusters, and one [3Fe4S] cluster in H2 or a [4Fe3S] proximal cluster instead of a [4Fe4S] cluster in H1. Even slight Ni contaminations of ∼5% would diminish the apparent Fe/Ni ratio to a value of ∼11.5. Presumably, both H_2ases therefore contained 12 Fe ions per active site Ni.

The four proteins of H1 with mutations in the small subunit, i.e., amino acid exchanges at or close to the site of the proximal FeS cluster, in the cases of C19G, C115S, and C120G also showed close to 12 Fe/Ni (Figure 4.1), i.e., likely all metal cofactor species were assembled completely. However, for C120G the total Fe and Ni concentrations were about 4-fold lowered and an increase of the Zn content above the Ni level was observed. This suggested additional Zn binding to the protein and instability of the metal cofactors in part of the preparation. The C20S mutant revealed an Fe/Ni ratio which was diminished to a value of 7 – 8 (Figure 4.1), suggesting loss of one FeS species from the protein, presumably the four Fe ions of the proximal FeS cluster.

XAS analysis of H_2ase proteins. XAS at the Fe K-edge was used to determine the iron oxidation state and average coordination environment. XANES spectra of the H_2ase preparations are shown in Figure 4.2. The spectrum of oxidized WTH1 differed from that of H2 by a ∼0.5 eV higher edge energy and slight changes in the edge shape and a smaller pre-edge feature due to 1s→3d electronic transitions. The latter changes suggested overall more oxidized Fe and a different mean iron coordination, i.e., more asymmetric Fe ions in H1. On the basis of an edge up-shift of ∼3 eV per single-electron oxidation of mono-Fe compounds [Lambertz et al., 2014], the edge shift suggested the presence of 1 – 2 more oxidized, i.e., Fe(III) ions in H1 compared to H2. Hydrogen-reduced H1 showed an edge down-shift by ∼0.9 eV, due to the reduction of 3 – 4 Fe(III) ions to the Fe(II) level.

All H1 mutants revealed changes in the edge shape and energy compared to WT (Figure 4.2), suggesting variations in the coordination of the proximal FeS cluster.

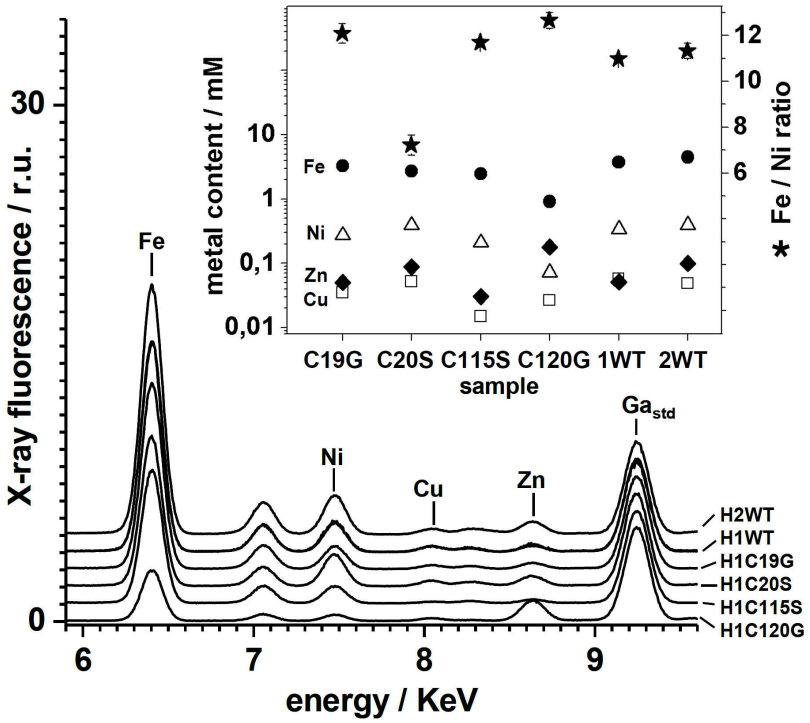

Figure 4.1: Metal quantification in H1 and H2 proteins by TXRF. X-ray fluorescence spectra of H_2ase samples were normalized on the peak of the gallium standard (Ga_{std}) and vertically displaced for comparison. For WTH1, spectra of oxidized and H_2-reduced preparations are overlaid. K_α fluorescence emission lines are marked, remaining features are K_β lines. Inset: metal concentrations (left y-axis) and respective Fe/Ni ratios (right y-axis).

For H1C19G, the edge features were rather similar to WTH2, meaning that FeS_p had become more similar to the [4Fe4S] cluster in H2. H1C20S showed a pre-edge feature which was in between the ones of WTH1 and H2. Higher edge energies in H1C115S and H1C120G presumably did not reflect additional iron oxidation, but, because of the increased primary edge maxima and steeper edge slope, likely were related to the binding of additional ligands, i.e., oxygen species, to some iron atoms. At least for H1C115S, this may be due to the binding of serine (SerO) instead of cysteine (CysS) to an Fe ion of FeS_p.

By EXAFS analysis Fe−Fe and Fe−ligand distances and respective coordination numbers were derived (Figure 4.3). All FTs of EXAFS spectra showed two major peak features, mostly due to Fe−S bonds (peak I) and Fe−Fe distances (peak II) of ∼2.7 Å, typical for FeS clusters [Beinert et al., 1997; Buhrke et al., 2005b]. The FT of WTH1 differed from the one of H2 in particular by its much smaller peak II. This

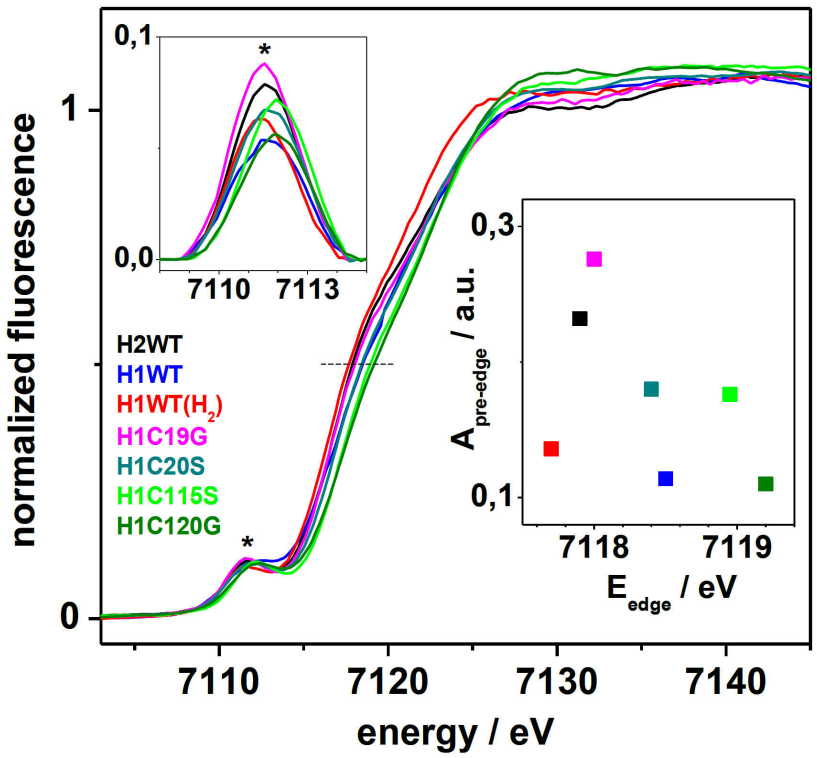

Figure 4.2: Fe XANES spectra of H_2ase preparations. (H_2) denotes hydrogen-reduced H1WT, all other proteins were oxidized. The dashed line marks the edge half-height, the asterisk the pre-edge feature. Respective edge energies and integral pre-edge areas are shown in the inset.

suggested less Fe−Fe distances of 2.7 Å in H1. Results of simulations of the H1 and H2 EXAFS spectra using a previously developed approach involving six coordination shells [Fritsch et al., 2011a] are shown in Figure 4.4. The H2 result was in agreement with a standard-type content of iron clusters, i.e., 2 x [4Fe4S], 1 x [3Fe4S], and the active-site Fe in this protein. Respective experimental coordination numbers per Fe ion (N) were very close to the calculated ones (∼0.35 Fe−C,O of ∼1.95 Å due to the Fe−$O(CN)_2(CO)$ bonds in the Ni-A, -B states, ∼3.85 Fe−S bonds of ∼2.3 Å, and ∼2.6 Fe−Fe distances of ∼2.7 Å (Figure 4.4) [Stein and Lubitz, 2002; Siegbahn et al., 2007]).

The main EXAFS differences for H1 were (i) decreased numbers of Fe−S distances of ∼2.3 Å and increased numbers of long Fe−S bonds of ∼2.6 Å, (ii) a lowered coordination number of about 2 of ∼2.7 Å Fe−Fe distances, (iii) a larger spread of about 2.67 – 2.75 Å of the shorter Fe−Fe distances, and (iv) an increased number of Fe−Fe distances of ∼3.4 Å. However, the number of Fe−C,O bonds was similar to H2. Assuming 12 Fe

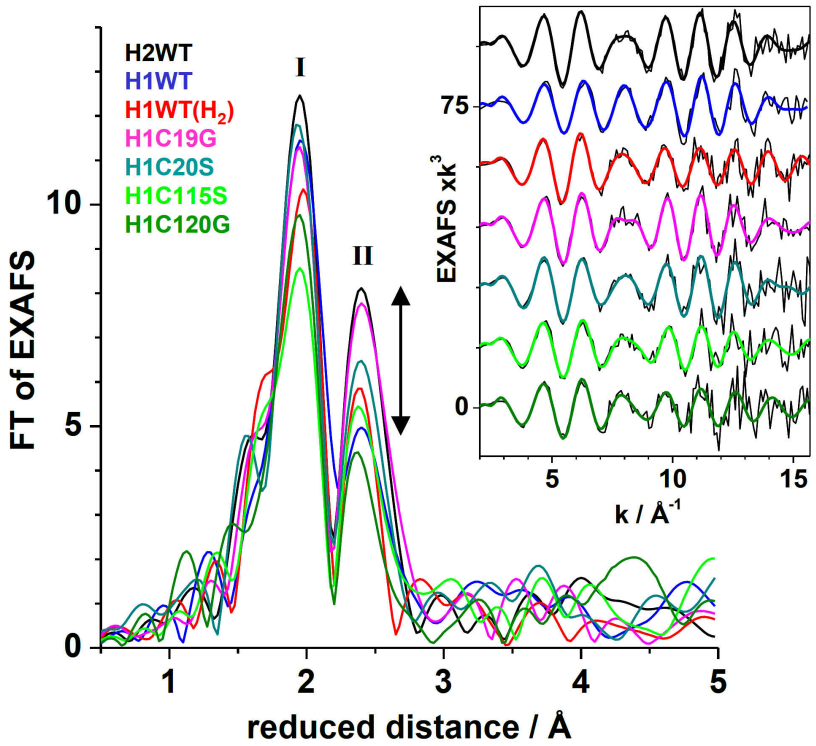

Figure 4.3: EXAFS spectra of H_2ase preparations. Fourier-transforms (FTs) correspond to the experimental EXAFS spectra in the inset (black lines); colored lines in the inset are simulations with parameters shown in Figure 4.4 (see legend). FT peaks I and II mostly reflect Fe−S and Fe−Fe interactions. The arrow shows the amplitude reduction of FT peak II due to ∼2.7 Å Fe−Fe distances in H1 compared to H2.

ions, normal distal [4Fe4S] and medial [3Fe4S] clusters, and the active site mainly in the Ni-B state in H1, the EXAFS data suggested that only about 6 Fe−Fe distances of ∼2.7 Å and 5 – 7 distances of ∼3.4 Å were present in FeS_p. A value of 6 Fe−Fe distances of ∼2.7 Å is typical for [3Fe4S] clusters (each Fe−Fe pair contributes a sum of 2 to this number). The N-value of the longer Fe−Fe distances suggested that one Fe ion was at a larger distance to three Fe ions, i.e., in a 3Fe cluster. Detection of particularly short Fe−Fe distances of ≤2.67 Å in H1 may point to a bridging coordination of the thiol group of one of the additional cysteines (C19, C120) in an Fe(μS_{Cys})Fe motif, similar to the observations in the *Ralstonia eutropha* MBH.

Changes in the EXAFS were observed for all H1 mutants (Figures 4.3 and 4.4). Particularly interesting was C19S, which revealed an Fe coordination different from WTH1, but very similar to that of H2, i.e., similar numbers of ∼2.3 Å Fe−S bonds and ∼2.7 Å Fe−Fe distances and low numbers of long Fe−S and Fe−Fe interactions.

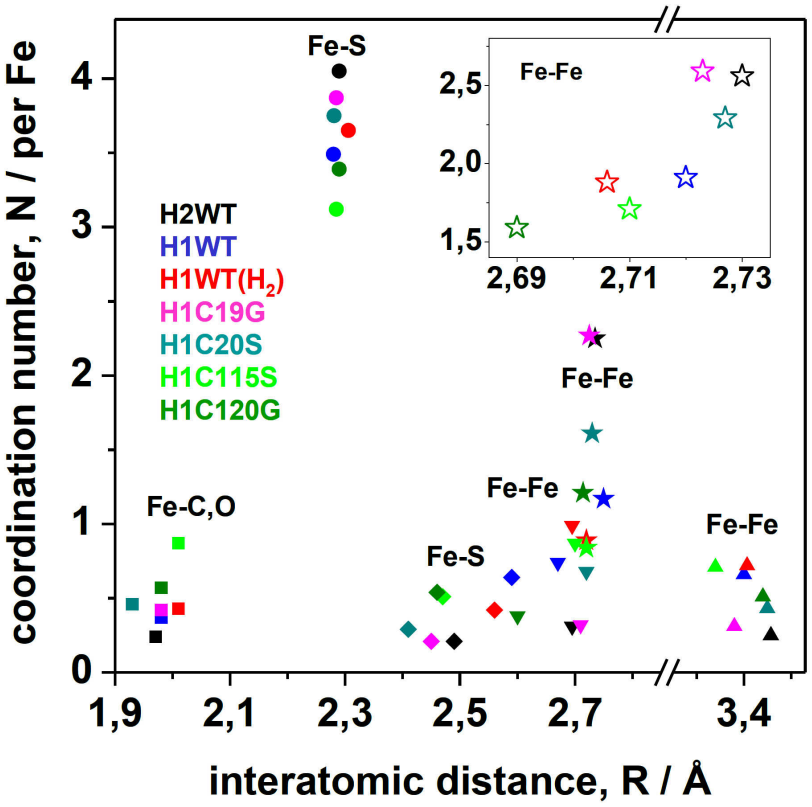

Figure 4.4: EXAFS simulation results. Coordination numbers and interatomic distances were derived from a global analysis of data in Figure 4.3. EXAFS fits further included Debye-Waller factors ($2\sigma^2$) of 0.002 Å^2 (Fe−C,O), 0.007 Å^2 (Fe−S), and 0.008 Å^2 (Fe−Fe). The sum of the N-values of Fe−C,O and Fe−S shells was restraint to 4.5 in the simulations. The error sum (R_F [Dau et al., 2003]) was 10.2% for the joint fit of the seven spectra. Inset: mean short Fe−Fe distances derived from the N-weighted sum of Fe−Fe distances around ∼2.7 Å in the main figure.

A straightforward interpretation of the XANES and EXAFS results is the conversion of the proximal [4Fe3S] cluster in WTH1 to a standard [4Fe4S] cluster in H1C19G.

H1C20S showed an increase to ∼2.3 in the number of Fe−Fe distances of ∼2.7 Å, a smaller Fe−Fe distance spread, lower numbers of long Fe−S and Fe−Fe distances, and overall shorter Fe−C,O bonds compared to WTH1 (Figures 4.3 and 4.4). A value of ∼2.4 Fe−Fe distances of ∼2.7 Å was expected for the presence of only the distal [4Fe4S] and medial [3Fe4S] clusters in the protein. The EXAFS result and the loss of ∼4 Fe ions detected by TXRF thus were in agreement with the complete loss of FeS_p from the H1C20S protein. Apparently, the serine was unable to coordinate to iron leading to destabilization of FeS_p.

For H1C115S, an about doubled number of longer Fe−C,O bonds and decreased number of Fe−S bonds were detected. Otherwise the iron coordination was relatively similar to WTH1. The increase in $N_{Fe-C,O}$ suggested the binding of one or several oxygen species to iron. Possibly, a SerO−Fe bond was formed instead of CysS−Fe. Such a coordination change may facilitate binding of further oxygen species, i.e., water molecules, to some of the iron ions of FeS_p. However, the overall structure of FeS_p apparently was not much affected by these coordination changes.

For H1C120G, the situation was less clear. A diminished number of overall shorter ∼2.7 Å Fe−Fe distances and of longer Fe−Fe interactions and slightly more Fe−C,O bonds were detected. As this mutant contained increased Zn levels, a possible explanation of the decreased numbers of Fe−Fe distances was the replacement of Fe by Zn in a fraction of protein. Zn may then be at distances exceeding 3.4 Å from Fe, so that respective interactions became undetectable in the EXAFS spectrum. The C120G mutation seemed to reduce the content of all cofactors in the protein, pointing to a destabilization of the structure. However, in protein with remaining structural integrity, an overall similar FeS_p species as in WT may be formed, perhaps sometimes with a Zn ion instead of Fe more remotely from the 3Fe site.

4.2.5 Discussion

Recent crystal structures of O_2-tolerant MBHs have revealed a novel [4Fe3S] cluster in the small subunit proximal to the [NiFe] cofactor. This holds also for the MBH from *E. coli* (H1). The structural differences between H1 and H2 and the mutation effects therefore are discussed with respect to the organization of the proximal FeS cluster. The results on wild-type H1 and H2 enzymes are similar to the ones previously obtained by comparison of *D. gigas* standard periplasmic [NiFe] H_2ase and the *R. eutropha* MBH [Fritsch et al., 2011b,a, 2013].

Structural attributions for the proximal FeS cluster in H1 and H2, based on the XAS data and the crystal structures, are summarized in Figure 4.5. In H2, FeS_p is a standard [4Fe4S] cluster, in agreement with the amino acid sequence. In H1 there are two additional cysteines (C19, C120) at the site of the proximal cluster. For this enzyme, the EXAFS results suggest a 3Fe+1Fe arrangement for FeS_p, i.e., a modified 3Fe cluster plus a more remote Fe ion at ∼3.4 Å to several of the other three ions. In the 3Fe unit, there may be a bridging cysteine, which, according to the crystal structure of H1, is C19. C120 then may be a ligand to the remote Fe ion (Figure 4.5), as also seen in the structure. This structure presumably explains EPR results (i.e., the split g = 2 signal due to the modified cluster), the two-electron oxidation of FeS_p [Pandelia et al., 2010a, 2011, 2012a], and the 1 – 2 more oxidized Fe ions in H1 compared to H2 found in the present work.

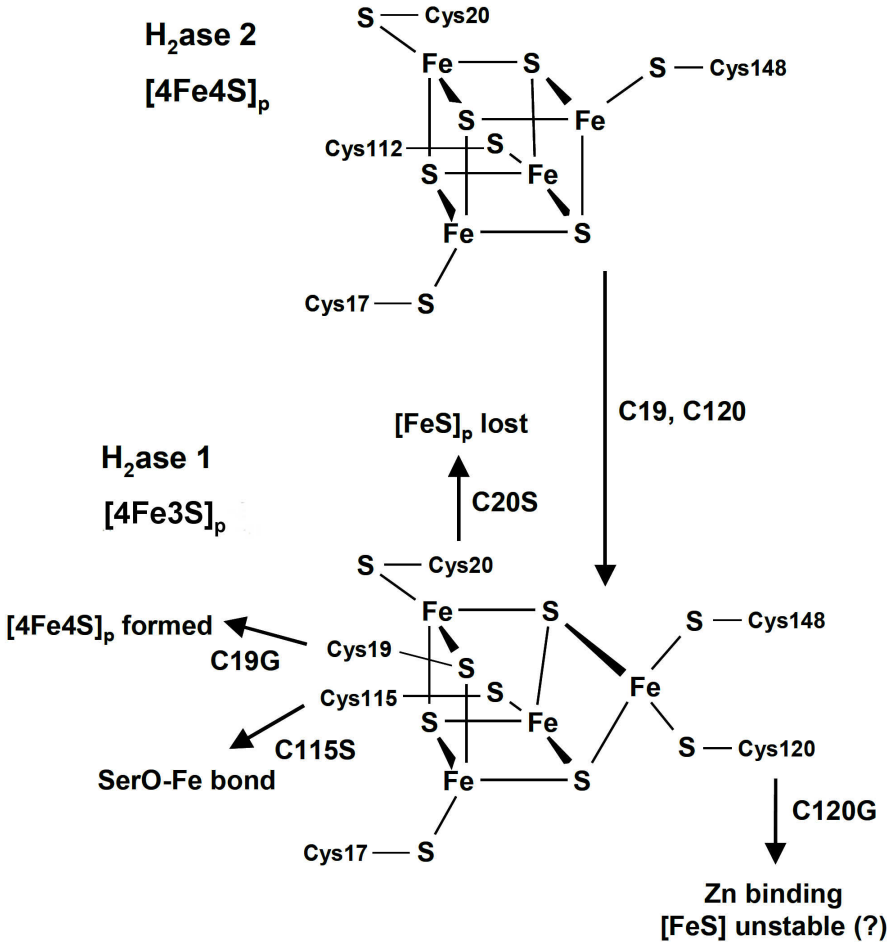

Figure 4.5: Structural models for the proximal FeS cluster in wild-type and mutated *E. coli* hydrogenases. Top: conventional [4Fe4S] cluster in H2. Bottom: model of the proximal [4Fe3S] cluster in H1. The coordination of C19 in an Fe−Fe bridging position and of C120 at the remote Fe ion are in agreement with the XAS results and crystal data. The indicated effects of the cysteine mutations are in agreement with the EXAFS and TXRF analyses. For further details see the text.

The mutation effects support the modified FeS_p structure in WTH1 (Figure 4.5). C120G may lead to the loss of the remote Fe of FeS_p, to its replacement by Zn, or even to destabilization of the protein. C20S likely leads to the loss of FeS_p because serine apparently cannot coordinate the respective Fe ion. Removal of the bridging CysS in the C19G mutant almost quantitatively recovers a normal [4Fe4S] cluster at the proximal position. Interestingly, a similar effect, i.e., commission of $[4Fe3S]_p$ to $[4Fe4S]_p$, was induced in the C19,120G double mutant in the *R. eutropha* MBH. This

means that the replacement of Cys19 by Glycine is sufficient for the conversion of FeS_p to a [4Fe4S] cluster. This is further evidence for C19 being a bridging ligand which replaces a µS bridge, i.e., in its absence, a µS atom is incorporated into FeS_p, so that the Fe bound by C120 is stabilized. C115 seems to be a more flexible ligand, because the alternative serine seems to bind to the Fe ion. This may cause only minor structural changes of FeS_p, such as perhaps binding of one or several further water molecules to Fe.

In summary, our TXRF and XAS results strongly support that FeS_p is an unusual [4Fe3S] species in the O_2-tolerant MBHs. The unusual coordination of Fe by the additional two cysteines in the small subunit, which results in the modified structure, as well as structural alterations at FeS_p in response to site-directed mutagenesis, can clearly be detected by XAS. The conversion of the [4Fe3S] cluster to a [4Fe4S] cluster is a key finding in the XAS data. Whether and how the structural changes at FeS_p affect the O_2-tolerance level of the MBH H1 remains to be investigated.

4.3 Protein-Protein Complex Formation Affects the Ni-Fe and Fe-S Centers in the H_2-Sensing Regulatory Hydrogenase from Ralstonia eutropha H16

Previously published in: S. Löscher, A. Gebler, M. Stein, O. Sanganas, T. Buhrke, I. Zebger, H. Dau, B. Friedrich, O. Lenz and M. Haumann (2010). Protein-Protein Complex Formation Affects the Ni-Fe and Fe-S Centers in the H_2-Sensing Regulatory Hydrogenase from *Ralstonia eutropha* H16, *ChemPhysChem*, 11:1297-1306.

https://dx.doi.org/10.1002/cphc.200901007

Content removed due to copyright restrictions.

Previously published in: S. Löscher, A. Gebler, M. Stein, O. Sanganas, T. Buhrke, I. Zebger, H. Dau, B. Friedrich, O. Lenz and M. Haumann (2010). Protein-Protein Complex Formation Affects the Ni-Fe and Fe-S Centers in the H_2-Sensing Regulatory Hydrogenase from *Ralstonia eutropha* H16, *ChemPhysChem*, 11:1297-1306.

https://dx.doi.org/10.1002/cphc.200901007

Content removed due to copyright restrictions.

Previously published in: S. Löscher, A. Gebler, M. Stein, O. Sanganas, T. Buhrke, I. Zebger, H. Dau, B. Friedrich, O. Lenz and M. Haumann (2010). Protein-Protein Complex Formation Affects the Ni-Fe and Fe-S Centers in the H_2-Sensing Regulatory Hydrogenase from *Ralstonia eutropha* H16, *ChemPhysChem*, 11:1297-1306.

https://dx.doi.org/10.1002/cphc.200901007

Content removed due to copyright restrictions.

Previously published in: S. Löscher, A. Gebler, M. Stein, O. Sanganas, T. Buhrke, I. Zebger, H. Dau, B. Friedrich, O. Lenz and M. Haumann (2010). Protein-Protein Complex Formation Affects the Ni-Fe and Fe-S Centers in the H_2-Sensing Regulatory Hydrogenase from *Ralstonia eutropha* H16, *ChemPhysChem*, 11:1297-1306.

https://dx.doi.org/10.1002/cphc.200901007

Content removed due to copyright restrictions.

Previously published in: S. Löscher, A. Gebler, M. Stein, O. Sanganas, T. Buhrke, I. Zebger, H. Dau, B. Friedrich, O. Lenz and M. Haumann (2010). Protein-Protein Complex Formation Affects the Ni-Fe and Fe-S Centers in the H_2-Sensing Regulatory Hydrogenase from *Ralstonia eutropha* H16, *ChemPhysChem*, 11:1297-1306.

https://dx.doi.org/10.1002/cphc.200901007

Previously published in: S. Löscher, A. Gebler, M. Stein, O. Sanganas, T. Buhrke, I. Zebger, H. Dau, B. Friedrich, O. Lenz and M. Haumann (2010). Protein-Protein Complex Formation Affects the Ni-Fe and Fe-S Centers in the H_2-Sensing Regulatory Hydrogenase from *Ralstonia eutropha* H16, *ChemPhysChem*, 11:1297-1306.

https://dx.doi.org/10.1002/cphc.200901007

Content removed due to copyright restrictions.

Previously published in: S. Löscher, A. Gebler, M. Stein, O. Sanganas, T. Buhrke, I. Zebger, H. Dau, B. Friedrich, O. Lenz and M. Haumann (2010). Protein-Protein Complex Formation Affects the Ni-Fe and Fe-S Centers in the H_2-Sensing Regulatory Hydrogenase from *Ralstonia eutropha* H16, *ChemPhysChem*, 11:1297-1306.

https://dx.doi.org/10.1002/cphc.200901007

Content removed due to copyright restrictions.

Previously published in: S. Löscher, A. Gebler, M. Stein, O. Sanganas, T. Buhrke, I. Zebger, H. Dau, B. Friedrich, O. Lenz and M. Haumann (2010). Protein-Protein Complex Formation Affects the Ni-Fe and Fe-S Centers in the H_2-Sensing Regulatory Hydrogenase from *Ralstonia eutropha* H16, *ChemPhysChem*, 11:1297-1306.

https://dx.doi.org/10.1002/cphc.200901007

Content removed due to copyright restrictions.

Previously published in: S. Löscher, A. Gebler, M. Stein, O. Sanganas, T. Buhrke, I. Zebger, H. Dau, B. Friedrich, O. Lenz and M. Haumann (2010). Protein-Protein Complex Formation Affects the Ni-Fe and Fe-S Centers in the H_2-Sensing Regulatory Hydrogenase from *Ralstonia eutropha* H16, *ChemPhysChem*, 11:1297-1306.

https://dx.doi.org/10.1002/cphc.200901007

Content removed due to copyright restrictions.

Previously published in: S. Löscher, A. Gebler, M. Stein, O. Sanganas, T. Buhrke, I. Zebger, H. Dau, B. Friedrich, O. Lenz and M. Haumann (2010). Protein-Protein Complex Formation Affects the Ni-Fe and Fe-S Centers in the H_2-Sensing Regulatory Hydrogenase from *Ralstonia eutropha* H16, *ChemPhysChem*, 11:1297-1306.

https://dx.doi.org/10.1002/cphc.200901007

Content removed due to copyright restrictions.

Previously published in: S. Löscher, A. Gebler, M. Stein, O. Sanganas, T. Buhrke, I. Zebger, H. Dau, B. Friedrich, O. Lenz and M. Haumann (2010). Protein-Protein Complex Formation Affects the Ni-Fe and Fe-S Centers in the H_2-Sensing Regulatory Hydrogenase from *Ralstonia eutropha* H16, *ChemPhysChem*, 11:1297-1306.

https://dx.doi.org/10.1002/cphc.200901007

Content removed due to copyright restrictions.

Previously published in: S. Löscher, A. Gebler, M. Stein, O. Sanganas, T. Buhrke, I. Zebger, H. Dau, B. Friedrich, O. Lenz and M. Haumann (2010). Protein-Protein Complex Formation Affects the Ni-Fe and Fe-S Centers in the H_2-Sensing Regulatory Hydrogenase from *Ralstonia eutropha* H16, *ChemPhysChem*, 11:1297-1306.

https://dx.doi.org/10.1002/cphc.200901007

Content removed due to copyright restrictions.

Previously published in: S. Löscher, A. Gebler, M. Stein, O. Sanganas, T. Buhrke, I. Zebger, H. Dau, B. Friedrich, O. Lenz and M. Haumann (2010). Protein-Protein Complex Formation Affects the Ni-Fe and Fe-S Centers in the H_2-Sensing Regulatory Hydrogenase from *Ralstonia eutropha* H16, *ChemPhysChem*, 11:1297-1306.

https://dx.doi.org/10.1002/cphc.200901007

Content removed due to copyright restrictions.

Previously published in: S. Löscher, A. Gebler, M. Stein, O. Sanganas, T. Buhrke, I. Zebger, H. Dau, B. Friedrich, O. Lenz and M. Haumann (2010). Protein-Protein Complex Formation Affects the Ni-Fe and Fe-S Centers in the H_2-Sensing Regulatory Hydrogenase from *Ralstonia eutropha* H16, *ChemPhysChem*, 11:1297-1306.

https://dx.doi.org/10.1002/cphc.200901007

Content removed due to copyright restrictions.

Previously published in: S. Löscher, A. Gebler, M. Stein, O. Sanganas, T. Buhrke, I. Zebger, H. Dau, B. Friedrich, O. Lenz and M. Haumann (2010). Protein-Protein Complex Formation Affects the Ni-Fe and Fe-S Centers in the H_2-Sensing Regulatory Hydrogenase from *Ralstonia eutropha* H16, *ChemPhysChem*, 11:1297-1306.

https://dx.doi.org/10.1002/cphc.200901007

Content removed due to copyright restrictions.

Previously published in: S. Löscher, A. Gebler, M. Stein, O. Sanganas, T. Buhrke, I. Zebger, H. Dau, B. Friedrich, O. Lenz and M. Haumann (2010). Protein-Protein Complex Formation Affects the Ni-Fe and Fe-S Centers in the H_2-Sensing Regulatory Hydrogenase from *Ralstonia eutropha* H16, *ChemPhysChem*, 11:1297-1306.

https://dx.doi.org/10.1002/cphc.200901007

Content removed due to copyright restrictions.

Previously published in: S. Löscher, A. Gebler, M. Stein, O. Sanganas, T. Buhrke, I. Zebger, H. Dau, B. Friedrich, O. Lenz and M. Haumann (2010). Protein-Protein Complex Formation Affects the Ni-Fe and Fe-S Centers in the H_2-Sensing Regulatory Hydrogenase from *Ralstonia eutropha* H16, *ChemPhysChem*, 11:1297-1306.

https://dx.doi.org/10.1002/cphc.200901007

Content removed due to copyright restrictions.

Previously published in: S. Löscher, A. Gebler, M. Stein, O. Sanganas, T. Buhrke, I. Zebger, H. Dau, B. Friedrich, O. Lenz and M. Haumann (2010). Protein-Protein Complex Formation Affects the Ni-Fe and Fe-S Centers in the H_2-Sensing Regulatory Hydrogenase from *Ralstonia eutropha* H16, *ChemPhysChem*, 11:1297-1306.

https://dx.doi.org/10.1002/cphc.200901007

Content removed due to copyright restrictions.

Previously published in: S. Löscher, A. Gebler, M. Stein, O. Sanganas, T. Buhrke, I. Zebger, H. Dau, B. Friedrich, O. Lenz and M. Haumann (2010). Protein-Protein Complex Formation Affects the Ni-Fe and Fe-S Centers in the H_2-Sensing Regulatory Hydrogenase from *Ralstonia eutropha* H16, *ChemPhysChem*, 11:1297-1306.

https://dx.doi.org/10.1002/cphc.200901007

Content removed due to copyright restrictions.

Previously published in: S. Löscher, A. Gebler, M. Stein, O. Sanganas, T. Buhrke, I. Zebger, H. Dau, B. Friedrich, O. Lenz and M. Haumann (2010). Protein-Protein Complex Formation Affects the Ni-Fe and Fe-S Centers in the H_2-Sensing Regulatory Hydrogenase from *Ralstonia eutropha* H16, *ChemPhysChem*, 11:1297-1306.

https://dx.doi.org/10.1002/cphc.200901007

4.4 X-ray Absorption Spectroscopy on the Hydrogenase Subcomplex of the NAD$^+$-Reducing [NiFe] Hydrogenase from Ralstonia eutropha

Omitted parts previously published as part of: L. Lauterbach, J. Liu, M. Horch, P. Hummel, A. Schwarze, M. Haumann, K.A. Vincent, O. Lenz and I. Zebger (2011). The Hydrogenase Subcomplex of the NAD$^+$-Reducing [NiFe] Hydrogenase from *Ralstonia eutropha* − Insights into Catalysis and Redox Interconversions, *European Journal of Inorganic Chemistry*, 7:1067–1079.

https://dx.doi.org/10.1002/ejic.201001053

Content removed due to copyright restrictions.

Omitted parts previously published as part of: L. Lauterbach, J. Liu, M. Horch, P. Hummel, A. Schwarze, M. Haumann, K.A. Vincent, O. Lenz and I. Zebger (2011). The Hydrogenase Subcomplex of the NAD^+-Reducing [NiFe] Hydrogenase from *Ralstonia eutropha* − Insights into Catalysis and Redox Interconversions, *European Journal of Inorganic Chemistry*, 7:1067–1079.

https://dx.doi.org/10.1002/ejic.201001053

Content removed due to copyright restrictions.

Omitted parts previously published as part of: L. Lauterbach, J. Liu, M. Horch, P. Hummel, A. Schwarze, M. Haumann, K.A. Vincent, O. Lenz and I. Zebger (2011). The Hydrogenase Subcomplex of the NAD^+-Reducing [NiFe] Hydrogenase from *Ralstonia eutropha* − Insights into Catalysis and Redox Interconversions, *European Journal of Inorganic Chemistry*, 7:1067–1079.

https://dx.doi.org/10.1002/ejic.201001053

Omitted parts previously published as part of: L. Lauterbach, J. Liu, M. Horch, P. Hummel, A. Schwarze, M. Haumann, K.A. Vincent, O. Lenz and I. Zebger (2011). The Hydrogenase Subcomplex of the NAD^+-Reducing [NiFe] Hydrogenase from *Ralstonia eutropha* − Insights into Catalysis and Redox Interconversions, *European Journal of Inorganic Chemistry*, 7:1067–1079.

https://dx.doi.org/10.1002/ejic.201001053

Results and Discussion

Metal content. By TXRF, average concentrations of 0.78 ± 0.05 mM Fe and 0.15 ± 0.05 mM Ni were determined for five HoxHY samples (SH_{dimer}). The average ratio of Fe per Ni ions was 5.5 ± 1.6. The relatively large variations in the metal ratio presumably was due to a partially occupied Ni site in a fraction of protein and/or to small amounts of unspecific Fe, depending on the preparation. However, the finding of close to five Fe ions per Ni was compatible with the presence of the active-site iron atom in the HoxH subunit and of four iron atoms in an FeS cluster in HoxY.

X-ray absorption spectroscopy. By XAS, the coordination environment of the active-site Ni and the nature of the FeS cluster in the as-isolated HoxHY moiety were studied. The Ni K-edge showed an energy (at 50% level) of 8341.9 ± 0.1 eV, a moderate slope of the absorption rise, and a relatively large primary maximum at ∼8350 eV (Figure 4.6), suggesting five-coordinated metal presumably in the Ni(II) oxidation state and coordinated by sulfur ligands and additional oxygen species [Haumann et al., 2003; Burgdorf et al., 2005b; Löscher et al., 2006]. The Fourier-transform (FT) of the corresponding EXAFS spectrum showed one major peak with comparably small magnitude (Figure 4.6), likely due to interference between Ni−S, Ni−O, and Ni−Fe contributions to the EXAFS. A quantitative simulation of the spectrum was achieved using four Ni−backscatterer interactions (Table 4.1), i.e., close to two shorter (2.28 Å)

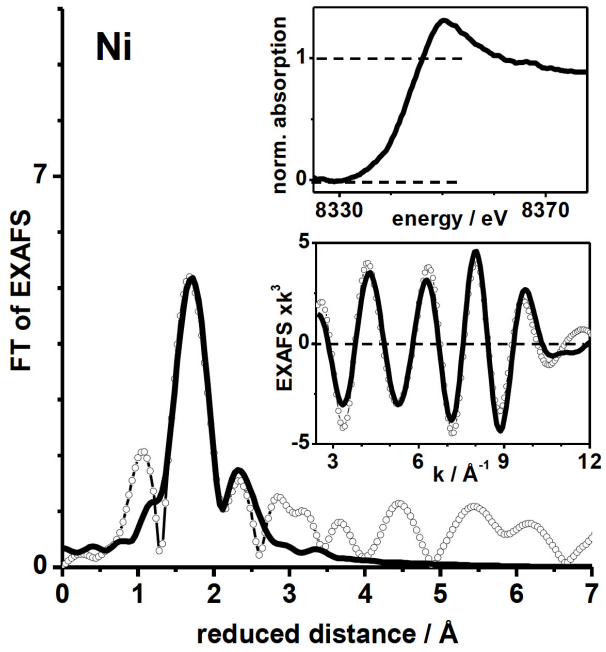

Figure 4.6: XAS spectrum at the Ni K-edge. Fourier-transform (FT) of Ni EXAFS data. Respective EXAFS oscillations are shown in the lower inset. Corresponding K-edge spectrum is shown in the upper inset. Experimental data, open circles; EXAFS simulations with parameters in Table 4.1, solid lines. FTs were calculated using $\cos^2$ windows extending over 10% at both k-range ends. XAS spectrum at the Fe K-edge removed due to copyright restrictions (for reference see text).

Table 4.1: EXAFS simulation parameters.

shell	N_i [per metal]	R_i [Å]	$2\sigma^2{}_i$ [Å^2]	R_F [%]
Nickel				
O	1.18$^{\#}$	2.02	0.002*	13.5
S	2.01$^{\#}$	2.28	0.015	
S	1.81$^{\#}$	2.51	0.005*	
Fe	1*	2.53	0.005*	

N_i, coordination number; R_i metal-backscatterer distance; $2\sigma^2{}_i$, Debye-Waller parameter, R_F, fit error sum [Dau et al., 2003]. $^{\#}$The sum of the first-sphere coordination numbers was restricted to 5; *parameters that were fixed to physically reasonable values in the simulations. Iron EXAFS simulation parameters removed due to copyright restrictions (for reference see text).

and two longer (2.51 Å) Ni−S bonds and about one Ni−O bond (2.02 Å). Due to the limited k-range and signal-to-noise ratio of the EXAFS data resulting from the low Ni concentration in the samples, the Ni−Fe distance (∼2.5 Å) could only tentatively be determined. The EXAFS analysis suggested that the four conserved cysteine residues in HoxH coordinated the Ni via their thiolate sulfur atoms. The large distance spread in the Ni−S bonds pointed to sample heterogeneity, i.e., the presence of several states of the Ni−Fe site in the preparation. The Ni−O interaction, according to its bond length >2 Å, is attributable to a terminal ligand and not to a Ni−Fe bridging oxygen [Dementin et al., 2009].

Content removed due to copyright restrictions.

Omitted parts previously published as part of: L. Lauterbach, J. Liu, M. Horch, P. Hummel, A. Schwarze, M. Haumann, K.A. Vincent, O. Lenz and I. Zebger (2011). The Hydrogenase Subcomplex of the NAD^+-Reducing [NiFe] Hydrogenase from *Ralstonia eutropha* − Insights into Catalysis and Redox Interconversions, *European Journal of Inorganic Chemistry*, 7:1067–1079.

https://dx.doi.org/10.1002/ejic.201001053

Omitted parts previously published as part of: L. Lauterbach, J. Liu, M. Horch, P. Hummel, A. Schwarze, M. Haumann, K.A. Vincent, O. Lenz and I. Zebger (2011). The Hydrogenase Subcomplex of the NAD^+-Reducing [NiFe] Hydrogenase from *Ralstonia eutropha* − Insights into Catalysis and Redox Interconversions, *European Journal of Inorganic Chemistry*, 7:1067–1079.

https://dx.doi.org/10.1002/ejic.201001053

Conclusions

In the present study we characterized the smallest active [NiFe] hydrogenase subcomplex, the heterodimeric hydrogenase moiety, HoxHY, of the bidirectional SH of *R. eutropha* by XAS. Ni-XAS suggests ligation of the Ni by four sulfurs from conserved cysteine residues in HoxH and one oxygen in a terminal position. The large distance spread in the Ni−S bonds of the samples is probably due to heterogeneity, i.e., several oxidation states were likely present. The bond lengths at the [NiFe] active site iron are in agreement with, e.g., crystal structures of [NiFe] hydrogenases. Fe-XAS focused on the nature of the FeS species. The EXAFS analysis in combination with the metal content determined by TXRF and the conserved cysteines suggested the binding of a [4Fe4S] cluster in HoxY in the dominant protein fraction and some oxidatively modified species in addition. In a minor proportion of the sample, this cluster may have been converted by oxidative modification to a [4Fe-nS-nO] species [Buhrke et al., 2005b]. The HoxHY is the smallest active subcomplex of a [NiFe] hydrogenase with the [NiFe] active site in HoxH plus a [4Fe4S] cluster in HoxY. This situation is somewhat similar to the one in [FeFe] hydrogenases (H-cluster with 4Fe and 2Fe units), but in this case a direct cysteine link between the units is present. How the putative [4Fe4S] cluster in HoxY is located relative to the [NiFe] cofactor in the SH protein remains to be shown.

4.5 Resonant Inelastic X-ray Scattering on Synthetic Nickel Compounds and Ni-Fe Hydrogenase Protein

Previously published in: O. Sanganas, S. Löscher, S. Pfirrmann, N. Marinos, P. Glatzel, T.-C. Weng, C. Limberg, M. Driess, H. Dau and M. Haumann (2009). Resonant inelastic X-ray scattering on synthetic nickel compounds and Ni-Fe hydrogenase protein, *XAFS14, Journal of Physics: Conference Series*, 190:012199-202.

https://dx.doi.org/10.1088/1742-6596/190/1/012199

Content removed due to copyright restrictions.

Previously published in: O. Sanganas, S. Löscher, S. Pfirrmann, N. Marinos, P. Glatzel, T.-C. Weng, C. Limberg, M. Driess, H. Dau and M. Haumann (2009). Resonant inelastic X-ray scattering on synthetic nickel compounds and Ni-Fe hydrogenase protein, *XAFS14, Journal of Physics: Conference Series*, 190:012199-202.

https://dx.doi.org/10.1088/1742-6596/190/1/012199

Content removed due to copyright restrictions.

Previously published in: O. Sanganas, S. Löscher, S. Pfirrmann, N. Marinos, P. Glatzel, T.-C. Weng, C. Limberg, M. Driess, H. Dau and M. Haumann (2009). Resonant inelastic X-ray scattering on synthetic nickel compounds and Ni-Fe hydrogenase protein, *XAFS14, Journal of Physics: Conference Series*, 190:012199-202.

https://dx.doi.org/10.1088/1742-6596/190/1/012199

Content removed due to copyright restrictions.

Previously published in: O. Sanganas, S. Löscher, S. Pfirrmann, N. Marinos, P. Glatzel, T.-C. Weng, C. Limberg, M. Driess, H. Dau and M. Haumann (2009). Resonant inelastic X-ray scattering on synthetic nickel compounds and Ni-Fe hydrogenase protein, *XAFS14, Journal of Physics: Conference Series*, 190:012199-202.

https://dx.doi.org/10.1088/1742-6596/190/1/012199

Content removed due to copyright restrictions.

Previously published in: O. Sanganas, S. Löscher, S. Pfirrmann, N. Marinos, P. Glatzel, T.-C. Weng, C. Limberg, M. Driess, H. Dau and M. Haumann (2009). Resonant inelastic X-ray scattering on synthetic nickel compounds and Ni-Fe hydrogenase protein, *XAFS14, Journal of Physics: Conference Series*, 190:012199-202.

https://dx.doi.org/10.1088/1742-6596/190/1/012199

Content removed due to copyright restrictions.

Previously published in: O. Sanganas, S. Löscher, S. Pfirrmann, N. Marinos, P. Glatzel, T.-C. Weng, C. Limberg, M. Driess, H. Dau and M. Haumann (2009). Resonant inelastic X-ray scattering on synthetic nickel compounds and Ni-Fe hydrogenase protein, *XAFS14, Journal of Physics: Conference Series*, 190:012199-202.

https://dx.doi.org/10.1088/1742-6596/190/1/012199

Content removed due to copyright restrictions.

Previously published in: O. Sanganas, S. Löscher, S. Pfirrmann, N. Marinos, P. Glatzel, T.-C. Weng, C. Limberg, M. Driess, H. Dau and M. Haumann (2009). Resonant inelastic X-ray scattering on synthetic nickel compounds and Ni-Fe hydrogenase protein, *XAFS14, Journal of Physics: Conference Series*, 190:012199-202.

https://dx.doi.org/10.1088/1742-6596/190/1/012199

4.6 The Structure of the Active Site H-Cluster of [FeFe] Hydrogenase from the Green Alga Chlamydomonas reinhardtii Studied by X-ray Absorption Spectroscopy

Previously published in: S. Stripp*, O. Sanganas*, T. Happe and M. Haumann (2009). The Structure of the Active Site H-Cluster of [FeFe] Hydrogenase from the Green Alga *Chlamydomonas reinhardtii* Studied by X-ray Absorption Spectroscopy, *Biochemistry*, 48:5042-5049. *co-first author

https://dx.doi.org/10.1021/bi900010b

Content removed due to copyright restrictions.

Previously published in: S. Stripp*, O. Sanganas*, T. Happe and M. Haumann (2009). The Structure of the Active Site H-Cluster of [FeFe] Hydrogenase from the Green Alga *Chlamydomonas reinhardtii* Studied by X-ray Absorption Spectroscopy, *Biochemistry*, 48:5042-5049. *co-first author

https://dx.doi.org/10.1021/bi900010b

Content removed due to copyright restrictions.

Previously published in: S. Stripp*, O. Sanganas*, T. Happe and M. Haumann (2009). The Structure of the Active Site H-Cluster of [FeFe] Hydrogenase from the Green Alga *Chlamydomonas reinhardtii* Studied by X-ray Absorption Spectroscopy, *Biochemistry*, 48:5042-5049. *co-first author

https://dx.doi.org/10.1021/bi900010b

Content removed due to copyright restrictions.

Previously published in: S. Stripp*, O. Sanganas*, T. Happe and M. Haumann (2009). The Structure of the Active Site H-Cluster of [FeFe] Hydrogenase from the Green Alga *Chlamydomonas reinhardtii* Studied by X-ray Absorption Spectroscopy, *Biochemistry*, 48:5042-5049. *co-first author

https://dx.doi.org/10.1021/bi900010b

Content removed due to copyright restrictions.

Previously published in: S. Stripp*, O. Sanganas*, T. Happe and M. Haumann (2009). The Structure of the Active Site H-Cluster of [FeFe] Hydrogenase from the Green Alga *Chlamydomonas reinhardtii* Studied by X-ray Absorption Spectroscopy, *Biochemistry*, 48:5042-5049. *co-first author

https://dx.doi.org/10.1021/bi900010b

Content removed due to copyright restrictions.

Previously published in: S. Stripp*, O. Sanganas*, T. Happe and M. Haumann (2009). The Structure of the Active Site H-Cluster of [FeFe] Hydrogenase from the Green Alga *Chlamydomonas reinhardtii* Studied by X-ray Absorption Spectroscopy, *Biochemistry*, 48:5042-5049. *co-first author

https://dx.doi.org/10.1021/bi900010b

Content removed due to copyright restrictions.

Previously published in: S. Stripp*, O. Sanganas*, T. Happe and M. Haumann (2009). The Structure of the Active Site H-Cluster of [FeFe] Hydrogenase from the Green Alga *Chlamydomonas reinhardtii* Studied by X-ray Absorption Spectroscopy, *Biochemistry*, 48:5042-5049. *co-first author

https://dx.doi.org/10.1021/bi900010b

Content removed due to copyright restrictions.

Previously published in: S. Stripp*, O. Sanganas*, T. Happe and M. Haumann (2009). The Structure of the Active Site H-Cluster of [FeFe] Hydrogenase from the Green Alga *Chlamydomonas reinhardtii* Studied by X-ray Absorption Spectroscopy, *Biochemistry*, 48:5042-5049. *co-first author

https://dx.doi.org/10.1021/bi900010b

Content removed due to copyright restrictions.

Previously published in: S. Stripp*, O. Sanganas*, T. Happe and M. Haumann (2009). The Structure of the Active Site H-Cluster of [FeFe] Hydrogenase from the Green Alga *Chlamydomonas reinhardtii* Studied by X-ray Absorption Spectroscopy, *Biochemistry*, 48:5042-5049. *co-first author

https://dx.doi.org/10.1021/bi900010b

Content removed due to copyright restrictions.

Previously published in: S. Stripp*, O. Sanganas*, T. Happe and M. Haumann (2009). The Structure of the Active Site H-Cluster of [FeFe] Hydrogenase from the Green Alga *Chlamydomonas reinhardtii* Studied by X-ray Absorption Spectroscopy, *Biochemistry*, 48:5042-5049. *co-first author

https://dx.doi.org/10.1021/bi900010b

Content removed due to copyright restrictions.

Previously published in: S. Stripp*, O. Sanganas*, T. Happe and M. Haumann (2009). The Structure of the Active Site H-Cluster of [FeFe] Hydrogenase from the Green Alga *Chlamydomonas reinhardtii* Studied by X-ray Absorption Spectroscopy, *Biochemistry*, 48:5042-5049. *co-first author

https://dx.doi.org/10.1021/bi900010b

Content removed due to copyright restrictions.

Previously published in: S. Stripp*, O. Sanganas*, T. Happe and M. Haumann (2009). The Structure of the Active Site H-Cluster of [FeFe] Hydrogenase from the Green Alga *Chlamydomonas reinhardtii* Studied by X-ray Absorption Spectroscopy, *Biochemistry*, 48:5042-5049. *co-first author

https://dx.doi.org/10.1021/bi900010b

Content removed due to copyright restrictions.

Previously published in: S. Stripp*, O. Sanganas*, T. Happe and M. Haumann (2009). The Structure of the Active Site H-Cluster of [FeFe] Hydrogenase from the Green Alga *Chlamydomonas reinhardtii* Studied by X-ray Absorption Spectroscopy, *Biochemistry*, 48:5042-5049. *co-first author

https://dx.doi.org/10.1021/bi900010b

Content removed due to copyright restrictions.

Previously published in: S. Stripp*, O. Sanganas*, T. Happe and M. Haumann (2009). The Structure of the Active Site H-Cluster of [FeFe] Hydrogenase from the Green Alga *Chlamydomonas reinhardtii* Studied by X-ray Absorption Spectroscopy, *Biochemistry*, 48:5042-5049. *co-first author

https://dx.doi.org/10.1021/bi900010b

Content removed due to copyright restrictions.

Previously published in: S. Stripp*, O. Sanganas*, T. Happe and M. Haumann (2009). The Structure of the Active Site H-Cluster of [FeFe] Hydrogenase from the Green Alga *Chlamydomonas reinhardtii* Studied by X-ray Absorption Spectroscopy, *Biochemistry*, 48:5042-5049. *co-first author

https://dx.doi.org/10.1021/bi900010b

Content removed due to copyright restrictions.

Previously published in: S. Stripp*, O. Sanganas*, T. Happe and M. Haumann (2009). The Structure of the Active Site H-Cluster of [FeFe] Hydrogenase from the Green Alga *Chlamydomonas reinhardtii* Studied by X-ray Absorption Spectroscopy, *Biochemistry*, 48:5042-5049. *co-first author

https://dx.doi.org/10.1021/bi900010b

Chapter 5

Summary and Outlook

The understanding of the catalytic cycle of hydrogenases is essential for their potential use as hydrogen fuel production catalysts, for example in design cells. This includes the structural and electronic features of all intermediate states as well as the activation and inhibition reactions. Of particular interest are hydrogenases showing specific unusual features such as O_2-tolerance, particularly high activity, or altered redox potentials [Vincent et al., 2005; Friedrich et al., 2011].

X-ray absorption spectroscopy (XAS) is a valuable tool to study metal cofactors in hydrogenase enzymes as it can detect all reaction intermediates and yields element-specific information. The prime advantage of XAS is that interatomic distances can be determined at unprecedented subangstrom resolution. In addition, the metal oxidation state, the site symmetry, and the nature of the surrounding ligands can be derived. In this work, XAS at the Fe and Ni K-edges was employed to study the FeS clusters and the [NiFe] and [FeFe] active sites in various hydrogenases and synthetic model compounds.

A primary goal was the search for structural differences between several standard-type and O_2-tolerant **[NiFe] hydrogenases**. Therefore, O_2-tolerant membrane-bound enzymes (**MBH**) and "standard" O_2-sensitive periplasmic enzymes (**PH**) were compared by XAS:

Fe-EXAFS for the various PH samples consistently revealed 12 Fe−Fe distances of ∼2.7 Å, in line with the expected 2 x [4Fe4S] plus 1 x [3Fe4S] cluster complement (Sections 4.1, 4.2). At variance with the PHs, the O_2-tolerant MBH proteins showed a diminished coordination number of at most 6 Fe−Fe distances of 2.6 – 2.85 Å and up to 4 longer Fe−Fe distances of ∼3.4 Å (Sections 4.1, 4.2). This can be interpreted as an unusual 3Fe+1Fe arrangement of the Fe atoms in the proximal cluster, i.e., three Fe−Fe pairs separated by 2.6 – 2.85 Å and one Fe ion at ∼3.4 Å to the other three . O_2-tolerant MBHs have two additional cysteine residues close to the position of the proximal cluster [Goris et al., 2011], e.g., Cys19 and Cys120 in the MBH of *R. eutropha*.

The XAS results were in agreement with the binding of the extra cysteines to the proximal cluster (Sections 4.1, 4.2).

Recently, crystal structures of three O_2-tolerant MBHs have become available [Fritsch et al., 2011b; Shomura et al., 2011; Volbeda et al., 2012, 2013]. The structures have confirmed the 3Fe+1Fe arrangement of the Fe atoms in the proximal cluster, which is a new [4Fe3S] type, and, in agreement with our published data [Fritsch et al., 2011a], also showed the coordination of its Fe atoms by the two additional cysteines (Figure 5.1) [Fritsch et al., 2014; Frielingsdorf et al., 2014]. Further XAS studies were carried out to compare wild-type MBHs and enzymes, in which the additional cysteines have been mutated to glycines (Sections 4.1, 4.2). Broadly speaking, Cys→Gly conversion changed the proximal cluster back to a structure close to a conventional [4Fe4S] site. This corroborated the essential character of the additional cysteines for formation of a [4Fe3S] cluster.

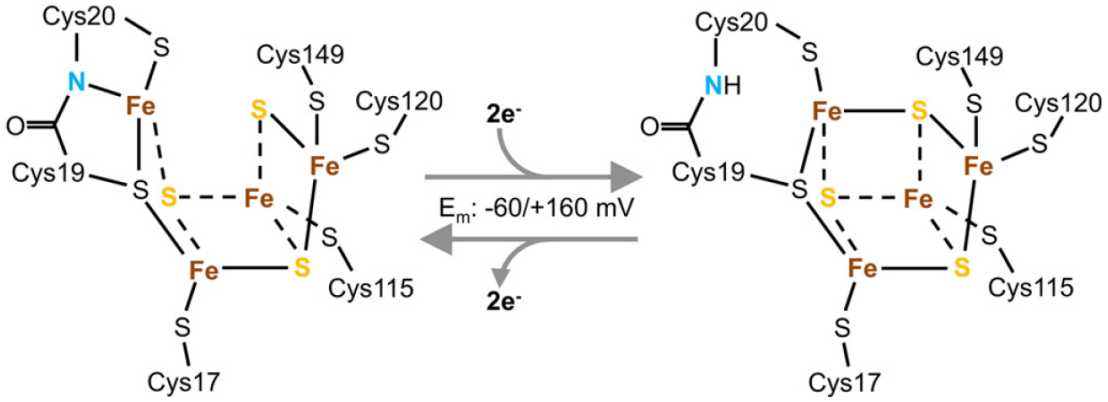

Figure 5.1: Structure of the proximal [4Fe3S] cluster in MBH enzymes, e.g., from *R. eutropha*, and the possible structural changes upon redox transitions. Two electrons can be transferred within a very narrow midpoint potential (E_m) range. Dashed lines indicate the more remote Fe and S atoms of the 3Fe+1Fe arrangement; from [Fritsch et al., 2014].

Fe-XANES data have revealed considerably more oxidized Fe in all oxidized MBH samples (Sections 4.1, 4.2), supporting a higher oxidation state and oxidative transitions of the proximal cluster at variance with the [4Fe4S] cluster in the PHs [Saggu et al., 2010b; Pandelia et al., 2011; Roessler et al., 2012]. In conclusion, recent EPR and FTIR studies [Saggu et al., 2009; Yoon et al., 2009; Saggu et al., 2010b; Lukey et al., 2010; Lenz et al., 2010; Pandelia et al., 2010a,b, 2011; Goris et al., 2011], crystal structures [Fritsch et al., 2011b; Shomura et al., 2011; Volbeda et al., 2012, 2013], and our XAS results (Sections 4.1, 4.2) have shown that the modified proximal [4Fe3S] cluster is

essential for O_2-tolerance in the MBHs. The surplus electron donation capacity of the proximal cluster possibly explains why the Ni-B state of the [NiFe] active site is favored over Ni-A prevailing in the PHs [Cracknell et al., 2009; Goris et al., 2011; Pandelia et al., 2011]. In the MBHs, O_2 may be fully reduced (to H_2O) so that potentially harmful reactive oxygen species (ROS) can be safely disposed.

In summary, we have shown that **Fe-XAS** can detect the modified proximal [4Fe3S] cluster both in crystallized MBHs and also in those enzymes, for which crystal structures are not yet available. In addition, structural changes at the proximal cluster in response to mutations also are detectable.

Our **Ni-XAS** studies indicated a similar coordination of the [NiFe] active site, in both MBH and PH proteins, with Ni surrounded by the thiolate sulfurs of four conserved cysteines (Section 4.1). However, more subtle structural differences seem to exist between MBHs and PHs. The Ni-B state of the O_2-tolerant MBHs shows a longer Ni−O bond, probably due to a bridging OH^- group, than the Ni-A state of standard hydrogenases. Further, Ni-B in the MBHs shows longer and more diverse Ni−S bonds and a shorter Ni−Fe distance. This suggests weaker binding of the O_2 species (OH^-) to Ni in the Ni-B state and may be related to the faster activation of Ni-B in the MBHs compared to Ni-A and Ni-B in the PHs. Consistently and in agreement with other studies, Ni-A was not found in the MBHs, and its absence seems to be crucial for O_2-tolerant H_2 catalysis.

Although crystal structures of several redox states and extensive spectroscopic data are available, even for standard hydrogenases, several questions concerning the O_2-inactivation, the mechanism of H_2 catalysis at the [NiFe] active site, the electronic and molecular structures of the [NiFe] active site remain. This is true in particular for less stable intermediate states that are not easily populated in protein samples. Our XAS results suggest that, besides of Ni-A and Ni-B, several further oxidized [NiFe] species exist in MBHs and PHs. Understanding the role of these states, in particular the distribution of O_2 species around the active sites, require further XAS studies on well defined [NiFe] hydrogenase samples.

The O_2-tolerant **regulatory [NiFe] hydrogenase (RH)** is special in showing a complex protein composition (Section 4.3). Four constructs of the H_2-sensing RH of *R. eutropha* differing in their subunit complement were investigated by Ni- and Fe-XAS. H_2 activation and near-quantitative formation of the EPR-detectable Ni^{III}-C state of the [NiFe] active site in HoxC as well as the reduction of several Fe ions of FeS clusters in HoxB were observed for all samples. Therefore, a tetrameric structure, the C-terminal extension of HoxB, or the HoxJ protein histidine kinase are not necessary for a functional active site. The light-induced formation of the Ni-L state was also possible in all constructs.

The distal FeS cluster is presumably missing in the C-terminally truncated construct RH_{stop}, which has a standard-like [NiFe] active site with four S from cysteines at the Ni, while RH-HoxJ complexes have less direct S ligands and additional O bonds at the Ni. The FeS clusters in the RH may not be of the standard [4Fe4S] or [3Fe4S] types. Our XAS results may favor two [2Fe2S] cluster in the proximal and medial position and one [4Fe-3O-3S] species as distal cluster. However, further investigations are needed to clarify the structures of the FeS clusters in the RH. In general, HoxBC dimerization and HoxJ binding stabilizes the [NiFe] active site coordination and the FeS clusters but does not affect the formation of the Ni-C state, which is similar in all constructs [Buhrke et al., 2005a; Gebler et al., 2007]. The possible quantitative preparation of both states makes the RH an ideal candidate to apply advanced X-ray spectroscopy techniques in the future. The nature of the FeS clusters, their role concerning the O_2-tolerance and O_2-reduction without the Ni-A or Ni-B state, and the reasons for the unusual oxidized Ni^{II} silent ready state should be further studied by spectroscopic methods.

The O_2-tolerant NAD^+-reducing **soluble [NiFe] hydrogenase (SH)** from *R. eutropha* H16 usually consists of six conserved subunits $HoxHYFUI_2$ harboring the [NiFe] active site and several FeS clusters distributed within these subunits. For the first time, the smallest active subcomplex HoxHY containing only the heterodimeric hydrogenase module HoxHY was investigated by XAS (Section 4.4). The focus was the determination of the nature of the solely present FeS cluster in the HoxY subunit and deeper insight into the [NiFe] active site environment. Our Ni-XAS results suggest four S ligands of conserved cysteines and one O ligand, probably in a teminal position, at the Ni. The large distance deviation in the Ni−S bonds point to a high heterogeneity in the samples. The Fe-XAS suggests C(=O/N) and S ligands at the Fe of the [NiFe] active site as well as the Fe in the FeS cluster. From the EXAFS simulations, in combination with the TXRF metal quantification data, a [4Fe4S] cluster in HoxY in the dominant protein sample fraction is the most probable conclusion. A minor species may have a modified [4Fe-nS-nO] unit present. Although the situation is similar to the [FeFe] hydrogenase from the green alga *C. reinhardtii*, where only the H-cluster is present, due to the lower metal content and, therefore, the limited measurement range a separation of the individual Fe−Fe distances was not possible.

Synthetic nickel model compounds, which mimic relevant features of hydrogenases, and the **soluble hydrogenase (SH)** of *R. eutropha* were studied by resonant inelastic X-ray scattering (RIXS) to evaluate the feasibility of advanced X-ray spectroscopy (Section 4.5). As the structure of the synthetic models is well known, their spectroscopic data can be compared to spectra of biological samples. Our published XAS and XES studies show the possibility to gain L-edge type spectra with direct information on d orbitals from resonant inelastic X-ray scattering (RIXS) experiments using K-edge energies. Further, the investigated model compounds provided reference data of Ni^{II} in varying coordination environments.

In the absence of additional FeS clusters, the **[FeFe] hydrogenase** from the green alga *C. reinhardtii* (*Cr*HydA1) binds only the H-cluster and is the smallest known hydrogenase. Therefore, a detailed investigation of the minimal catalytically active unit for H_2 production was feasible (Section 4.6). For the first time, extended-range XAS at the Fe K-edge to particularly high energy values ($k = 19.5\,\text{Å}^{-1}$) was applied to *Cr*HydA1 to study the site geometry and electronic configuration of the H-cluster. The data revealed that the general structural organization of the H-cluster in *Cr*HydA1 is overall similar to the one in bacterial [FeFe] hydrogenases, with a $[4Fe4S]_H$ cluster and a diiron $2Fe_H$ site. This result is consistent with EPR and FTIR data [Kamp et al., 2008; von Abendroth et al., 2008]. The absence of relay FeS clusters in *Cr*HydA1 facilitated the precise determination of the Fe−ligand distances and of the Fe−Fe distances individually for the $[4Fe4S]_H$ cluster and the $2Fe_H$ site. These results (Section 4.6) and further investigations on *Cr*HydA1 [Stripp et al., 2009; Czech et al., 2011] have been published.

Bond length changes at the diiron site upon CO and H_2 exposure were detected for the first time. Treatment with H_2 led to a slight oxidation of the iron in $2Fe_H$ without significant variations in the interatomic distances, suggesting that no additional ligand was bound to $2Fe_H$. CO exposure elongated the Fe−Fe distance in $2Fe_H$ and increased the coordination number for C(=O) ligands due to binding of exogenous CO at Fe_d. This is consistent with studies by other groups [Peters, 1999; Lemon and Peters, 1999; Nicolet et al., 2002; Kamp et al., 2008; Stripp et al., 2009; Czech et al., 2011; Winkler et al., 2013]. The blocking of the open binding site at Fe_d likely is the reason for CO-inactivation of *Cr*HydA1. Our XAS studies showed the structural changes on an atomic level at the H-cluster during H_2 production and led to further extensive investigations of the catalytic cycle of *Cr*HydA1.

References

Adams, M. W. (1990). The structure and mechanism of iron-hydrogenases. *Biochimica et Biophysica Acta (BBA) - Bioenergetics*, 1020(2):115–145.

Akhmanova, A., Voncken, F., van Alen, T., van Hoek, A., Boxma, B., Vogels, G., Veenhuis, M., and Hackstein, J. H. (1998). A hydrogenosome with a genome. *Nature*, 396(6711):527–528.

Albracht, S. P. J. (1994). Nickel hydrogenases: In search of the active site. *Biochimica et Biophysica Acta (BBA) - Bioenergetics*, 1188(3):167–204.

Ankudinov, A. L. and Rehr, J. J. (2003). Development of XAFS theory. *Journal of Synchrotron Radiation*, 10(5):366–368.

Armstrong, F. H., Artero, V., Dau, H., Friedrich, B., Happe, T., Kurz, P., Lubitz, W., and Rogner, M. (2012). Biological and bio-inspired solar dihydrogen production. In Anton, C. and Steinicke, H., editors, *Bioenergy - Chances and Limits*, pages 63–76. German National Academy of Science Leopoldina, Halle (Saale).

Bagley, K. A., Garderen, C. J. V., Chen, M., Duin, E. C., Albracht, S. P., and Woodruff, W. H. (1994). Infrared studies on the interaction of carbon monoxide with divalent nickel in hydrogenase from *Chromatium vinosum*. *Biochemistry*, 33(31):9229–9236.

Beinert, H., Holm, R. H., and Munck, E. (1997). Iron-sulfur clusters: Nature's modular, multipurpose structures. *Science*, 277(5326):653–659.

Berggren, G., Adamska, A., Lambertz, C., Simmons, T. R., Esselborn, J., Atta, M., Gambarelli, S., Mouesca, J.-M., Reijerse, E., Lubitz, W., Happe, T., Artero, V., and Fontecave, M. (2013). Biomimetic assembly and activation of [FeFe]-hydrogenases. *Nature*, 499(7456):66–69.

Bernhard, M., Buhrke, T., Bleijlevens, B., Lacey, A. L. D., Fernandez, V. M., Albracht, S. P. J., and Friedrich, B. (2001). The H_2 sensor of *Ralstonia eutropha*: Biochemical characteristics, spectroscopic properties, and its interaction with a histidine protein kinase. *Journal of Biological Chemistry*, 276(19):15592–15597.

Bleijlevens, B., Faber, B., and Albracht, S. (2001). The [NiFe] hydrogenase from *Allochromatium vinosum* studied in EPR-detectable states: H/D exchange experiments that yield new information about the structure of the active site. *JBIC Journal of Biological Inorganic Chemistry*, 6(8):763–769.

Brecht, M., van Gastel, M., Buhrke, T., Friedrich, B., and Lubitz, W. (2003). Direct detection of a hydrogen ligand in the [NiFe] center of the regulatory H_2-sensing hydrogenase from *Ralstonia eutropha* in its reduced state by HYSCORE and ENDOR spectroscopy. *Journal of the American Chemical Society*, 125(43):13075–13083.

Buhrke, T., Lenz, O., Krauss, N., and Friedrich, B. (2005a). Oxygen tolerance of the H_2-sensing [NiFe] hydrogenase from *Ralstonia eutropha* H16 is based on limited access of oxygen to the active site. *Journal of Biological Chemistry*, 280(25):23791–23796.

Buhrke, T., Lenz, O., Porthun, A., and Friedrich, B. (2004). The H_2-sensing complex of *Ralstonia eutropha*: Interaction between a regulatory [NiFe] hydrogenase and a histidine protein kinase. *Molecular Microbiology*, 51(6):1677–1689.

Buhrke, T., Loscher, S., Lenz, O., Schlodder, E., Zebger, I., Andersen, L. K., Hildebrandt, P., Meyer-Klaucke, W., Dau, H., Friedrich, B., and Haumann, M. (2005b). Reduction of unusual iron-sulfur clusters in the H_2-sensing regulatory Ni-Fe hydrogenase from *Ralstonia eutropha* H16. *Journal of Biological Chemistry*, 280(20):19488–19495.

Burgdorf, T., Lenz, O., Buhrke, T., van der Linden, E., Jones, A. K., Albracht, S. P., and Friedrich, B. (2005a). [NiFe]-hydrogenases of *Ralstonia eutropha* H16: Modular enzymes for oxygen-tolerant biological hydrogen oxidation. *Journal of Molecular Microbiology and Biotechnology*, 10(2-4):181–196.

Burgdorf, T., Löscher, S., Liebisch, P., der Linden, E. V., Galander, M., Lendzian, F., Meyer-Klaucke, W., Albracht, S. P. J., Friedrich, B., Dau, H., and Haumann, M. (2005b). Structural and oxidation-state changes at its nonstandard Ni-Fe site during activation of the NAD-reducing hydrogenase from *Ralstonia eutropha* detected by X-ray absorption, EPR, and FTIR spectroscopy. *Journal of the American Chemical Society*, 127(2):576–592.

Burgdorf, T., van der Linden, E., Bernhard, M., Yin, Q. Y., Back, J. W., Hartog, A. F., Muijsers, A. O., de Koster, C. G., Albracht, S. P. J., and Friedrich, B. (2005c). The soluble NAD^+-reducing [NiFe]-hydrogenase from *Ralstonia eutropha* H16 consists of six subunits and can be specifically activated by NADPH. *Journal of Bacteriology*, 187(9):3122–3132.

Buurman, G., Shima, S., and Thauer, R. K. (2000). The metal-free hydrogenase from methanogenic archaea: Evidence for a bound cofactor. *FEBS Letters*, 485(2):200–204.

Cammack, R., Frey, M., and Robson, R. (1997). *Hydrogen as a Fuel: Learning from Nature*. Taylor & Francis, London, U.K.

Cracknell, J. A., Wait, A. F., Lenz, O., Friedrich, B., and Armstrong, F. A. (2009). A kinetic and thermodynamic understanding of O_2 tolerance in [NiFe]-hydrogenases. *Proceedings of the National Academy of Sciences*, 106(49):20681–20686.

Czech, I., Silakov, A., Lubitz, W., and Happe, T. (2010). The [FeFe]-hydrogenase maturase HydF from *Clostridium acetobutylicum* contains a CO and CN^- ligated iron cofactor. *FEBS Letters*, 584:638–642.

Czech, I., Stripp, S., Sanganas, O., Leidel, N., Happe, T., and Haumann, M. (2011). The [FeFe]-hydrogenase maturation protein HydF contains a H-cluster like [4Fe4S]-2Fe site. *FEBS Letters*, 585(1):225–230.

Dau, H., Liebisch, P., and Haumann, M. (2003). X-ray absorption spectroscopy to analyze nuclear geometry and electronic structure of biological metal centers–potential and questions examined with special focus on the tetra-nuclear manganese complex of oxygenic photosynthesis. *Analytical and Bioanalytical Chemistry*, 376(5):562–583.

Dau, H., Liebisch, P., and Haumann, M. (2004). The structure of the manganese complex of photosystem II in its dark-stable S_1-state: EXAFS results in relation to recent crystallographic data. *Physical Chemistry Chemical Physics*, 6(20):4781–4792.

De Lacey, A. L., Fernandez, V. M., Rousset, M., and Cammack, R. (2007). Activation and inactivation of hydrogenase function and the catalytic cycle: Spectroelectrochemical studies. *Chemical Reviews*, 107(10):4304–4330.

De Lacey, A. L., Gutierrez-Sanchez, C., Fernandez, V. M., Pacheco, I., and Pereira, I. A. (2008). FTIR spectroelectrochemical characterization of the Ni-Fe-Se hydrogenase from *Desulfovibrio vulgaris* Hildenborough. *JBIC Journal of Biological Inorganic Chemistry*, 13(8):1315–1320.

Dementin, S., Leroux, F., Cournac, L., de Lacey, A. L., Volbeda, A., Leger, C., Burlat, B., Martinez, N., Champ, S., Martin, L., Sanganas, O., Haumann, M., Fernandez, V. M., Guigliarelli, B., Fontecilla-Camps, J. C., and Rousset, M. (2009). Introduction of methionines in the gas channel makes [NiFe] hydrogenase aero-tolerant. *Journal of the American Chemical Society*, 131(29):10156–10164.

Dittmer, J., Iuzzolino, L., Drner, W., Nolting, H. F., Meyer-Klaucke, W., and Dau, H. (1998). A new method for determination of the edge position of X-ray absorption spectra. In Garab, G., editor, *Photosynthesis: Mechanisms and Effects*, volume 2 of *Photosynthesis: Mechanismas and Effects*, pages 1339–1342. Kluwer Academic Publishers, Dortrecht, 1. edition.

Erbes, D. L., King, D., and Gibbs, M. (1979). Inactivation of hydrogenase in cell-free extracts and whole cells of *Chlamydomonas reinhardtii* by oxygen. *Plant Physiology*, 63(6):1138–42.

Evans, R. M., Parkin, A., Roessler, M. M., Murphy, B. J., Adamson, H., Lukey, M. J., Sargent, F., Volbeda, A., Fontecilla-Camps, J. C., and Armstrong, F. A. (2013). Principles of sustained enzymatic hydrogen oxidation in the presence of oxygen - the crucial influence of high potential Fe-S clusters in the electron relay of [NiFe]-hydrogenases. *Journal of the American Chemical Society*, 135(7):2694–2707.

Fichtner, C., Laurich, C., Bothe, E., and Lubitz, W. (2006). Spectroelectrochemical characterization of the [NiFe] hydrogenase of *Desulfovibrio vulgaris* Miyazaki F. *Biochemistry*, 45(32):9706–9716.

Foerster, S. (2003). *EPR Spectroscopic Investigation of the active site of [NiFe] hydrogenase: A contribution to the elucidation of the reaction mechanism.* PhD thesis, Technische Universitat Berlin.

Foerster, S., Stein, M., Brecht, M., Ogata, H., Higuchi, Y., and Lubitz, W. (2003). Single crystal EPR studies of the reduced active site of [NiFe] hydrogenase from *Desulfovibrio vulgaris* Miyazaki F. *Journal of the American Chemical Society*, 125(1):83–93.

Fontecilla-Camps, J., Frey, M., Garcin, E., Hatchikian, C., Montet, Y., Piras, C., Vernede, X., and Volbeda, A. (1997). Hydrogenase: A hydrogen-metabolizing enzyme. What do the crystal structures tell us about its mode of action? *Biochimie*, 79(11):661–666.

Fontecilla-Camps, J. C., Volbeda, A., Cavazza, C., and Nicolet, Y. (2007). Structure/Function relationships of [NiFe]- and [FeFe]-hydrogenases. *Chemical Reviews*, 107(10):4273–4303.

Frey, M. (1998). Nickel-iron hydrogenases: Structural and functional properties. In Hill, H., Sadler, P., and Thomson, A., editors, *Metal Sites in Proteins and Models Redox Centres*, volume 90 of *Structure & Bonding*, pages 97–126. Springer Berlin Heidelberg.

Friedrich, B., Fritsch, J., and Lenz, O. (2011). Oxygen-tolerant hydrogenases in hydrogen-based technologies. *Current Opinion in Biotechnology*, 22:358–364.

Frielingsdorf, S., Fritsch, J., Schmidt, A., Hammer, M., Lowenstein, J., Siebert, E., Pelmenschikov, V., Jaenicke, T., Kalms, J., Rippers, Y., Lendzian, F., Zebger, I., Teutloff, C., Kaupp, M., Bittl, R., Hildebrandt, P., Friedrich, B., Lenz, O., and Scheerer, P. (2014). Reversible [4Fe-3S] cluster morphing in an O_2-tolerant [NiFe] hydrogenase. *Nature Chemical Biology*, advance online publication:–.

Frielingsdorf, S., Schubert, T., Pohlmann, A., Lenz, O., and Friedrich, B. (2011). A trimeric supercomplex of the oxygen-tolerant membrane-bound [NiFe]-hydrogenase from *Ralstonia eutropha* H16. *Biochemistry*, 50(50):10836–10843.

Fritsch, J., Lenz, O., and Friedrich, B. (2013). Structure, function and biosynthesis of O_2-tolerant hydrogenases. *Nature Reviews Microbiology*, 11(2):106–114.

Fritsch, J., Löscher, S., Sanganas, O., Siebert, E., Zebger, I., Stein, M., Ludwig, M., De Lacey, A. L., Dau, H., Friedrich, B., Lenz, O., and Haumann, M. (2011a). [NiFe] and [FeS] cofactors in the membrane-bound hydrogenase of *Ralstonia eutropha* investigated by X-ray absorption spectroscopy: Insights into O_2-tolerant H_2 cleavage. *Biochemistry*, 50(26):5858–69.

Fritsch, J., Scheerer, P., Frielingsdorf, S., Kroschinsky, S., Friedrich, B., Lenz, O., and Spahn, C. M. T. (2011b). The crystal structure of an oxygen-tolerant hydrogenase uncovers a novel iron-sulphur centre. *Nature*, 479(7372):249–252.

Fritsch, J., Siebert, E., Priebe, J., Zebger, I., Lendzian, F., Teutloff, C., Friedrich, B., and Lenz, O. (2014). Rubredoxin-related maturation factor guarantees metal cofactor integrity

during aerobic biosynthesis of membrane-bound [NiFe] hydrogenase. *Journal of Biological Chemistry*, 289(11):7982–7993.

Froimowitz, M. (1993). HyperChem: A software package for computational chemistry and molecular modeling. *Biotechniques*, 14(6):1010–1013.

Garcin, E., Vernede, X., Hatchikian, E., Volbeda, A., Frey, M., and Fontecilla-Camps, J. (1999). The crystal structure of a reduced [NiFeSe] hydrogenase provides an image of the activated catalytic center. *Structure*, 7(5):557–566.

Gebler, A., Burgdorf, T., De Lacey, A. L., Rudiger, O., Martinez-Arias, A., Lenz, O., and Friedrich, B. (2007). Impact of alterations near the [NiFe] active site on the function of the H_2 sensor from *Ralstoniaeutropha*. *FEBS Journal*, 274(1):74–85.

Ghirardi, M. L., Posewitz, M. C., Maness, P.-C., Dubini, A., Yu, J., and Seibert, M. (2007). Hydrogenases and hydrogen photoproduction in oxygenic photosynthetic organisms. *Annual Review of Plant Biology*, 58(1):71–91.

Goldet, G., Brandmayr, C., Stripp, S., Happe, T., Cavazza, C., Fontecilla-Camps, J., and Armstrong, F. (2009). Electrochemical kinetic investigations of the reactions of [FeFe]-hydrogenases with carbon monoxide and oxygen: comparing the importance of gas tunnels and active-site electronic/redox effects. *Journal of the American Chemical Society*, 131:14979–14989.

Goldet, G., Wait, A. F., Cracknell, J. A., Vincent, K. A., Ludwig, M., Lenz, O., Friedrich, B., and Armstrong, F. A. (2008). Hydrogen production under aerobic conditions by membrane-bound hydrogenases from *Ralstonia Species*. *Journal of the American Chemical Society*, 130(33):11106–11113.

Goris, T., Wait, A. F., Saggu, M., Fritsch, J., Heidary, N., Stein, M., Zebger, I., Lendzian, F., Armstrong, F. A., Friedrich, B., and Lenz, O. (2011). A unique iron-sulfur cluster is crucial for oxygen tolerance of a [NiFe]-hydrogenase. *Nature Chemical Biology*, 7(5):310–318.

Gray, C. T. and Gest, H. (1965). Biological formation of molecular hydrogen: A "hydrogen valve" facilitates regulation of anaerobic energy metabolism in many microorganisms. *Science*, 148(3667):186–192.

Grundmeier, A. P. (2011). *The water-oxidizing manganese complex of oxygenic photosynthesis: Structural models based on X-ray absorption spectroscopy*. PhD thesis, Freie Universitat Berlin.

Guiral, M., Aubert, C., and Giudici-Orticoni, M.-T. (2005). Hydrogen metabolism in the hyperthermophilic bacterium *Aquifex aeolicus*. *Biochemical Society Transactions*, 33(Pt 1):22–24.

Haken, H. and Wolf, H. C. (1996). *Atom- und Quantenphysik*. Springer, Berlin/Heidelberg, Germany, 6th edition.

Happe, R. P., Roseboom, W., Pierik, A. J., Albracht, S. P. J., and Bagley, K. A. (1997). Biological activition of hydrogen. *Nature*, 385(6612):126.

Happe, T. and Kaminski, A. (2002). Differential regulation of the Fe-hydrogenase during anaerobic adaptation in the green alga *Chlamydomonas reinhardtii*. *European Journal of Biochemistry*, 269(3):1022–1032.

Happe, T. and Naber, J. D. (1993). Isolation, characterization and N-terminal amino acid sequence of hydrogenase from the green alga *Chlamydomonas reinhardtii*. *European Journal of Biochemistry*, 214(2):475–481.

Hartmann, G., Klein, A., Linder, M., and Thauer, R. (1996). Purification, properties and primary structure of H_2-forming N5, N10-methylenetetrahydromethanopterin dehydrogenase from *Methanococcus thermolithotrophicus*. *Archives of Microbiology*, 165(3):187–193.

Haumann, M., Porthun, A., Buhrke, T., Liebisch, P., Meyer-Klaucke, W., Friedrich, B., and Dau, H. (2003). Hydrogen-induced structural changes at the nickel site of the regulatory [NiFe] hydrogenase from *Ralstonia eutropha* detected by X-ray absorption spectroscopy. *Biochemistry*, 42(37):11004–11015.

Higuchi, Y., Ogata, H., Miki, K., Yasuoka, N., and Yagi, T. (1999). Removal of the bridging ligand atom in the Ni-Fe active site of [NiFe] hydrogenase upon reduction with H_2, as revealed by X-ray structure analysis at 1.4 Å resolution. *Structure*, 7(5):549–557.

Higuchi, Y., Yagi, T., and Yasuoka, N. (1997). Unusual ligand structure in Ni-Fe active center and an additional Mg site in hydrogenase revealed by high resolution X-ray structure analysis. *Structure*, 5(12):1671–1680.

Holtz, C., Kaspari, H., and Klemme, J.-H. (1991). Production and properties of xylanases from thermophilic actinomycetes. *Antonie van Leeuwenhoek*, 59(1):1–7.

Horch, M., Lauterbach, L., Saggu, M., Hildebrandt, P., Lendzian, F., Bittl, R., Lenz, O., and Zebger, I. (2010). Probing the active site of an O_2-tolerant NAD^+-reducing [NiFe]-hydrogenase from *Ralstonia eutropha* H16 by *in situ* EPR and FTIR spectroscopy. *Angewandte Chemie International Edition*, 49(43):8026–8029.

Huyett, J. E., Carepo, M., Pamplona, A., Franco, R., Moura, I., Moura, J. J. G., and Hoffman, B. M. (1997). ^{57}Fe Q-band pulsed ENDOR of the hetero-dinuclear site of nickel hydrogenase: Comparison of the Ni-A, Ni-B, and Ni-C states. *Journal of the American Chemical Society*, 119(39):9291–9292.

Hypercube (2007). HyperChem(TM) Professional, Hypercube, Inc.

Kamp, C., Silakov, A., Winkler, M., Reijerse, E. J., Lubitz, W., and Happe, T. (2008). Isolation and first EPR characterization of the [FeFe]-hydrogenases from green algae. *Biochimica et Biophysica Acta (BBA) - Bioenergetics*, 1777(5):410–416.

Kellers, P., Pandelia, M.-E., Currell, L. J., Gorner, H., and Lubitz, W. (2009). FTIR study on the light sensitivity of the [NiFe] hydrogenase from *Desulfovibrio vulgaris* Miyazaki F: Ni-C to Ni-L photoconversion kinetics of proton rebinding and H/D isotope effect. *Physical Chemistry Chemical Physics*, 11:8680–8683.

Kleihues, L., Lenz, O., Bernhard, M., Buhrke, T., and Friedrich, B. (2000). The H_2 sensor of *Ralstonia eutropha* is a member of the subclass of regulatory [NiFe] hydrogenases. *Journal of Bacteriology*, 182:2716–2724.

Klementiev, K. V. (2005). XANES dactyloscope for windows, freeware: www.desy.de/∼klmn/xanda.html.

Klockenkamper, R. (1996). *Total-Reflection X-Ray Fluorescence Analysis*. Wiley-VCH, London, UK.

Koningsberger, D. C. and Prins, R., e. (1988). *X-Ray Absorption: Principles, Applications, Techniques of EXAFS, SEXAFS and XANES*. John Wiley & Sons, New York/Chichester/Brisbane/Toronto/Singapore.

Lambertz, C., Chernev, P., Klingan, K., Leidel, N., Sigfridsson, K. G. V., Happe, T., and Haumann, M. (2014). Electronic and molecular structures of the active-site H-cluster in [FeFe]-hydrogenase determined by site-selective X-ray spectroscopy and quantum chemical calculations. *Chemical Science*, 5:1187–1203.

Lambertz, C., Leidel, N., Havelius, K. G., Noth, J., Chernev, P., Winkler, M., Happe, T., and Haumann, M. (2011). O_2-reactions at the six-iron active site (H-cluster) in [FeFe]-hydrogenase. *Journal of Biological Chemistry*, 286(47):40614–40623.

Lemon, B. J. and Peters, J. W. (1999). Binding of exogenously added carbon monoxide at the active site of the iron-only hydrogenase (CpI) from *Clostridium pasteurianum*. *Biochemistry*, 38(40):12969–12973.

Lenz, O., Bernhard, M., Buhrke, T., Schwartz, E., and Friedrich, B. (2002). The hydrogen-sensing apparatus in *Ralstonia eutropha*. *Journal of Molecular Microbiology and Biotechnology*, 4(3):255–262.

Lenz, O. and Friedrich, B. (1998). A novel multicomponent regulatory system mediates H_2 sensing in *Alcaligenes eutrophus*. *Proceedings of the National Academy of Sciences of the United States of America*, 95:12474–12479.

Lenz, O., Ludwig, M., Schubert, T., Burstel, I., Ganskow, S., Goris, T., Schwarze, A., and Friedrich, B. (2010). H_2 conversion in the presence of O_2 as performed by the membrane-bound [NiFe]-hydrogenase of *Ralstonia eutropha*. *ChemPhysChem*, 11(6):1107–1119.

Löscher, S. (2007). *X-Ray Absorption Spectroscopy on the Ni-Fe and Fe-S Cofactors of the Oxygen-Tolerant Hydrogenases from Ralstonia eutropha: Variations on a Common Theme*. PhD thesis, Freie Universitat Berlin.

Löscher, S., Burgdorf, T., Zebger, I., Hildebrandt, P., Dau, H., Friedrich, B., and Haumann, M. (2006). Bias from H_2 cleavage to production and coordination changes at the Ni-Fe active site in the NAD^+-reducing hydrogenase from *Ralstonia eutropha*. *Biochemistry*, 45(38):11658–65.

Löscher, S., Schwartz, L., Stein, M., Ott, S., and Haumann, M. (2007). Facilitated hydride binding in an Fe-Fe hydrogenase active-site biomimic revealed by X-ray absorption spectroscopy and DFT calculations. *Inorganic Chemistry*, 46(26):11094–105.

Löscher, S., Zebger, I., Andersen, L. K., Hildebrandt, P., Meyer-Klaucke, W., and Haumann, M. (2005). The structure of the Ni-Fe site in the isolated HoxC subunit of the hydrogen-sensing hydrogenase from *Ralstonia eutropha*. *FEBS Letters*, 579(20):4287–91.

Lubitz, W., Ogata, H., Rudiger, O., and Reijerse, E. (2014). Hydrogenases. *Chemical Reviews*, online publication, DOI: 10.1021/cr4005814(0).

Lubitz, W., Reijerse, E., and van Gastel, M. (2007). [NiFe] and [FeFe] hydrogenases studied by advanced magnetic resonance techniques. *Chemical Reviews*, 107(10):4331–4365.

Lukey, M. J., Parkin, A., Roessler, M. M., Murphy, B. J., Harmer, J., Palmer, T., Sargent, F., and Armstrong, F. A. (2010). How *Escherichia coli* is equipped to oxidize hydrogen under different redox conditions. *Journal of Biological Chemistry*, 285(6):3928–3938.

Lyon, E. J., Shima, S., Boecher, R., Thauer, R. K., Grevels, F.-W., Bill, E., Roseboom, W., and Albracht, S. P. J. (2004a). Carbon monoxide as an intrinsic ligand to iron in the active site of the iron-sulfur-cluster-free hydrogenase H_2-forming methylenetetrahydromethanopterin dehydrogenase as revealed by infrared spectroscopy. *Journal of the American Chemical Society*, 126(43):14239–14248.

Lyon, E. J., Shima, S., Buurman, G., Chowdhuri, S., Batschauer, A., Steinbach, K., and Thauer, R. K. (2004b). UV-A/blue-light inactivation of the metal-free hydrogenase (Hmd) from methanogenic archaea. *European Journal of Biochemistry*, 271(1):195–204.

Madigan, M. T., Martinko, J. M., Stahl, D. A., and Clark, D. P. (2010). *Brock Biology of Microorganisms*. Benjamin Cummings; 13 edition.

Matias, P. M., Soares, C. M., Saraiva, L. M., Coelho, R., Morais, J., Le Gall, J., and Carrondo, M. A. (2001). [NiFe] hydrogenase from *Desulfovibrio desulfuricans* ATCC 27774: Gene sequencing, three-dimensional structure determination and refinement at 1.8 Å and modelling studies of its interaction with the tetrahaem cytochrome c 3. *JBIC Journal of Biological Inorganic Chemistry*, 6(1):63–81.

Medina, M., Hatchikian, E. C., and Cammack, R. (1996). Studies of light-induced nickel EPR signals in hydrogenase: Comparison of enzymes with and without selenium. *Biochimica et Biophysica Acta (BBA) - Bioenergetics*, 1275(3):227–236.

Melis, A. and Happe, T. (2001). Hydrogen production. green algae as a source of energy. *Plant Physiology*, 127(3):740–748.

Montet, Y., Amara, P., Volbeda, A., Vernede, X., Hatchikian, E. C., Field, M. J., Frey, M., and Fontecilla-Camps, J. C. (1997). Gas access to the active site of Ni-Fe hydrogenases probed by X-ray crystallography and molecular dynamics. *Nature Structural and Molecular Biology*, 4(7):523–526.

Mustre de Leon, J., Rehr, J. J., Zabinsky, S. I., and Albers, R. C. (1991). Ab initio curved-wave X-ray-absorption fine structure. *Physcal Review B*, 44(9):4146–4156.

Newville, M. (2004). *Fundamentals of XAFS*. Consortium for Advanced Radiation Sources, University of Chicago, Chicago, USA.

Nicolet, Y., Cavazza, C., and Fontecilla-Camps, J. (2002). Fe-only hydrogenases: Structure, function and evolution. *Journal of Inorganic Biochemistry*, 91(1):1–8.

Nicolet, Y., de Lacey, A. L., Vernde, X., Fernandez, V. M., Hatchikian, E. C., and Fontecilla-Camps, J. C. (2001). Crystallographic and FTIR spectroscopic evidence of changes in Fe coordination upon reduction of the active site of the Fe-only hydrogenase from *Desulfovibrio desulfuricans*. *Journal of the American Chemical Society*, 123(8):1596–1601.

Nicolet, Y., Lemon, B. J., Fontecilla-Camps, J. C., and Peters, J. W. (2000). A novel FeS cluster in Fe-only hydrogenases. *Trends in Biochemical Sciences*, 25(3):138–143.

Nicolet, Y., Piras, C., Legrand, P., Hatchikian, C. E., and Fontecilla-Camps, J. C. (1999). *Desulfovibrio desulfuricans* iron hydrogenase: The structure shows unusual coordination to an active site Fe binuclear center. *Structure*, 7(1):13–23.

Ogata, H., Hirota, S., Nakahara, A., Komori, H., Shibata, N., Kato, T., Kano, K., and Higuchi, Y. (2005). Activation process of [NiFe] hydrogenase elucidated by high-resolution X-ray analyses: Conversion of the ready to the unready state. *Structure*, 13(11):1635–1642.

Ogata, H., Kellers, P., and Lubitz, W. (2010). The crystal structure of the [NiFe] hydrogenase from the photosynthetic bacterium *Allochromatium vinosum*: Characterization of the oxidized enzyme (Ni-A state). *Journal of Molecular Biology*, 402(2):428 – 444.

Pandelia, M.-E., Bykov, D., Izsak, R., Infossi, P., Giudici-Orticoni, M.-T., Bill, E., Neese, F., and Lubitz, W. (2013). Electronic structure of the unique [4Fe-3S] cluster in O_2-tolerant hydrogenases characterized by ^{57}Fe Mössbauer and EPR spectroscopy. *Proceedings of the National Academy of Sciences*, 110(2):483–488.

Pandelia, M.-E., Fourmond, V., Tron-Infossi, P., Lojou, E., Bertrand, P., Leger, C., Giudici-Orticoni, M.-T., and Lubitz, W. (2010a). Membrane-bound hydrogenase I from the hyperthermophilic bacterium *Aquifex aeolicus*: Enzyme activation, redox intermediates and oxygen tolerance. *Journal of the American Chemical Society*, 132(20):6991–7004.

Pandelia, M.-E., Infossi, P., Giudici-Orticoni, M. T., and Lubitz, W. (2010b). The oxygen-tolerant hydrogenase I from *Aquifex aeolicus* weakly interacts with carbon monoxide: An electrochemical and time-resolved FTIR study. *Biochemistry*, 49(41):8873–8881.

Pandelia, M.-E., Infossi, P., Stein, M., Giudici-Orticoni, M.-T., and Lubitz, W. (2012a). Spectroscopic characterization of the key catalytic intermediate Ni-C in the O_2-tolerant [NiFe] hydrogenase I from *Aquifex aeolicus*: Evidence of a weakly bound hydride. *Chemical Communications*, 48:823–825.

Pandelia, M.-E., Lubitz, W., and Nitschke, W. (2012b). Evolution and diversification of group 1 [NiFe] hydrogenases. Is there a phylogenetic marker for O_2-tolerance? *Biochimica et Biophysica Acta (BBA) - Bioenergetics*, 1817(9):1565 – 1575.

Pandelia, M.-E., Nitschke, W., Infossi, P., Giudici-Orticoni, M.-T., Bill, E., and Lubitz, W. (2011). Characterization of a unique [FeS] cluster in the electron transfer chain of the oxygen tolerant [NiFe] hydrogenase from *Aquifex aeolicus*. *Proceedings of the National Academy of Sciences*, 108(15):6097–6102.

Pandelia, M.-E., Ogata, H., Currell, L., Flores, M., and Lubitz, W. (2009). Probing intermediates in the activation cycle of [NiFe] hydrogenase by infrared spectroscopy: The Ni-SI_r state and its light sensitivity. *JBIC Journal of Biological Inorganic Chemistry*, 14(8):1227–1241.

Pandelia, M.-E., Ogata, H., Currell, L. J., Flores, M., and Lubitz, W. (2010c). Inhibition of the [NiFe] hydrogenase from *Desulfovibrio vulgaris* Miyazaki F by carbon monoxide: An FTIR and EPR spectroscopic study. *Biochimica et Biophysica Acta (BBA) - Bioenergetics*, 1797(2):304–313.

Pandey, A. S., Harris, T. V., Giles, L. J., Peters, J. W., and Szilagyi, R. K. (2008). Dithiomethylether as a ligand in the hydrogenase H-cluster. *Journal of the American Chemical Society*, 130(13):4533–4540.

Parkin, A., Bowman, L., Roessler, M. M., Davies, R. A., Palmer, T., Armstrong, F. A., and Sargent, F. (2012). How *Salmonella oxidises* H_2 under aerobic conditions. *FEBS Letters*, 586(5):536–544.

Parkin, A. and Sargent, F. (2012). The hows and whys of aerobic H_2 metabolism. *Current Opinion in Chemical Biology*, 16(12):26–34.

Peters, J. W. (1999). Structure and mechanism of iron-only hydrogenases. *Current Opinion in Structural Biology*, 9(6):670–676.

Peters, J. W., Lanzilotta, W. N., Lemon, B. J., and Seefeldt, L. C. (1998). X-ray crystal structure of the Fe-only hydrogenase (CpI) from *Clostridium pasteurianum* to 1.8 Å resolution. *Science*, 282(5395):1853–1858.

Pierik, A. J., Hulstein, M., Hagen, W. R., and Albracht, S. P. J. (1998a). A low-spin iron with CN and CO as intrinsic ligands forms the core of the active site in [Fe]-hydrogenases. *European Journal of Biochemistry*, 258(2):572–578.

Pierik, A. J., Roseboom, W., Happe, R. P., Bagley, K. A., and Albracht, S. P. J. (1999). Carbon monoxide and cyanide as intrinsic ligands to iron in the active site of [NiFe]-hydrogenases: $NiFe(CN)_2CO$, biology's way to activate H_2. *Journal of Biological Chemistry*, 274(6):3331–3337.

Pierik, A. J., Schmelz, M., Lenz, O., Friedrich, B., and Albracht, S. P. (1998b). Characterization of the active site of a hydrogen sensor from alcaligenes eutrophus. *FEBS letters*, 438(3):231–235.

Pilak, O., Mamat, B., Vogt, S., Hagemeier, C. H., Thauer, R. K., Shima, S., Vonrhein, C., Warkentin, E., and Ermler, U. (2006). The crystal structure of the apoenzyme of the iron-sulphur cluster-free hydrogenase. *Journal of Molecular Biology*, 358(3):798 – 809.

Przybyla, A. E., Robbins, J., Menon, N., and Peck, H. D., J. (1992). Structure-function relationships among the nickel-containing hydrogenases. *FEMS Microbiology Reviews*, 8(2):109–35.

Rehr, J. J. and Albers, R. C. (2000). Theoretical approaches to X-ray absorption fine structure. *Reviews of Modern Physics*, 72(3):621–654.

Rehr, J. J., Kas, J. J., Vila, F. D., Prange, M. P., and Jorissen, K. (2010). Parameter-free calculations of X-ray spectra with FEFF9. *Physical Chemistry Chemical Physics*, 12:5503–5513.

Roessler, M. M., Evans, R. M., Davies, R. A., Harmer, J., and Armstrong, F. A. (2012). EPR spectroscopic studies of the Fe−S clusters in the O_2-tolerant [NiFe]-hydrogenase Hyd-1 from *Escherichia coli* and characterization of the unique [4Fe−3S] cluster by HYSCORE. *Journal of the American Chemical Society*, 134(37):15581–15594.

Roseboom, W., Lacey, A., Fernandez, V., Hatchikian, E., and Albracht, S. (2006). The active site of the [FeFe]-hydrogenase from *Desulfovibrio desulfuricans*. II. Redox properties, light sensitivity and CO-ligand exchange as observed by infrared spectroscopy. *Journal of Biological Inorganic Chemistry*, 11(1):102–118.

Saggu, M., Ludwig, M., Friedrich, B., Hildebrandt, P., Bittl, R., Lendzian, F., Lenz, O., and Zebger, I. (2010a). Impact of amino acid substitutions near the catalytic site on the spectral properties of an O_2-tolerant membrane-bound [NiFe] hydrogenase. *ChemPhysChem*, 11(6):1215–1224.

Saggu, M., Teutloff, C., Ludwig, M., Brecht, M., Pandelia, M.-E., Lenz, O., Friedrich, B., Lubitz, W., Hildebrandt, P., Lendzian, F., and Bittl, R. (2010b). Comparison of the membrane-bound [NiFe] hydrogenases from *R. eutropha* H16 and *D. vulgaris* Miyazaki F in the oxidized ready state by pulsed EPR. *Physical Chemistry Chemical Physics*, 12:2139–2148.

Saggu, M., Zebger, I., Ludwig, M., Lenz, O., Friedrich, B., Hildebrandt, P., and Lendzian, F. (2009). Spectroscopic insights into the oxygen-tolerant membrane-associated [NiFe]-hydrogenase of *Ralstonia eutropha* H16. *Journal of Biological Chemistry*, 184:16264–16276.

Schaefers, F., Mertin, M., and Gorgoi, M. (2007). KMC-1: A high resolution and high flux soft X-ray beamline at BESSY. *Review of Scientific Instruments*, 78(12):1–14.

Schwartz, E. and Friedrich, B. (2003). The H_2-metabolizing prokaryotes. In Dworkin, M., Falkow, S., Rosenberg, E., Schleifer, K.-H., and Stackebrandt, E., editors, *The Prokaryotes*, chapter The prokaryotes: An evolving electronic resource for the microbiological community, pages 496–563. Springer New York.

Shafaat, H. S., Rudiger, O., Ogata, H., and Lubitz, W. (2013). [NiFe] hydrogenases: A common active site for hydrogen metabolism under diverse conditions. *Biochimica et Biophysica Acta (BBA) - Bioenergetics*, 1827(8-9):986–1002.

Shepard, E., McGlynn, S., Bueling, A., Grady-Smith, C., George, S., Winslow, M., Cramer, S., Peters, J., and Broderick, J. (2010). Synthesis of the 2Fe subcluster of the [FeFe]-hydrogenase H cluster on the HydF scaffold. *Proceedings of the National Academy of Sciences of the United States of America*, 107:10448–10453.

Shima, S., Schick, M., and Tamura, H. (2011). Chapter seven - preparation of [Fe]-hydrogenase from methanogenic archaea. In Rosenzweig, A. C. and Ragsdale, S. W., editors, *Methods in Methane Metabolism, Part A*, volume 494 of *Methods in Enzymology*, pages 119 – 137. Academic Press.

Shomura, Y., Yoon, K.-S., Nishihara, H., and Higuchi, Y. (2011). Structural basis for a [4Fe-3S] cluster in the oxygen-tolerant membrane-bound [NiFe]-hydrogenase. *Nature*, 479(7372):253–256.

Siegbahn, P. E. M., Tye, J. W., and Hall, M. B. (2007). Computational studies of [NiFe] and [FeFe] hydrogenases. *Chemical Reviews*, 107(10):4414–4435.

Silakov, A., Wenk, B., Reijerse, E., and Lubitz, W. (2009). ^{14}N HYSCORE investigation of the H-cluster of [FeFe] hydrogenase: Evidence for a nitrogen in the dithiol bridge. *Physical Chemistry Chemical Physics*, 11:6592–6599.

Special Issue on Hydrogenases (2007). American Chemical Society, Washington, DC. *Chemical Reviews*, 107.

Stein, M. (2001). *Insight into the mechanism of [NiFe] Hydrogenase by means of magnetic resonance Experiments and DFT calculations.* PhD thesis, Technische Universitat Berlin.

Stein, M. and Lubitz, W. (2001). DFT calculations of the electronic structure of the paramagnetic states Ni-A, Ni-B and Ni-C of [NiFe] hydrogenase. *Physical Chemistry Chemical Physics*, 13(3):2668–2675.

Stein, M. and Lubitz, W. (2002). Quantum chemical calculations of [NiFe] hydrogenase. *Current Opinion in Chemical Biology*, 6(2):243–249.

Stephenson, M. and Stickland, L. H. (1931). Hydrogenase: A bacterial enzyme activating molecular hydrogen: The properties of the enzyme. *Biochem. J.*, 25(1):205–214.

Stohr, J. (1992). *NEXAFS spectroscopy*, volume 25 of *Springer series in surface sciences*. Springer Verlag, Berlin/Heidelberg, Germany.

Stripp, S. T., Goldet, G., Brandmayr, C., Sanganas, O., Vincent, K. A., Haumann, M., Armstrong, F. A., and Happe, T. (2009). How oxygen attacks [FeFe] hydrogenases from photosynthetic organisms. *Proceedings of the National Academy of Sciences of the United States of America*, 106(41):17331–6.

Teixeira, M., Moura, I., Xavier, A. V., Huynh, B. H., DerVartanian, D. V., Peck, H. D., LeGall, J., and Moura, J. J. (1985). Electron paramagnetic resonance studies on the mechanism of activation and the catalytic cycle of the nickel-containing hydrogenase from *Desulfovibrio gigas*. *Journal of Biological Chemistry*, 260(15):8942–8950.

Teo, B. (1986). *EXAFS: Basic Principles and Data Analysis*. Springer Verlag, Berlin/Heidelberg, Germany.

Teo, B.-K. and Joy, D. C. (1981). *EXAFS Spectroscopy*. Plenum Press, New York, USA.

Thauer, R. K., Klein, A. R., and Hartmann, G. C. (1996). Reactions with molecular hydrogen in microorganisms: Evidence for a purely organic hydrogenation catalyst. *Chemical Reviews*, 96(7):3031–3042.

Tomic, S., Searle, B. G., Wander, A., Harrison, M. N., Dent, A. J., Mosselmans, J. F. W., and Inglesfield, J. E. (2005). New tools for the analysis of EXAFS: The DL EXCURV package. *CCLRC Technical Report DL-TR-2005-001*, ISSN 1362-0207.

van der Linden, E., Faber, B. W., Bleijlevens, B., Burgdorf, T., Bernhard, M., Friedrich, B., and Albracht, S. P. J. (2004). Selective release and function of one of the two FMN groups in the cytoplasmic NAD^+-reducing [NiFe]-hydrogenase from *Ralstonia eutropha*. *European Journal of Biochemistry*, 271(4):801–808.

van der Zwaan, J., Albracht, S., Fontijn, R., and Slater, E. (1985). Monovalent nickel in hydrogenase from *Chromatium vinosum*: Light sensitivity and evidence for direct interaction with hydrogen. *FEBS Letters*, 179(2):271 – 277.

Vignais, P. M. and Billoud, B. (2007). Occurrence, classification, and biological function of hydrogenases: An overview. *Chemical Reviews*, 107(10):4206–4272.

Vignais, P. M., Billoud, B., and Meyer, J. (2001). Classification and phylogeny of hydrogenases. *FEMS Microbiology Reviews*, 25(4):455–501.

Vignais, P. M. and Colbeau, A. (2004). Molecular biology of microbial hydrogenases. *Current Issues of Molecular Biology*, 6:159–188.

Vincent, K. A., Parkin, A., and Armstrong, F. A. (2007). Investigating and exploiting the electrocatalytic properties of hydrogenases. *Chemical Reviews*, 107(10):4366–4413.

Vincent, K. A., Parkin, A., Lenz, O., Albracht, S. P. J., Fontecilla-Camps, J. C., Cammack, R., Friedrich, B., and Armstrong, F. A. (2005). Electrochemical definitions of O_2 sensitivity and oxidative inactivation in hydrogenases. *Journal of the American Chemical Society*, 127(51):18179–18189.

Volbeda, A., Amara, P., Darnault, C., Mouesca, J.-M., Parkin, A., Roessler, M. M., Armstrong, F. A., and Fontecilla-Camps, J. C. (2012). X-ray crystallographic and computational studies of the O_2-tolerant [NiFe]-hydrogenase 1 from *Escherichia coli*. *Proceedings of the National Academy of Sciences*, 109(14):5305–5310.

Volbeda, A., Charon, M. H., Piras, C., Hatchikian, E. C., Frey, M., and Fontecilla-Camps, J. C. (1995). Crystal structure of the nickel-iron hydrogenase from *Desulfovibrio gigas*. *Nature*, 373(6515):580–587.

Volbeda, A., Darnault, C., Parkin, A., Sargent, F., Armstrong, F., and Fontecilla-Camps, J. (2013). Crystal structure of the O_2-tolerant membrane-bound hydrogenase 1 from *Escherichia coli* in complex with its cognate cytochrome b. *Structure*, 21(1):184–190.

Volbeda, A., Fontecilla-Camps, J. C., and Frey, M. (1996). Novel metal sites in protein structures. *Current Opinion in Structural Biology*, 6(6):804–812.

Volbeda, A., Martin, L., Cavazza, C., Matho, M., Faber, B. W., Roseboom, W., Albracht, S. P. J., Garcin, E., Rousset, M., and Fontecilla-Camps, J. C. (2005). Structural differences between the ready and unready oxidized states of [NiFe] hydrogenases. *Journal of Biological Inorganic Chemistry*, 10(3):239–249.

von Abendroth, G., Stripp, S., Silakov, A., Croux, C., Soucaille, P., Girbal, L., and Happe, T. (2008). Optimized over-expression of [FeFe] hydrogenases with high specific activity in *Clostridium acetobutylicum*. *International Journal of Hydrogen Energy*, 33(21):6076–6081.

Winkler, M., Esselborn, J., and Happe, T. (2013). Molecular basis of [FeFe]-hydrogenase function: An insight into the complex interplay between protein and catalytic cofactor. *Biochimica et Biophysica Acta*, 1827:874–985.

Yoon, K., Sakai, Y., Tsukada, N., Fujisawa, K., and Nishihara, H. (2009). Purification and biochemical characterization of a membrane-bound [NiFe]-hydrogenase from a hydrogen-oxidizing, lithotrophic bacterium, *Hydrogenophaga sp.* AH-24. *FEMS Microbiology Letters*, 290(1):114–120.

Zabinsky, S. I., Rehr, J. J., Ankudinov, A., Albers, R. C., and Eller, M. J. (1995). Multiple-scattering calculations of X-ray-absorption spectra. *Physical Review B*, 52(4):2995–3009.

Zirngibl, C., van Dongen, W., Schworer, B., Von Bunau, R., Richter, M., Klein, A., and Thauer, R. K. (1992). H_2-forming methylenetetrahydromethanopterin dehydrogenase, a novel type of hydrogenase without iron-sulfur clusters in methanogenic archaea. *European Journal of Biochemistry*, 208(2):511–520.

Abstract

Hydrogenases of the [NiFe] and [FeFe] types catalyze reversible hydrogen turnover and are of prime interest for renewable energy applications. Important questions address the reaction cycle mechanisms and the unusual oxygen-tolerance of certain hydrogenases. Achieving O_2-tolerance also in synthetic catalysts would be a major step towards a hydrogen economy (**Chapters 1, 2**).

Here, the main task was the comparison of molecular and electronic structures of metal cofactors in O_2-tolerant and O_2-inhibited [NiFe] hydrogenases and in an irreversibly O_2-deactivated [FeFe] hydrogenase using synchrotron-based X-ray absorption spectroscopy (XAS) methods (**Chapter 3**). The primary goal was the characterization of differences at their metal cofactors.

Comparative Ni- and Fe-XAS studies on O_2-tolerant membrane-bound (MBH) and O_2-sensitive periplasmic (PH) [NiFe] hydrogenases from six organisms (**Chapters 4.1, 4.2**) have revealed globally similar coordination of the nickel, but also altered locations of reduced oxygen species at the [NiFe] cofactor in the MBHs. The latter may be related to an alternative mechanism for disposal of reactive oxygen species. A highlight was the detection of altered structures of FeS clusters in the MBHs, assigned to an unusual 3+1 arrangement of iron in the proximal cluster, as confirmed by MBH crystal structures disclosing a unique [4Fe3S] proximal cluster. XAS showed that cysteine ligand mutation can revert the [4Fe3S] to a normal [4Fe4S] cluster. The [4Fe3S] cluster and altered O_2-handling at the active site may synergetically provide O_2-tolerance in the MBHs.

Regulatory [NiFe] hydrogenases (RH) are H_2-sensors and comprise hydrogenase, PAS, and kinase domains. XAS on the O_2-tolerant RH from *R. eutropha* has revealed considerable plasticity at the [NiFe] site with respect to oxidative modifications and altered FeS clusters undergoing EPR-silent redox transitions (**Chapter 4.3**). In a truncated RH construct one FeS cluster is lost. Our data suggest unusual structural and redox FeS cluster properties in the RH, but a rather standard [NiFe] site. However, these features are influenced by the protein composition in a still undefined way. Further studies are required to clarify the nature of the FeS clusters in the RH.

Soluble [NiFe] hydrogenases (SH) catalyze reversible H_2-turnover and have a hydrogenase and a diaphorase domain. A minimal active construct with only the hydrogenase domain of the *R. eutropha* SH was studied by XAS (**Chapter 4.4**), which has revealed a single [4Fe4S] cluster in the HoxY subunit. This cluster in concert with a FMN in HoxY likely is crucial for electron transfer.

Experimentally demanding high-resolution X-ray absorption and emission methods, e.g., resonant inelastic X-ray scattering (RIXS), facilitate electronic structure determination. First Ni RIXS experiments were carried out on synthetic compounds and the SH of *R. eutropha* (**Chapter 4.5**). This revealed the applicability of RIXS to dilute protein samples and the superior resolution of electronic transitions.

The [FeFe] hydrogenase HydA1 from green algae is the most active H_2-producer in nature (**Chapter 4.6**). Its active site (H-cluster) consists of a $[4Fe4S]_H$ cluster connected to a diiron unit, $2Fe_H$. Extended-range Fe-XAS on HydA1 from *C. reinhardtii* facilitated determination of bond-lengths and Fe−Fe distances individually for the two subcomplexes and detection of structural changes upon exposure to O_2 or CO. These studies have paved the way for more detailed X-ray spectroscopy studies on HydA1, which have been carried out in the meantime.

In conclusion, extensive XAS studies were conducted on various O_2-tolerant and O_2-sensitive [NiFe] and [FeFe] hydrogenases from different organisms. They have provided deeper insight into the metal cofactor structures and possible reasons for their unusual catalytic behavior (**Chapter 5**). Advanced X-ray spectroscopy methods were further developed. However, firmly establishing the molecular basis of the H_2 and O_2 chemistry in all enzymes requires further studies. The application of high-resolution X-ray spectroscopy methods will contribute to clarify these questions.

Zusammenfassung

[NiFe] und [FeFe] Hydrogenasen katalysieren die reversible Wasserstoffbildung und sind von besonderem Interesse für erneuerbare Energie Anwendungen. Offene Fragen bestehen zu Reaktionsmechanismen und der ungewöhnlichen Sauerstofftoleranz macher Hydrogenasen. O_2-Toleranz der H_2-Katalyse ist ein wichtiger Faktor für eine künftige Wasserstoff Ökonomie (**Kapitel 1, 2**).

Die Aufgabe hier war die vergleichende Untersuchung der molekularen und elektronischen Struktur von Metall-Kofaktoren in O_2-toleranten und O_2-inhibierten [NiFe] Hydrogenasen und in einer O_2-deaktivierten [FeFe] Hydrogenase mittels Synchrotron-basierter Röntgenabsorptions-Spektroskopie (XAS) (**Kapitel 3**) zur Herausarbeitung funktionell relevanter Unterschiede.

Vergleichende Ni- und Fe-XAS Untersuchungen an O_2-toleranten Membran-gebundenen (MBH) und O_2-sensitiven (PH) [NiFe] Hydrogenasen aus sechs Organismen (**Kapitel 4.1, 4.2**) zeigten ähnliche Ni Bindestellen aber eine veränderte Anordnung von Sauerstoffspezies am [NiFe] Kofaktor in den MBHs. Dies legt einen alternativen Weg für die „Entschärfung“ reaktiver Sauerstoffspezies nahe. Besonders interessant war die Detektion von veränderten FeS Cluster Strukturen in den MBHs, interpretiert als 3+1 Anordnung der Eisenatome im proximalen Cluster, was in MBH Kristallen, die einen neuen proximalen [4Fe3S] Cluster zeigen, bestätigt wird. XAS hat gezeigt, dass der [4Fe3S] Cluster durch Mutagenese in einen [4Fe4S] Cluster konvertiert wird. Der [4Fe3S] Cluster und eine veränderte O_2-Chemie könnten synergetisch die O_2-Toleranz der MBHs verantworten.

Regulatorische [NiFe] Hydrogenasen (RH) sind H_2-Sensoren bestehend aus Hydrogenase, PAS, und Kinase Domänen. XAS an der O_2-toleranten RH aus *R. eutropha* zeigte die Plastizität des [NiFe] Kofaktors für oxidative Modifikation und veränderte FeS Cluster mit EPR-unsichtbaren Redox-Übergängen (**Kapitel 4.3**). In einem verkürzten RH Konstrukt geht ein FeS Cluster verloren. Unsere Daten zeigen ungewöhnliche Eigenschaften der FeS Cluster und einen normalen [NiFe] Kofaktor, die jedoch in bisher unklarer Weise durch den Aufbau des Proteinkomplexes beeinflusst werden. Weitere Studien sind nötig zur Aufklärung der FeS Cluster in der RH.

Lösliche [NiFe] Hydrogenasen (SH) sind reversible H_2-Bildner und haben Hydrogenase und Diaphorase Domänen. XAS an einem aktiven Minimalkonstrukt, der Hydrogenase Domäne der SH aus *R. eutropha* (**Kapitel 4.4**), zeigte einen einzigen [4Fe4S] Cluster in der HoxY Untereinheit. Dieser Cluster und ein FMN in HoxY sind wahrscheinlich essentiell für den Elektronentransfer.

Anspruchsvolle hochauflösende Röntgenabsorptions und -emissions Methoden wie resonante inelastische Röntgenstreuung (RIXS) dienen der elektronischen Strukturbestimmung. Erste Ni RIXS Experimente an synthetischen Komplexen und der SH aus *R. eutropha* (**Kapitel 4.5**) belegten die Anwendbarkeit der Methode auf verdünnte Proteinproben und die gute Auflösung elektronischer Übergänge.

Die [FeFe] Hydrogenase HydA1 aus Grünalgen ist der aktivste H_2-Produzent in der Natur (**Kapitel 4.6**). Das aktive Zentrum (H-cluster) besteht aus einem $[4Fe4S]_H$ Cluster, der an ein Zweieisen-Zentrum ($2Fe_H$) bindet. Fe-XAS mit besonders hohen Anregungsenergien an HydA1 aus *C. reinhardtii* erlaubte die Bestimmung von individuellen Bindungslängen und Metallabständen in den beiden Subkomplexen und die Detektion von Änderungen unter O_2 oder CO. Diese Ergebnisse haben den Weg bereitet für die später ausgeführten detaillierteren Röntgenstudien an HydA1.

Zusammenfassend ist festzustellen, dass umfangreiche XAS Studien an O_2-toleranten und O_2-sensitiven [NiFe] und [FeFe] Hydrogenasen aus mehreren Organismen durchgeführt wurden, die vertiefte Einblicke in die Strukturen der Metall-Kofaktoren und mögliche Gründe für die ungewöhnlichen katalytischen Eigenschaften geliefert haben (**Kapitel 5**). Fortgeschrittene Röntgenmethoden wurden weiterentwickelt. Zur vollständigen Aufklärung der molekularen Grundlagen der H_2- und O_2-Reaktionen in den verschiedenen Systemen sind jedoch weitere Untersuchungen nötig, besonders auch mit hochauflösenden Röntgenspektroskopiemethoden.

List of Publications

K.G.V. Sigfridsson, N. Leidel, **O. Sanganas**, P. Chernev, O. Lenz, K.-S. Yoon, H. Nishihara, A. Parkin, F.A. Armstrong, S. Dementin, M. Rousset, A.L. De Lacey, M. Haumann (2015). Structural differences of oxidized iron-sulfur and nickel-iron cofactors in O_2-tolerant and O_2-sensitive hydrogenases studied by X-ray absorption spectroscopy, *Biochimica et Biophysica Acta (BBA) - Bioenergetics*, 1847:162-170, Epub ahead of print.

J. Fritsch, S. Löscher, **O. Sanganas**, E. Siebert, I. Zebger, M. Stein, M. Ludwig, A.L. De Lacey, H. Dau, B. Friedrich, O. Lenz, M. Haumann (2011). [NiFe] and [FeS] cofactors in the membrane-bound hydrogenase of *Ralstonia eutropha* investigated by X-ray absorption spectroscopy: Insights into O_2-tolerant H_2 cleavage, *Biochemistry*, 50:5858-5869.

I. Czech, S. Stripp, **O. Sanganas**, N. Leidel, T. Happe, M. Haumann (2011). The [FeFe]-hydrogenase maturation protein HydF contains a H-cluster like [4Fe4S]-2Fe site, *FEBS Letters*, 585:225-230.

S. Löscher, A. Gebler, M. Stein, **O. Sanganas**, T. Buhrke, I. Zebger, H. Dau, B. Friedrich, O. Lenz, M. Haumann (2010). Protein-protein complex formation affects the Ni-Fe and Fe-S centers in the H_2-sensing regulatory hydrogenase from *Ralstonia eutropha* H16, *ChemPhysChem*, 11:1297-1306.

S.T. Stripp, G. Goldet, C. Brandmayr, **O. Sanganas**, K.A. Vincent, M. Haumann, F.A. Armstrong, T. Happe (2009). How oxygen attacks [FeFe] hydrogenases from photosynthetic organisms, *Proceedings of the National Academy of Sciences of the United States of America*, 106:17331-17336.

S. Dementin, F. Leroux, L. Cournac, A.L. De Lacey, A. Volbeda, C. Leger, B. Burlat, N. Martinez, S. Champ, L. Martin, **O. Sanganas**, M. Haumann, V.M. Fernandez, B. Guigliarelli, J.C. Fontecilla-Camps, M. Rousset (2009). Introduction of methionines in the gas channel makes [NiFe] hydrogenase aero-tolerant, *Journal of the American Chemical Society*, 131:10156-10164.

S. Stripp*, **O. Sanganas***, T. Happe, M. Haumann (2009). The structure of the active site H-cluster of [FeFe] hydrogenase from the green alga *Chlamydomonas reinhardtii* studied by X-ray absorption spectroscopy, *Biochemistry*, 48:5042-5049.
*co-first author

O. Sanganas, S. Löscher, S. Pfirrmann, N. Marinos, P. Glatzel, T.-C. Weng, C. Limberg, M. Driess, H. Dau, M. Haumann (2009). Resonant inelastic X-ray scattering on synthetic nickel compounds and Ni-Fe hydrogenase protein, *XAFS14, Journal of Physics: Conference Series*, 190:012199-202.

N. Voevodskaya, F. Lendzian, **O. Sanganas**, A. Grundmeier, A. Graslund, M. Haumann (2009). Redox Intermediates of the Mn-Fe Site in Subunit R2 of *Chlamydia trachomatis* Ribonucleotide Reductase: An X-Ray Absorption and EPR Study, *Journal of Biological Chemistry*, 2844555-4566.

O. Sanganas, A. Grundmeier, M. Risch, I. Zaharieva, P. Chernev, V. Khare, T. Weyhermuller, K. Wieghardt, N. Voevodskaya, A. Graslund, S. Stripp, T. Happe, H. Dau, M. Haumann (2008). X-ray absorption spectroscopy investigations on binuclear metal sites in proteins and models at the Mn and Fe K-edges, *BESSY Annual Report 2008*, 405406.

A. Grundmeier, M. Risch, **O. Sanganas**, L. Gerencser, S. Löscher, I. Zaharieva, P. Chernev, S. Pfirrmann, C. Limberg, N. Marinos, M. Driess, M. Hörnke, B. Koksch, V. Kraehmer, D. Rehder, M. Anderlund, A. Magnuson, M. Haumann, H. Dau (2008). Synthetic models of biological metal centers studied by X-ray absorption spectroscopy at V, Mn Fe, Ni, and Zn Kedges, *BESSY Annual Report 2008*, 403404.

M. Risch, V. Khare, A. Grundmeier, **O. Sanganas**, L. Gerencser, I. Zaharieva, S. Löscher, P. Chernev, M. Haumann, H. Dau (2008). Characterization of a novel water-oxidizing cobalt catalyst by X-ray absorption spectroscopy, *BESSY Annual Report 2008*, 68-69.

Danksagung

Als erstes möchte ich Priv.-Doz. Dr. Michael Haumann ganz herzlich für die Möglichkeit, an diesem spannenden und attraktiven Thema arbeiten zu können, sowie für seine Betreuung und fachliche Unterstützung während meiner Dissertation danken. Dies gilt insbesondere für die vielen interessanten Projekte während meiner Zeit sowie die damit verbundene Interdisziplinarität und tieferen wissenschaftlichen Einblicke in diverse Forschungsgebiete.

Herrn Prof. Holger Dau danke ich für die vorbildliche Zusammenarbeit der beiden Arbeitsgruppen und der damit verbundenen gemeinsamen Nutzung von geistigen und materiellen Ressourcen. Besonders erwähnenswert sind die zahlreichen gemeinschaftlich organisierten und durchgeführten Synchrotronmeßzeiten sowie die gemeinsamen Arbeitsgruppenbesprechungen.

Herrn Prof. Joachim Heberle möchte ich für die Übernahme des Zweitgutachtens danken.

Ein besonderer Dank gilt Alex für die angenehme Zeit als langjähriger Zimmerkollege und während zahlreicher Synchrotronmeßzeiten.

Ivelina, Petko und Marcel als fester Bestandteil der Synchrotronabteilung gilt ebenso mein Dank für die erfolgreiche Zusammenarbeit vor, während und nach den Synchrotronaufenthalten sowie während der täglichen Laborarbeit und Datenauswertung.

Des Weiteren möchte ich mich bei Joachim, Björn, Andre und Laszlo, sowie bei allen hier nicht namentlich genannten Mitarbeitern der Arbeitsgruppen AG Haumann und AG Dau für das angenehme Arbeitsklima, den freundschaftlichen Umgang und die gute Zusammenarbeit bedanken. Zudem gilt mein Dank Marion und Sylvia für ihre stete Hilfsbereitschaft in Verwaltungsangelegenheiten.

Diese Arbeit wäre ohne die Unterstützung zahlreicher weiterer Forschungseinrichtungen nicht möglich gewesen. Deshalb möchte ich mich bei den Mitarbeitern aller Kooperationspartner und Synchrotroneinrichtungen für die erfolgreiche Zusammenarbeit bedanken. Namentlich erwähnen möchte ich die Arbeitsgruppen von B. Friedrich und O. Lenz (Humboldt Universität Berlin), T. Happe (Ruhr Universität Bochum), M. Rousset (CNRS Marseille, Frankreich), F. Armstrong (Oxford Universität, Großbritannien), H. Nishihara (Ibaraki Universität, Japan), C. Limberg (Humboldt Universität Berlin) und M. Driess (Technische Universität Berlin), sowie BESSY II (KMC-1, Berlin, F. Schäfers und M. Mertin), EMBL (D2, HASYLAB, DESY, Hamburg, W. Meyer-Klaucke), SRS (16.5, Daresbury, Großbritannien, B. Bilsborough), ANKA (XAS, Karlsruhe Institut für Technologie, Karlsruhe, S. Mangold) und ESRF (ID26, Grenoble, Frankreich, P. Glatzel und T.-C. Weng).

Danksagung

Abschließend möchte ich ganz besonders meinen Eltern danken, die mich mein ganzes bisheriges Leben in allen Belangen uneingeschränkt unterstützt haben. Ohne ihre Hilfe und ihren Rückhalt wäre ein erfolgreicher Abschluß meines Studiums und meiner Dissertation nicht möglich gewesen. Zudem danke ich meinem Bruder für seine kontinuierliche Unterstützung während dieser Zeit.

Selbstständigkeitserklärung

Hiermit versichere ich, dass alle Hilfsmittel und Hilfen angegeben wurden und die Arbeit auf dieser Grundlage selbstständig verfasst wurde. Die Arbeit wurde nicht schon einmal in einem früheren Promotionsverfahren angenommen oder als ungenügend beurteilt.

Berlin,